

**MECHANICAL PROPERTIES OF
COLLAGEN FIBRILS AND ELASTIC FIBERS
EXPLORED BY AFM**

Lanti Yang

The research described in this thesis was financially supported by the Softlink program of ZonMw. Project number: 01SL056.

The printing of this thesis was sponsored by the Dutch Society for Biomaterials (NVB).

Mechanical properties of collagen fibrils and elastic fibers explored by AFM

Lanti Yang

Ph. D. Thesis, with references; with summary in English and Dutch.

University of Twente, Enschede, The Netherlands.

ISBN: 978-90-365-2623-4

Copyright © 2008 by L. Yang.

All rights reserved.

The cover was designed by Hao Gu and Lanti Yang.

Printed by PrintPartners Ipskamp, Enschede, The Netherlands, 2008.

**MECHANICAL PROPERTIES OF
COLLAGEN FIBRILS AND ELASTIC FIBERS
EXPLORED BY AFM**

DISSERTATION

to obtain
the degree of doctor at the University of Twente,
on the authority of the rector magnificus,
prof. dr. W. H. M. Zijm,
on account of the decision of the graduation committee,
to be publicly defended
on Friday, 15th February 2008 at 13.15

by

Lanti Yang

born on 15th April 1979
in Harbin, China

This dissertation has been approved by:

Promotor: Prof. dr. J. Feijen

Assistant Promotores: Dr. P. J. Dijkstra

Dr. ir. M. L. Bemmink

Contents

Chapter 1	1
General Introduction	
Chapter 2	7
Mechanical Properties of Collagen and AFM as a Tool for Mechanical Testing	
Chapter 3	31
Micromechanical Bending of Single Collagen Fibrils using AFM	
Chapter 4	47
Mechanical Properties of Native and Cross-linked Type I Collagen Fibrils	
Chapter 5	65
Mechanical Properties of Single Electrospun Collagen Type I Fibers	
Chapter 6	81
Micro-tensile Testing of Individual Native and Cross-linked Collagen Type I Fibrils	
Chapter 7	99
Viscoelastic Behavior of Collagen Type I Fibrils: Evidence for the Existence of Microfibrils?	
Chapter 8	115
Microscale Mechanical Properties of Single Elastic Fibers; the Role of Fibrillin-microfibrils	
Summary	135
Samenvatting	141
Acknowledgements	147
Curriculum Vitae	151

General Introduction

1.1 Collagen

Collagen is the most abundant protein in the human body. Of the 25 types of collagen known, fibril-forming collagen is the main component in many tissues such as tendons, cartilage and bone [1]. Fibril-forming collagen is characterized by a hierarchical assembly of substructures. In this hierarchical arrangement, collagen molecules consisting of three polypeptide chains assemble into fibrils with diameters in the range of 10 - 500 nm and the fibrils further assemble into fibers. Fascicles and tissues contain collagen fibers embedded in proteoglycan [2,3]. The main function of fibril-forming collagen is to provide the structural framework and the strength of tissues [2].

Collagen has been widely used in the manufacturing of cosmetics, glue and gelatin [4]. In the past 30 years, collagen-based biomaterials have been developed for a number of medical and tissue engineering applications, for example, heart valves, artificial skin substitutes and scaffolds for tissue engineering and drug delivery applications [5-7].

The outstanding mechanical properties of collagen are crucial for its function in tissue. The mechanical properties of collagen fibers, fascicles and collagen-based tissues have been studied for many years [2,8-10]. Due to the limitations in performing mechanical testing on the nanometer and micrometer scale, only very recently studies have been initiated to measure the mechanical properties of substructures like collagen fibrils and the respective influence of each substructure of the hierarchical structure on the overall mechanical properties of tissue [11-15].

1.2 Elastic Fibers

Next to collagen, elastic fibers are other important components responsible for the mechanical properties of tissues. Elastic fibers (Fig. 1.1A) are abundant in tissues such as blood vessels, elastic ligaments, and lung to provide the elasticity of these tissues [16]. The vertebrate elastic fiber contains at least two morphological components; amorphous

elastin, which accounts for 90% of the elastic fiber, and microfibrils (Fig. 1.1B) which are 10 - 12 nm in diameter and mainly composed of fibrillin-1 [17,18]. During elastic fiber formation, fibrillin-microfibrils appear first and serve as a scaffold for the deposition of tropo-elastin [17]. Studies suggest that fibrillin-microfibrils not only play a role as a scaffold for elastin but also contribute to the elastic properties of vertebrate organs [18,19]. There is still some debate as to how fibrillin-microfibrils contribute to the mechanical properties of the elastic fibers.

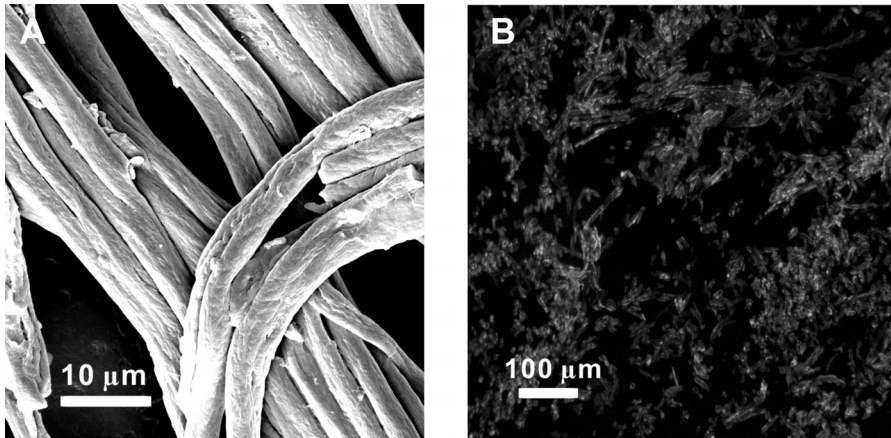


Figure 1.1 (A) SEM image of elastic fibers with diameters in the range of 3 to 5 μm . (B) Fluorescence microscope image of immunostained fibrillin-microfibrils in elastic fibers.

1.3 AFM Approach for Mechanical Testing

The atomic force microscope (AFM) was initially invented as an imaging tool for determining surface topographies at sub-nanometer resolution. In recent years, AFM has also been developed as a technique for micromanipulation and force spectroscopy of materials at the sub-micron scale or even at the single molecular level [20,21]. Conventional techniques for determining the mechanical properties of materials are based on direct manipulation and visual observation, which cannot be easily applied for materials with sub-micron size. With an AFM-based technique, samples at the sub-micron scale can be observed and manipulated. This technique with piconewton force sensitivity offers a novel means to measure the mechanical properties of materials at sub-micron scale.

1.4 Aim and Outline of this Thesis

It is the aim of this work to explore the relationship between the mechanical properties and structure of collagen fibrils and elastic fibers, which will provide a better insight in the micromechanical behavior of tissues. To achieve this aim, the mechanical properties of single collagen fibrils and elastic fibers will be determined using AFM-based micromanipulation techniques. Tensile properties, shear related properties and viscoelastic behavior of single collagen fibrils at ambient conditions and immersed in buffer will be determined. Furthermore, the influence of different cross-linking agents on the mechanical properties of collagen fibrils will be studied. The mechanical properties of these cross-linked collagen fibrils will provide insight into the existence of microfibrils. In a separate set of experiments, the mechanical properties of elastic fibers devoid of or containing fibrillin-microfibrils will be determined to evaluate the role of fibrillin-microfibrils in the mechanical properties of elastic fibers.

Chapter 2 presents a review of the current understanding of the structure and mechanical properties of collagen with emphasis on the collagen fibrils. AFM as a tool for determining the mechanical properties of materials in the sub-micron range is also described in this chapter.

In the next part of this thesis, the results of micro-mechanical bending experiments on single collagen fibrils are described. In **Chapter 3**, we report on experiments in which the Young's modulus of single native collagen fibrils at ambient conditions was determined from bending tests after successfully depositing the fibrils on a substrate containing micro-channels. The influence of glutaraldehyde cross-linking on the Young's modulus of single collagen fibrils was evaluated. In **Chapter 4**, we describe the development of micro-mechanical bending tests in a scanning mode which provides a more accurate determination of the mechanical properties of single collagen fibrils. The bending and shear moduli of native and carbodiimide cross-linked single collagen fibrils both at ambient conditions and in PBS buffer were determined. The shear modulus is two orders of magnitude lower than the Young's modulus of native collagen fibrils, which confirms the mechanical anisotropy of the fibrils. This micro-mechanical bending method was further applied to determine the mechanical properties of electrospun collagen fibers, as described in **Chapter 5**. Electrospun collagen fibers with diameters ranging from 100 to 600 nm were successfully produced by electrospinning of a solution of acid soluble collagen type I. The electrospun fibers were water soluble and became insoluble after cross-linking with glutaraldehyde vapor. The bending and shear moduli of both non- and

cross-linked single electrospun collagen fibers were determined by scanning mode bending after depositing the fibers on substrates containing micro-channels. An increase in the shear modulus of the fibers was found after cross-linking with glutaraldehyde vapor.

The following section of this thesis describes the tensile and viscoelastic properties of single collagen fibrils measured by micro-tensile testing and stress-relaxation measurements using AFM. In **Chapter 6**, we report on micro-tensile testing of (non)cross-linked single collagen fibrils both at ambient conditions and in PBS buffer of fibrils fixed between the substrate and the AFM cantilever. An AFM setup was used with ranges of displacement in the z direction sufficient to measure the breakage of the fibril. The stress-strain behavior, Young's modulus, failure stress and strain at break of (non)cross-linked fibrils were determined. The influence of different cross-linking agents on the tensile properties of single collagen fibrils was evaluated. In **Chapter 7**, the viscoelastic behavior of single collagen fibrils was studied in more detail by performing micro-tensile testing at different strain rates and stress relaxation measurements. The results indicate that the stress-strain behavior of individual collagen fibrils is rate-dependent. The relaxation process of individual collagen fibrils can be described by the two-term Prony series, which suggests that there are two stress relaxation regimes. A model is proposed to explain the stress relaxation of individual collagen fibrils.

The last part of this thesis, **Chapter 8** deals with the evaluation of the role of fibrillin-microfibrils in the mechanical properties of elastic fibers. The Young's moduli of elastic fibers devoid of and containing fibrillin-microfibrils were determined by bending the elastic fibers that were suspended across micro-channels with a tip-less AFM cantilever. Furthermore, layers of fibrillin-microfibrils were subjected to nano-indentation tests to understand the role of fibrillin-microfibrils in vertebrate elastic fibers. Combining the results from bending and indentation experiments, the role of fibrillin-microfibrils in the mechanical properties of vertebrate elastic fibers was discussed.

Most of the work described in this thesis has been published or will be published in the near future [22-27].

References

1. Prockop DJ, Kivirikko KI. Collagens: molecular biology, diseases, and potentials for therapy. *Annu. Rev. Biochem.* **1995**; 64: 403-434.
2. Silver FH, Freeman JW, Seehra GP. Collagen self-assembly and the development of

- tendon mechanical properties. *J. Biomech.* **2003**; 36: 1529-1553.
3. Ottani V, Martini D, Franchi M, Ruggeri A, Raspanti M. Hierarchical structures in fibrillar collagens. *Micron* **2002**; 33: 587-596.
 4. Weiss JB, Ayad S. *In Collagen in health and disease. Churchill Livingstone, Edinburgh, 1982.*
 5. Lee CH, Singla A, Lee Y. Biomedical applications of collagen. *Int. J. Pharm.* **2001**; 221: 1-22.
 6. Ruszczak Z. Effect of collagen matrices on dermal wound healing. *Adv. Drug. Deliver. Rev.* **2003**; 55: 1595-1611.
 7. Gentleman E, Lay AN, Dickerson DA, Nauman EA, Livesay GA, Dee KC. Mechanical characterization of collagen fibers and scaffolds for tissue engineering. *Biomaterials* **2003**; 24: 3805-3813.
 8. Wang JHC. Mechanobiology of tendon. *J. Biomech.* **2006**; 39: 1563-1582.
 9. Dowling BA, Dart AJ. Mechanical and functional properties of the equine superficial digital flexor tendon. *Vet. J.* **2005**; 170: 184-192.
 10. Fratzl P, Misof K, Zizak I. Fibrillar structure and mechanical properties of collagen. *J. Struct. Biol.* **1998**; 122: 119-122.
 11. Graham JS, Vomund AN, Phillips CL, Grandbois M. Structural changes in human type I collagen fibrils investigated by force spectroscopy. *Exp. Cell Res.* **2004**; 299: 335-342.
 12. van der Rijt JAJ, van der Werf KO, Bennink ML, Dijkstra PJ, Feijen J. Micromechanical testing of individual collagen fibrils. *Macromol. Biosci.* **2006**; 6: 697-702.
 13. Eppell SJ, Smith BN, Kahn H, Ballarini R. Nano measurements with micro-devices: mechanical properties of hydrated collagen fibrils. *J. R. Soc. Interface* **2006**; 3: 117-121.
 14. Strasser S, Zink A, Janko M, Heckl WM, Thalhammer S. Structural investigations on native collagen type I fibrils using AFM. *Biochem. Bioph. Res. Co.* **2007**; 354: 27-32.
 15. Wenger MPE, Bozec L, Horton MA, Mesquida P. Mechanical properties of collagen fibrils. *Biophys. J.* **2007**; 93: 1255-1263.
 16. Rosenbloom J, Abrams WR, Mecham R. Extracellular matrix 4: the elastic fiber. *FASEB J.* **1993**; 7: 1208-1218.
 17. Kielty CM, Sherratt MJ, Shuttleworth CA. Elastic fibres. *J. Cell Sci.* **2002**; 115: 2817-2828.
 18. Sherratt MJ, Baldock C, Haston JL, Holmes DF, Jones CJP, Shuttleworth CA, Wess TJ, Kielty CM. Fibrillin microfibrils are stiff reinforcing fibres in compliant tissues. *J. Mol. Biol.* **2003**; 332: 183-193.
 19. Lillie MA, David GJ, Gosline JM. Mechanical role of elastin-associated microfibrils in pig aortic elastic tissue. *Connect Tissue Res.* **1998**; 37: 121-141.
 20. Vinckier A, Semenza G. Measuring elasticity of biological materials by atomic

- force microscopy. *FEBS Lett.* **1998**; 430: 12-16.
21. Fisher TE, Oberhauser AF, Carrion-Vazquez M, Marszalek PE, Fernandez JM. The study of protein mechanics with the atomic force microscope. *Trends Biochem. Sci.* **1999**; 24: 379-384.
 22. Yang L, van der Werf KO, Koopman BFJM, Subramaniam V, Bennink ML, Dijkstra PJ, Feijen J. Micromechanical bending of single collagen fibrils using atomic force microscopy. *J. Biomed. Mater. Res. A* **2007**; 82: 160-168.
 23. Yang L, van der Werf KO, Fitié CFC, Bennink ML, Dijkstra PJ, Feijen J. Mechanical properties of native and cross-linked type I collagen fibrils. *Biophys. J.* **2007**; *Online*.
 24. Yang L, Fitié CFC, van der Werf KO, Bennink ML, Dijkstra PJ, Feijen J. Mechanical properties of single electrospun collagen type I fibers. *Biomaterials* **2008**; 29: 955- 962.
 25. Yang L, van der Werf KO, Bennink ML, Dijkstra PJ, Feijen J. Micro-tensile testing of individual native and cross-linked collagen type I fibrils. *To be submitted*.
 26. Yang L, van der Werf KO, Bennink ML, Dijkstra PJ, Feijen J. Viscoelastic behavior of individual collagen fibrils tested by AFM. *Tissue Eng.* **2007**; 13: 1777-1777.
 27. Yang L, Koenders MMJF, Wismans RG, van der Werf KO, Reinhardt DP, Bennink ML, Dijkstra PJ, van Kuppevelt TH, Feijen J. Microscale mechanics of single elastic fibers; the role of fibrillin-microfibrils. *To be submitted*.

Mechanical Properties of Collagen and AFM as a Tool for Mechanical Testing

2.1 Introduction

The mechanical properties of tissues like tendons, ligaments, and bone are directly related to the arrangement of their constituent components. Collagen type I is the most abundant protein in these tissues and is the principal, tensile stress-bearing component. In this fibrillar type collagen the collagen triple helices, also called collagen molecules, are assembled in fibrils and cross-linked via the amino acids lysine and hydroxyl lysine present in their telopeptide regions [1,2]. The way the collagen molecules assembled in a fibril has been a subject of extensive studies and the presence of subfibrillar and microfibrillar structure have been proposed. The fibrils are assembled in fibers, which depending on the tissue are assembled in fascicles like in tendon.

Because of the distinct hierarchical organization of the polypeptide chains up to the collagen fibers, over the past decades many studies have been initiated to elucidate the relation between the tissue mechanical properties and its distinct structure [1-10]. In this respect, mechanical testing of fibrils, an important substructure of the collagen fiber, is important to determine the contribution of such a substructure to the overall mechanical behavior of tissues.

The development of micromanipulation techniques like atomic force microscopy (AFM), offers a novel and direct means to measure the mechanical properties of materials on a micrometer and nanometer scale [11-15] or even at the single protein level [16,17]. Particularly, studies have been initiated on the mechanical properties of collagen single fibrils (10 - 500 nm in diameter) and molecules.

In section 2.2 an overview is given on the collagen hierarchical structure. Especially models describing the collagen molecular packing within collagen fibrils are discussed. In the next section (2.3) we will focus on the mechanical properties of collagen-based tendon

tissues, collagen fibers, fibrils and molecules. In section 2.4, a brief review on currently applied AFM-based mechanical tests methods is presented.

2.2 The Hierarchical Structure of Collagen

Collagen is the most abundant protein in vertebrates and accounts for 66% of all proteins in humans [18]. Up to now, 25 types of collagen have been identified [19]. Collagen can be found in both fibril and non-fibril forming structures. The fibril-forming collagens including type I, II, III, V and XI provide the structural framework and the mechanical strength of tissues [1]. In general, collagen type I is the most abundant and can be found throughout the human body [20]. Since the mechanical properties and structure of type I collagen are the main subjects of this research, we will focus in this chapter on fibril-forming collagen. Unlike most other proteins, collagen shows a highly organized structure with many hierarchical structural levels including the so-called collagen molecule, fibril, fiber, and even higher levels e.g. fascicles in a tendon (Fig. 2.1) [2,3].

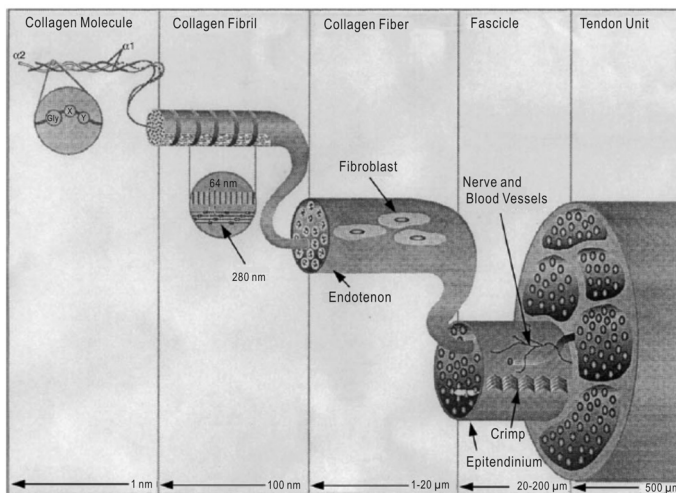


Figure 2.1 Schematic representation of the structural hierarchy in tendon. The diagram illustrates the relationship between collagen molecules, fibrils, fibers, fascicles and tendon units. The figure is reprinted from [1] with permission from Elsevier.

2.2.1 Collagen molecule

The primary structure of collagen is the polypeptide chain, a linear array of α -amino acids, mainly comprising the repeating tripeptide unit Gly-X-Y (Gly = glycine). The nature of the X and Y amino acid residues can vary but X is mostly proline (Pro) and Y is mostly hydroxyl-proline (Hyp) [21]. Three polypeptide chains are super-coiled around a common

axis forming a triple helix which is named the collagen molecule. Collagen molecules exhibit a long, rod-like structure with a diameter of ~ 1.5 nm, a length of 300 nm and a molecular weight of 285 kDa [2]. Depending on the collagen type, triple helices are composed of either homo- or heterotrimers. The triple helices of collagen type I are composed of two $\alpha 1$ -chains and one $\alpha 2$ -chain which differ only slightly in amino acid composition [22].

The causes of the high stability of the collagen molecule has been a subject of several studies [23-31] and is generally ascribed to hydrogen bonds between the backbones of the three α -chains and water-mediated hydrogen bonds [24-32]. The hydrogen bonds are formed between the N-H group of Gly residues in one chain and the C=O group of a residue at the X-position in an adjacent chain [33]. The importance of hydroxyproline in water-mediated hydrogen bonding and thereby stabilizing the triple helical collagen molecular structure has been recognized. It is hypothesized that one to four water molecules are involved in forming water bridges between the C=O (Hyp) and C=O (Gly) groups or between the OH (Hyp) and C=O (Gly) groups [26,27,29,31,33].

2.2.2 Molecular packing in the collagen fibril

The collagen fibril is formed by self-assembly of collagen molecules (Fig. 2.1). These fibrils show a cylindrical shape with diameters ranging from 10 to 500 nm [34]. Using electron microscopy or atomic force microscopy, a distinct and regular banded pattern in collagen fibrils can be observed. The periodicity of the pattern is ~ 67 nm, and is called the D-period. The observed banded pattern was first explained by the model of Hodge and Petruska [35]. In their model five collagen molecules are arranged in a staggered like structure as shown in Fig. 2.2. The model explains the appearance of dark bands, called "gap regions" or "gap zones" where only four molecules are present and light bands called "overlap regions" or "overlap zones" where five molecules are present.

The translation of the inherently 2D Hodge and Petruska model into a 3D dimensional molecular packing in the collagen fibrils has been debated for many years. Based on X-ray diffraction data and ultra structural techniques such as TEM, several models have been proposed to describe the molecular packing in collagen fibrils. These models can be divided into two principal categories. In the first category, five collagen molecules form an intermediate microfibrillar structure with connections in the telopeptide region. In the second category, collagen molecules form a crystalline (or quasi-crystalline) 3D array [2,34].

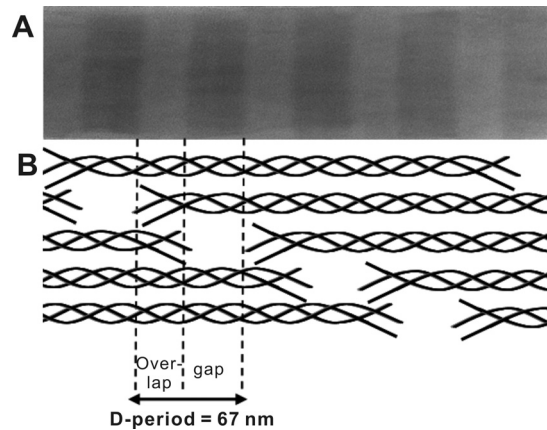


Figure 2.2 (A) Transmission electron microscopy (TEM) image of single fibrils with the 67 nm D-period visible. (B) Schematic representation of the two-dimensional axial arrangement of collagen molecules in a microfibril. The D-period originates from the staggered aggregation of the collagen molecules in microfibrils.

In the microfibrillar models, the collagen molecular segments are tightly packed in the overlap region and have more flexibility in the gap region [36]. The D-periodic five-stranded microfibril model for molecular packing of collagen, originally proposed by Smith has gained wide acceptance [37]. The model is consistent with electron microscopy and X-ray diffraction data. To further explain the packing of collagen molecules in microfibrils, Trus and Piez proposed the compressed microfibril model. In this model, the five-stranded microfibrils were compressed and the molecules were placed in cross-section on a near-hexagonal lattice unit cell [38]. The calculated intensities from an X-ray diffraction pattern of this near-hexagonal lattice unit cell agreed with the experimental X-ray diffraction data. However, this model is considered to be slightly simplistic. With the refinements in X-ray diffraction techniques, a model describing an interconnected microfibrillar structure was suggested by Wess *et al.* [36,39]. In this model, the fibril was formed from five-stranded microfibrils. The microfibril was compressed and was itself a helix with individual molecules wound in a left-handed manner. As presented in Fig. 2.3, in the overlap region, the five molecules in a microfibril are tightly packed leading to a well-ordered nearly crystalline structure. In the gap region, the molecular segments follow an individual path. In this model, it is proposed that the microfibrils are interconnected by the relative mobile telopeptides at the gap-overlap transitions. This explains the inherent disorder in the gap region and the impossibility of isolating microfibrils.

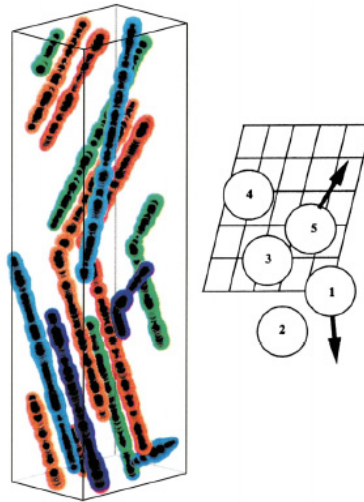


Figure 2.3 On the left, a 3D representation of the molecular arrangement of type I collagen according to Wess *et al.* On the right, the cyclic set of the final model and the telopeptide directions. Figure is reprinted from [36] with permission from Elsevier.

The second category comprises quasi-crystalline 3D array models which are based on X-ray diffraction data. X-ray diffraction reveals three-dimensional crystallinity in the molecular packing in the collagen fibril although diffuse scatter is present indicating significant disorder in the fibril. A major advancement was made by the quasi-hexagonal packing model proposed by Hulmes and Miller [40] in 1979. This model was based on a quasi-hexagonal molecular packing without microfibrillar sub-structure, which showed a much better agreement with their X-ray diffraction data. Later, cylindrical models were developed to explain the quasi-crystalline 3D array in collagen fibrils [41]. The most newly update was the concentric ring model developed by Hulmes *et al.* [4,34]. In this model a 3D crystallinity admixed with liquid-like lateral disorder in the collagen fibril and with molecules packed radially in concentric layers separated at a distance of ~ 4 nm was proposed.

Several attempts have been made to visualize the microfibrillar structure and recently the existence of such a sub-structure in collagen fibrils was suggested [42-46]. A longitudinal microfibrillar structure with a width of 4-8 nm was visualized in both hydrated (Fig. 2.4A) [43,44] and dehydrated [42] collagen type I fibrils using tapping mode AFM imaging. Furthermore, three-dimensional image reconstructions of 36 nm-diameter corneal collagen fibrils show a 4 nm repeat in a transverse section, which may be related to the microfibrillar structure [45]. Unexpectedly, the microfibrils exhibit a constant tilt angle of

$\sim 15^\circ$ to the fibril long axis in a right-handed helix. Interestingly, very recent work of Orgel *et al.* using X-ray diffraction culminating in an electron density map suggests microfibrillar structures similar as suggested by Holmes *et al.* [45]. As shown in Fig. 2.4 B and C, right-handed supertwisted microfibrillar structures can be identified by tracing the full path of each collagen molecule in the electron density map [46].

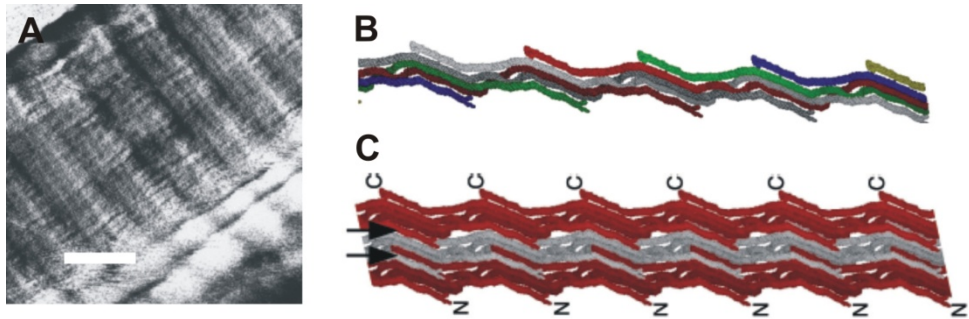


Figure 2.4 (A) Tapping mode AFM phase imaging of hydrated tendon revealing the microfibrillar structure in the collagen fibrils. The scale bar in the image represents 100 nm. The figure is reprinted from [43] with permission from Elsevier. From X-ray diffraction and electron density mapping models representing the single right-handed supertwisted microfibrillar structure (B) and three side by side microfibrils (C) is provided by Orgel *et al.* The figure is reprinted from [46] with permission from copyright (2006) National Academy of Sciences, U.S.A.

2.2.3 Collagen fibers

Collagen fibers form through the parallel arrangement of a large number of collagen fibrils. The fibrils within the fibers are tilted, resulting in a macroscopic crimped structure visible with an optical microscope [47]. Furthermore, small proteoglycans (PGs), especially the small leucine-rich proteoglycans (SLRPs) play an important role in the assembly of adjacent fibrils although the exact molecular interactions involved in the binding are not yet understood [2,45]. The structural skeleton of tissues is composed of an assembly of collagen fibers.

2.3 Mechanical Properties of Collagen

The main function of fibril-forming collagens is to provide the structural framework and the biomechanical properties of tissues [1]. Most studies concerning the mechanical properties of collagen make use of whole tendons or collagen fibers isolated from tendons. Therefore, the mechanical properties of collagen obtained from tendon are the best characterized up to now and will be reviewed in the next section.

2.3.1 Mechanical properties of tendon and collagen fibers

The stress-strain behavior of tendon and collagen fibers has been the subject of several studies in the past decades [1,3,7-10,48]. A typical stress-strain plot of tendon in the hydrated state shows three distinct regions as depicted in Fig. 2.5 [49]. The initial part of the curve with a strain up to 2% is characterized by a low stress and high strain and is called “toe region”. This toe region represents the removal of the macroscopic crimp in the collagen fibers, which can be visualized using an optical microscope [50,51]. The toe region is followed by the heel region where the slope increases due to the reduction of disorder in the lateral molecular packing in the fibril [49]. This reduction is reported to result from the removal of microscopic kinks in the gap region of collagen molecules [52]. Further increasing the stress leads to a linear stress-strain behavior of the tendon (start at ~ 3% strain). Several studies involving X-ray diffraction techniques have been carried out to explain the linear stress-strain behavior [5,6,53,54]. Folkhard *et al.* [53] stretched native fibers from rat tail tendon and monitored the changes in the D-period by time-resolved X-ray measurements using synchrotron radiation. From the results they suggested that there are two mechanisms that contribute to the linear stress-strain behavior, namely the stretching of the collagen molecules and sliding of molecules with respect to each other. X-ray diffractometry was performed by Sasaki *et al.* on loaded tendon samples to measure the strain at the fibril level. They suggested that molecular elongation is the main mechanism in the linear region of the stress-strain curve of tendon [6]. The slope of the linear region is taken as the Young’s modulus of the tendon. The Young’s moduli of dry tendon and collagen fibers presented in literature range from 1 to 8 GPa [10,55-57] and from 0.15 to 1 GPa of the samples in the hydrated state [55,57,58]. Beyond 8 - 10% strain, macroscopic failure occurs and further stretching causes rupture of the tendon [7].

Collagen based tendons usually exhibit viscoelastic properties, i.e. their mechanical behavior is rate dependent. The viscoelastic properties are considered to be important in the functioning of the tissue [59]. Various experiments have been performed on tendons and collagen fibers to study the viscoelastic behavior [3,60-70].

Tensile tests at different strain rates reveal that tendons and collagen fibers or fascicles from tendon show strain-rate dependent mechanical properties. Wu *et al.* [63] reported that the elastic moduli of fresh flexor tendons immersed in PBS buffer were 427 ± 10 , 653 ± 21 and 837 ± 11 MPa at strain rates of 0.6 %/s, 1.2 %/s and 5 %/s, respectively. Lynch *et al.* [64] investigated the strain rate dependent properties of tendon in detail and found that only the slope of the linear region (the modulus) was strain rate dependent. The elastic modulus of collagen fascicles increases from 160 ± 49 MPa to 216 ± 68 MPa when

increasing the strain rate from 0.01 %/s to 1 %/s [71]. Robinson *et al.* [62] found that the collagen fascicles from rat tail tendon without small proteoglycans (decorin) revealed a reduced strain rate dependency. Their results indicate that the proteoglycans play a role in the viscoelastic behavior of tendon.

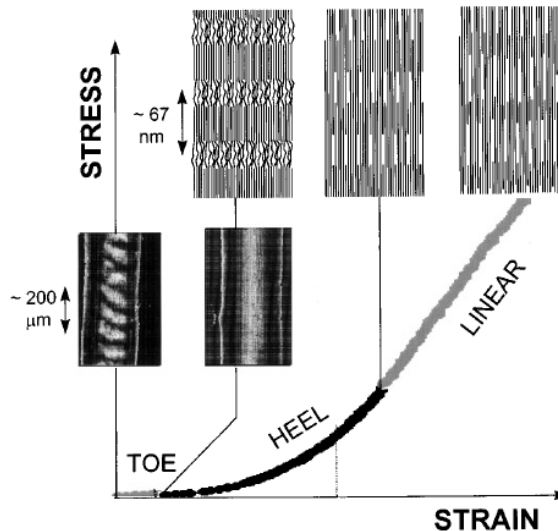


Figure 2.5 Typical stress-strain curve of a tendon. This curve qualitatively shows the different regions in the stress-strain curve of tendon and the main structural changes in the different regions (see text). The figure is reprinted from [49] with permission from Elsevier.

Besides tensile tests at different strain rates, stress-relaxation tests were performed to study the viscoelastic behavior of tendon and collagen fibers [63,65,66]. The experimental normalized stress as a function of time can be well described by the two-term Maxwell model (two-term Prony series) [72]. Applying this model to experimental results afforded two relaxation times, which means there are two stress relaxation regimes. A fast relaxation time of 200 s and a slow relaxation time of 20000 s were determined for rat tail tendon collagen fibers [66]. The authors proposed that the fast relaxation was related to the sliding between collagen molecules which was hindered by hydrogen bonding and the slow relaxation was related to the swelling and opening-up of the fiber bundles which was influenced by changes of pH values of buffers used.

Although the viscoelastic behavior of tendon and collagen fibers has been a subject of study for several years, the mechanism for the viscoelastic behavior is still not fully clear. Purslow and co-workers reported that a relaxation process within the collagen fibers or at the fiber-matrix interface may be responsible for the viscoelastic properties of these

tissues [59]. Simultaneous tensile testing and synchrotron X-ray diffraction were used to investigate the viscoelastic behavior of rat-tail tendon. It was found that the overall strain of tendon was always larger than the strain in individual fibrils, which demonstrated that some deformation is taking place in the matrix between fibrils [3]. Based on these results, the authors proposed a model in which the collagen fibrils and the interfibrillar matrix act as a coupled viscoelastic system. A similar conclusion was drawn by Silver *et al.* who showed that the specific binding of decorin to collagen fibrils enhances the viscous transfer of energy between collagen fibrils during tensile deformation. However, it was also suggested that the force within the tendon is directly transferred through collagen fibrils and not through an interfibrillar proteoglycan bridge [69] and that the sliding of collagen fibers with respect to each other is the main mechanism for the viscoelastic behavior of tendon [68].

2.3.2 Mechanical properties of collagen fibrils

Understanding the mechanical properties of collagen subunits provides insight in the contribution of each hierarchical level to the overall mechanical properties of tendon. However, the mechanical properties of collagen subunits like fibrils only received attention during the last few years due to a limitation of the available techniques.

The mechanical properties of the collagen fibrils were first studied using X-ray diffraction and simultaneous tensile testing on tissue samples [3,5,6,49,53,54]. The changes in the D-period detected from the X-ray diffraction data during loading the tissue sample was related to the strain on the collagen fibril level. A series of experiments were performed by Mosler and co-workers to study the mechanism of collagen fibril elongation [5,53,54]. In their research, stretching of the rat tail tendon was monitored in time-resolved X-ray measurements using synchrotron radiation. Their results suggest that there are two mechanisms contributing to the elongation of fibrils. The first mechanism is the stretching of the collagen molecule, which increases the D period from 67 nm to about 67.6 nm. The sliding of collagen molecules with respect to each other is the second mechanism which further increases the D period. Also, by holding the tendon at constant load, they found a continuous sliding of collagen molecules up to 300 s, which can be attributed to the viscous behavior of collagen fibrils. With a similar setup, Fratzl *et al.* [49] recorded simultaneously the strain at the tendon level and fibril level (relative changes in D-period). They found that the increase in the D-period is about 40 % of the total macroscopic strain applied, which implies that not all elongation of tendon is due to the stretching of the fibril. Sasaki and Odajima [6] studied the stress-strain behavior of collagen fibrils in

bovine Achilles tendon. In their measurements, small angle X-ray scattering (SAXS) was performed on the loaded tendon to measure the changes in the D-period, the strain at the fibril level, with changing the stress. Using the force applied to the bulk tendon they found a linear stress-strain relationship of the collagen fibrils as shown in Fig. 2.6. A Young's modulus of 400 MPa of the collagen fibrils in the hydrated state was estimated from the measurements. By analyzing the intensity of the X-ray diffraction pattern, they suggested that molecular elongation is the major contribution to fibril elongation.

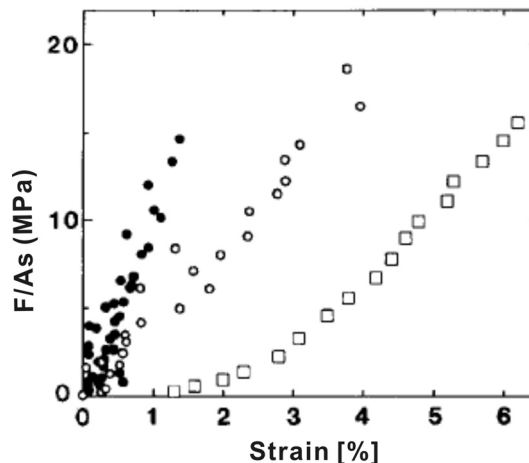


Figure 2.6 Stress-strain curves of a collagen molecule (filled circles), a collagen fibril (open circles) and tendon (open squares). The figure is reprinted from [6] with permission from Elsevier.

With the development of micro-manipulation techniques combined with force measurements, micro-mechanical testing on subunits of collagen [55,73,74] especially on individual collagen fibrils became possible [75-80]. In most studies, atomic force microscopy (AFM), a very sensitive tool to detect forces in the pN and nN range, was used.

Graham *et al.* [77] stretched in vitro-assembled type I collagen fibrils with a diameter of ~ 30 nm cultured from human fibroblasts using AFM, as shown in Fig. 2.7A. Due to the surface adhesion of collagen, a single collagen fibril adhered between the AFM cantilever and the glass surface. From the stress strain curves, the Young's modulus was determined to be 32 MPa above 4 % strain (Fig. 2.7B). Furthermore, discontinuities between 1.5 and 4.5 nN in force and 22 nm in length were observed in the elongation profile upon stretching of single fibrils, which were related to unfolding of the triple-helical polypeptides in the gap region.

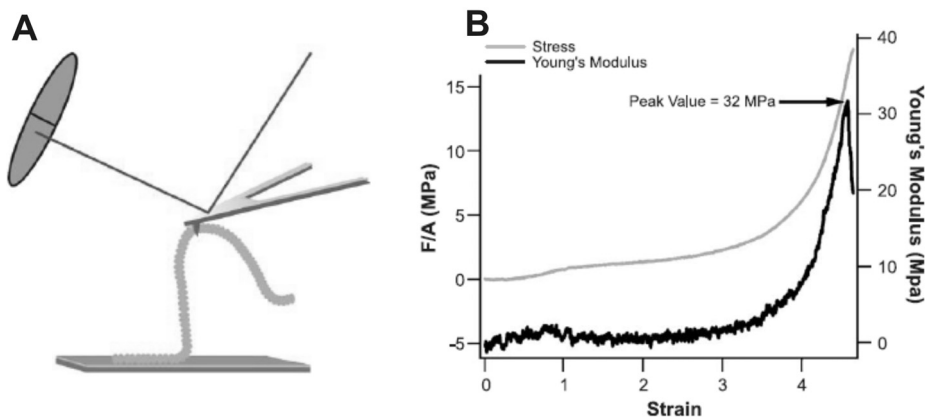


Figure 2.7 (A) Schematic representation of a force spectroscopy measurement on collagen fibrils. The fibril adhered between a clean glass surface and an AFM cantilever. (B) Stress strain curves for an individual collagen fibril. The gray curve is the stress in MPa (fibril diameter 20 nm). The black curve is the Young's modulus calculated by taking the derivative of the stress versus strain data. The figures are reprinted from [77] with permission from Elsevier.

Using microelectromechanical system (MEMS) technology, Eppell *et al.* [80] studied the stress-strain relationship of single type I collagen fibrils isolated from sea cucumber and found a Young's modulus of 550 MPa for a single collagen fibril in the hydrated state. With the device they used, it is possible to perform cyclic loading of a fibril. A decrease in the modulus of the fibril after large numbers of cyclic loading was determined (Fig. 2.8). However, their results did not show clear strain-rate dependency of the stress-strain behavior when increasing the strain rate from 1 Hz to 100 Hz.

In our previous work, we developed a method to tensile test single collagen fibrils isolated from bovine Achilles tendon using a home-built AFM system [75]. The collagen fibrils were deposited on a glass surface which was partly coated with Teflon. Before tensile testing, the fibril was fixed between the glass surface and the AFM cantilever using two component epoxy glue (Fig. 2.9A). Tensile tests of individual fibrils were both performed for fibrils at ambient conditions and fibrils in PBS buffer. A Young's modulus of 2 - 7 GPa was obtained at ambient conditions and 0.2 - 0.8 GPa for fibrils immersed in PBS buffer (Fig. 2.9B).

However, due to the limitation in micro-tensile techniques, the tests mentioned above [75,77,80] could only be performed up to a limited strain. The failure stress and strain at break still could not be measured.

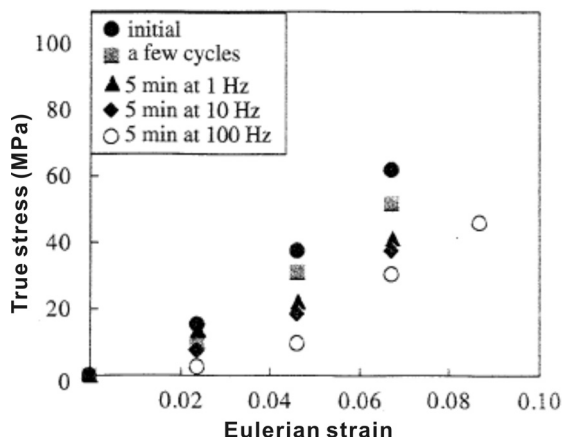


Figure 2.8 Stress-strain plots of a fibril measured before and after cyclic loading under specified conditions [80]. The Young's modulus measured from the first cycle is 0.93 GPa, and decreases to 0.78 GPa (after few cycles), 0.59 GPa (5 min at 1 Hz), 0.55 GPa (5 min at 10 Hz) and 0.55 GPa (5 min at 100 Hz). The figure is reprinted from [80] with permission from Royal Society.

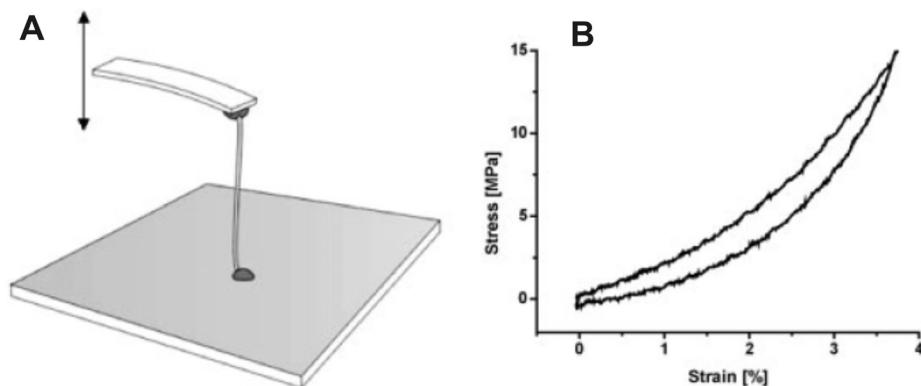


Figure 2.9 (A) Schematic drawing of the micro-tensile test experiment of single collagen fibrils performed using an AFM. The fibril is fixed between the AFM cantilever and the glass surface with epoxy glue. (B) Typical stress-strain curve of a single collagen fibril immersed in PBS buffer. The figure is reprinted from [75] with permission from Wiley-VCH Verlag GmbH & Co. KGaA.

Recently, both micromechanical bending and nano-indentation tests using AFM-based techniques have proven to be important tools in determining the mechanical properties of proteins and cells [14,81-84]. Besides tensile tests, some pioneering work has been done with bending and indentation techniques to understand the mechanical properties of single collagen fibrils [76,78,79]. Nano-indentation tests of single collagen fibrils using AFM were very recently reported by Wenger *et al.* [78]. From their results, reduced Young's moduli in the range of 5 to 11.5 GPa for collagen type I from rat tail tendon at ambient

conditions were determined. Furthermore, using an indenter with a tip apex smaller than the collagen fibril diameter, indentation on the fibril surface caused small imprints (Fig. 2.10). The nonuniform shape of the imprints indicates that the collagen fibril is anisotropic and supports the hypothesis that the fibrils consist of subfibrils, aligned along the fibril axis. Using an AFM based micro-dissection technique, the properties at the centre and the surface of the collagen fibrils isolated from calfskin were probed by Strasser and co-workers [79]. Nano-indentation was performed both at the surface and the centre of the fibril. A Young's modulus of 1.2 GPa without significant difference in the elasticity between core and shell was obtained from the measurements. However, they found a higher adhesion at the surface of the fibril compared to the central region, which they related to a higher number of cross-links near the fibril surface than in the central region as also suggested by Gutschmann *et al.* [85].

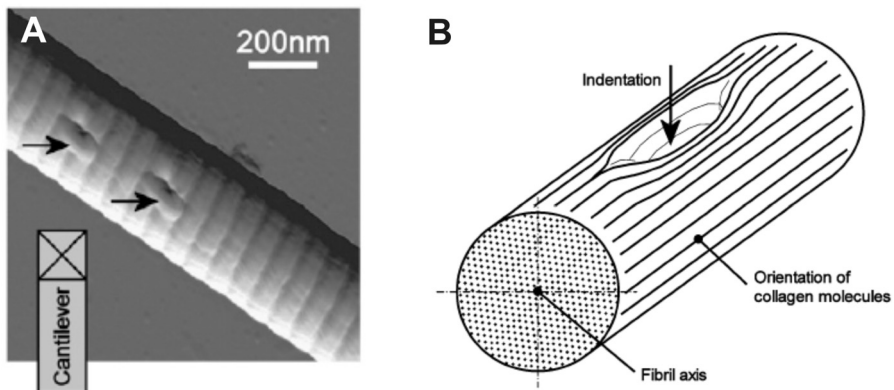


Figure 2.10 (A) Nonuniform shape of the imprints on a collagen fibril surface by high-load nano-indentation ($2 \mu\text{N}$). The imprint depth is $29 \pm 1 \text{ nm}$. (B) Schematic drawing of the nonuniform shaped imprints which imply an anisotropic fibril structure. The figure is reprinted from [78] with permission from Biophysical Society.

2.3.3 Mechanical properties of collagen molecules

A single collagen molecule is regarded as an elastic rod [86]. As shown in Fig. 2.6, using X-ray diffraction and simultaneous tensile testing of tissue samples, a linear stress-strain behavior was deduced for collagen molecules in the hydrated state. The deduced Young's modulus of collagen molecules ranged from 2.8 GPa to 3.0 GPa [87].

Recently, force spectroscopy measurements using AFM or optical tweezers were performed on collagen molecules [19,73,88,89]. Thompson *et al.* [88] pulled collagen molecules from insoluble collagen type I adsorbed on a glass substrate or directly from

polished bone. They reported that there are ‘sacrificial bonds’ in the collagen molecules that protect the collagen backbone and dissipate energy. The energy dissipation of the molecules was calculated from the hysteresis between the stretching and relaxation part of the force extension curves. They found that the longer the delay before the next pull, the more sacrificial bonds reform and thus the more energy dissipation is observed. The energy dissipation increased when calcium ions were present in the solution, which points to a possible role of these ions in the formation of sacrificial bonds in collagen molecules. Gutschmann *et al.* pulled subunits out of intact collagen fibers from rat tail tendon [73]. In the force extension curves, they found an exponential increase in force and two different periodic rupture events, one with strong binding with a periodicity of 78 nm and one with weak binding with a periodicity of 22 nm. They suggested that this pattern resulted from pulling an assembly of molecules out of the collagen fibrils. However, since the ECM surrounding was still present, the force-extension curves were complex and not reproducible, and no further conclusions were drawn from the study. Sun *et al.* [19] stretched a single collagen molecule using optical tweezers. The force-extension relationship was measured and analyzed by fitting the data with a worm-like chain model. The persistence length of the collagen molecules was determined to be 14.5 nm and the contour length was 309 nm. The elastic modulus derived from the persistence length of the molecule was estimated to be 0.35 - 12 GPa. The large deviation was caused by the difficulty in accurately measuring the diameter of the collagen molecule. A smaller contour length of collagen molecules (202 ± 5 nm) was found by Bozec *et al.* [89] using force spectroscopy measurements. This smaller contour length was explained by the fact that it was not possible to know where the AFM cantilever was adhered to the collagen molecule. In their study, no data on the mechanical properties of single collagen molecules were provided.

2.4 Mechanical Tests of Nano-sized Materials using AFM

2.4.1 Mechanical bending

An AFM-based three-point bending technique has been developed by different groups to measure the mechanical properties of nanometer scale beams and wires [90-97]. The nanometer scale beams or wires are first deposited on a substrate containing channels. As shown in Fig. 2.11, an AFM cantilever is used to bend the sample at the middle point of the channel. The force applied is related to the deflection of the cantilever which is detected by the laser system of the AFM. The displacement of the sample is calculated from the piezo movement in the z direction subtracting the deflection of the cantilever.

The gradient (dF/dz) of the force-displacement curve is fitted to a model describing bending of a rod to calculate the Young's modulus of the sample.



Figure 2.11 Schematic drawing of three-point bending tests using AFM.

The principle of this technique has also been applied in determining the mechanical properties of materials with a fibrillar structure of 20 - 200 nm in diameter [11-13,76]. In principle, the bending modulus (E_{bending}) related to the bending stiffness ($E_{\text{bending}}I$) representing the resistance of the material upon bending is determined from the bending tests. For isotropic materials, the bending modulus is equal to the Young's modulus. For anisotropic materials, the bending modulus can be different from the Young's modulus [12,96]. Kis *et al.* [12] further investigated the anisotropic properties of microtubules by determining the shear modulus. The shear modulus was deduced by bending the microtubules with different length to diameter ratios and fitting the data to the unit-load equation. The determined shear modulus of microtubules is two orders of magnitude lower than the Young's modulus, which confirms the mechanical anisotropy of the materials. Adapting the same approach, mechanical anisotropy in single vimentin intermediate filaments (IFs) was determined [13].

2.4.2 Nano-indentation

In nano-indentation measurements an AFM tip is pushed into a sample surface. From nano-indentation tests, the elasticity of a material can be determined from the force applied to the tip-sample system and the resulting deformation of the material [14]. Typical force-indentation curves obtained from indentation tests on hard and soft substrates are shown in Fig. 2.12. The elasticity (Young's modulus) of the material is deduced by fitting the force-indentation curve to the model described by Sneddon [98].

Nano-indentation tests have been applied to study for example cell elasticity [83,99-101]. The elasticity of living cells was first quantified by Weisenhorn *et al.* [83] to be in the range of 0.013 - 0.15 MPa. The elasticity of layers of proteins can also be explored by this method [81,82,102].

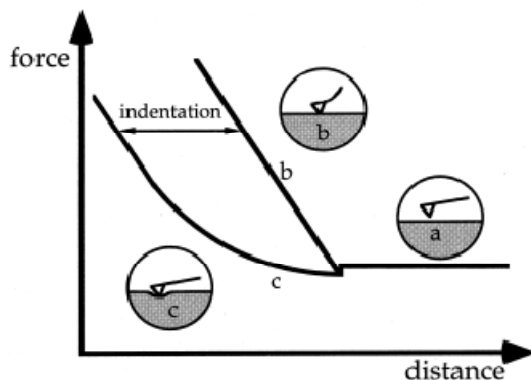


Figure 2.12 Typical approaching part of force versus distance curve on a hard (b) and a soft material (c). The picture (a) shows the situation of no contact between the tip and the sample. On a hard sample, there is practically no indentation of the sample when the AFM tip is pushed onto the surface. Deformation is observed when the AFM is pushed onto the soft sample. The figure is reprinted from [14] with permission from Elsevier.

2.4.3 Single molecule force spectroscopy

For most force spectroscopy measurements using AFM, layers of proteins or other biomolecules are deposited on a substrate. When an AFM tip is withdrawn from a substrate onto which biomolecules are adsorbed, there is a chance that one or more molecules attach between the tip and the substrate. Increasing the distance between the tip and the substrate will induce extension of the molecules generating a force that will bend the AFM cantilever. The AFM system records the deflection of the cantilever which relates the force applied to the extension of the protein [16,17]. Analysis of the force extension curve provides detailed mechanical behavior of the proteins at a single molecular level [103,104].

Single molecule force spectroscopy can for example be used to study entropic elasticity of a protein or the forces associated with the unfolding of sub-domains in the protein [105-107]. The entropic elasticity of biological polymers is described by the worm-like chain (WLC) model. The biological polymer is described as a polymer string of a given length. The persistence length which reflects the flexibility of the molecule and the contour length can be determined from fitting with the WLC model. Protein unfolding is in some cases also observed in the force-extension curves when stretching the protein with a higher force (Fig. 2.13) [108,109]. The force-extension curve displays a characteristic saw-tooth pattern with the number of peaks corresponding to the number of domains unraveled [16].

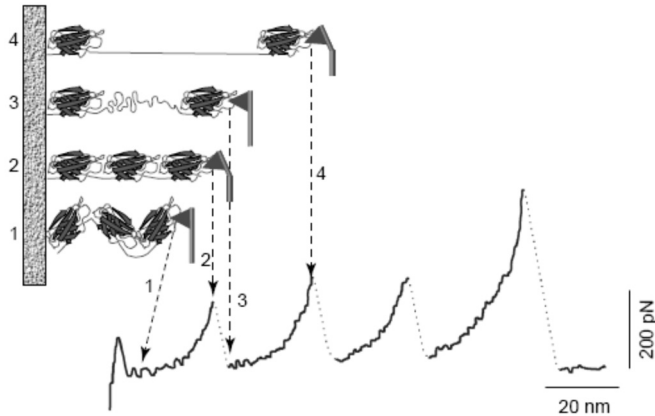


Figure 2.13 Typical force-extension curves of stretching a protein with folded domains using AFM. When the distance between substrate and tip increases (1 to 2), entropic elasticity of the protein can be determined by fitting the curve with the WLC model. Increasing the force (2 to 3), unfolding of folded sub-domains within the protein occurs, which can be seen as a drop of force and an increased contour length of the protein. This process repeats until all sub-domains are unfolded. The length of a folded domain can be determined from the distance between two successive peaks in the force extension curve. The figure is reprinted from [16] with permission from Elsevier.

2.5 Conclusions

Collagen fibrils appear to be an important structural unit in many tissues. Models describing the aggregation of collagen molecules into a microfibril, an intermediate structure in fibrils, are preferred based on recent studies. Collagen based tissues exhibit viscoelastic properties with a complex stress-strain behavior. There are some hypotheses on the mechanism of the viscoelastic behavior of collagen based tissues, which are mainly based on the simultaneous loading and X-ray monitoring of tissue samples. Micro-mechanical tests of single collagen fibrils will be helpful to further understand the overall mechanical properties of tissues.

Efforts have been made to perform micro-mechanical tests on single collagen fibrils. However, up to now the tests are limited to tensile tests in the low strain range of collagen fibrils (< 4%). The overall picture of the stress-strain behavior of single collagen fibrils until the point of breaking is still not possible. Furthermore, the mechanical tests are focused on the Young's modulus of the fibrils. The shear related properties of the fibril which are important to reveal (an)isotropic properties are not determined.

AFM has proven to be a powerful technique in measuring the mechanics of materials on a micrometer and nanometer scale. The force spectroscopy, mechanical bending and

nano-indentation studies show various possibilities to determine the mechanical properties of the materials. It seems promising to further develop AFM-based mechanical testing techniques that provide insight in the relation between the structure and the mechanical properties of collagen and other proteins.

References

1. Silver FH, Freeman JW, Seehra GP. Collagen self-assembly and the development of tendon mechanical properties. *J. Biomech.* **2003**; 36: 1529-1553.
2. Ottani V, Martini D, Franchi M, Ruggeri A, Raspanti M. Hierarchical structures in fibrillar collagens. *Micron* **2002**; 33: 587-596.
3. Puxkandl R, Zizak I, Paris O, Keckes J, Tesch W, Bernstorff S, Purslow P, Fratzl P. Viscoelastic properties of collagen: synchrotron radiation investigations and structural model. *Phil. Trans. R. Soc. Lond. B* **2002**; 357:191-197.
4. Hulmes DJS. Building collagen molecules, fibrils, and suprafibrillar structures. *J. Struct. Biol.* **2002**; 137: 2-10.
5. Mosler E, Folkhard W, Knorz E, Nemetschek-Gansler H, Nemetschek T, Koch MHJ. Stress-induced molecular rearrangement in tendon collagen. *J. Mol. Biol.* **1985**; 182: 589-596.
6. Sasaki N, Odajima S. Elongation mechanism of collagen fibrils and force-strain relations of tendon at each level of structural hierarchy. *J. Biomech.* **1996**; 29: 1131-1136.
7. Wang JHC. Mechanobiology of tendon. *J. Biomech.* **2006**; 39: 1563-1582.
8. Dowling BA, Dart AJ. Mechanical and functional properties of the equine superficial digital flexor tendon. *Vet. J.* **2005**; 170: 184-192.
9. Magnusson SP, Hansen P, Kjaer M. Tendon properties in relation to muscular activity and physical training. *Scand. J. Med. Sci. Sports* **2003**; 13: 211-223.
10. Silver FH, Christiansen D, Snowhill PB, Chen Y, Landis WJ. The role of mineral in the storage of elastic energy in turkey tendons. *Biomacromolecules* **2000**; 1: 180-185.
11. Smith JF, Knowles TPJ, Dobson CM, Macphee CE, Welland ME. Characterization of the nanoscale properties of individual amyloid fibrils. *Proc. Natl. Acad. Sci. USA* **2006**; 103: 15806-15811.
12. Kis A, Kasas S, Babić B, Kulik AJ, Benoît W, Briggs GAD, Schönenberger C, Catsicas S, Forró L. Nanomechanics of microtubules. *Phys. Rev. Lett.* **2002**; 89: 248101-1-4.
13. Guzmán C, Jeney S, Kreplak L, Kasas S, Kulik AJ, Aebi U, Forró L. Exploring the mechanical properties of single vimentin intermediate filaments by atomic force microscopy. *J. Mol. Biol.* **2006**; 360: 623-630.

14. Vinckier A, Semenza G. Measuring elasticity of biological materials by atomic force microscopy. *FEBS Lett.* **1998**; 430: 12-16.
15. Oliver WC, Pharr GM. Measurement of hardness and elastic modulus by instrumented indentation: Advances in understanding and refinement to methodology. *J. Mater. Res.* **2004**; 19: 3-20.
16. Fisher TE, Oberhauser AF, Carrion-Vazquez M, Marszalek PE, Fernandez JM. The study of protein mechanics with the atomic force microscope. *Trends Biochem. Sci.* **1999**; 24: 379-384.
17. Carrion-Vazquez M, Oberhauser AF, Fisher TE, Marszalek PE, Li HB, Fernandez JM. Mechanical design of proteins studied by single-molecule force spectroscopy and protein engineering. *Prog. Biophys. Mol. Bio.* **2000**; 74: 63-91.
18. Kadler K. Extracellular matrix. 1: fibril-forming collagens. *Protein Profile* **1994**; 1: 519-638.
19. Sun YL, Luo ZP, Fertala A, An KN. Direct quantification of the flexibility of type I collagen monomer. *Biochem. Biophys. Res. Co.* **2002**; 295: 382-386.
20. Lee CH, Singla A, Lee Y. Biomedical applications of collagen. *Int. J. Pharm.* **2001**; 221: 1-22.
21. Persikov AV, Ramshaw JAM, Kirkpatrick A, Brodsky B. Amino acid propensities for the collagen triple-helix. *Biochemistry* **2000**; 39: 14960-14967.
22. Huang L, Nagapudi K, Apkarian RP, Chaikof EL. Engineered collagen-PEO nanofibers and fabrics. *J. Biomater. Sci. Polymer Edn.* **2001**; 12: 979-993.
23. Holmgren SK, Bretscher LE, Taylor KM, Raines RT. A hyperstable collagen mimic. *Chem. Biol.* **1999**; 6: 63-70.
24. Traub W. Some stereochemical implications of the molecular conformation of collagen. *Israel J. Chem.* **1974**; 12: 435-439.
25. Fraser RDB, Macrae TT, Suzuki E. Chain conformation in the collagen molecule. *J. Mol. Biol.* **1979**; 129: 463-481.
26. Bella J, Eaton M, Brodsky B, Berman HM. Crystal structure and molecular structure of a collagen-like peptide at 1.9 angstrom resolution. *Science* **1994**; 266: 75-81.
27. Bella J, Brodsky B, Berman HM. Hydration structure of a collagen peptide. *Structure* **1995**; 3: 893-906.
28. Holmgren SK, Taylor KM, Bretscher LE, Raines RT. Code for collagen's stability deciphered. *Nature* **1998**; 392: 666-667.
29. Kramer RZ, Vitagliano L, Bella J, Berisio R, Mazzarella L, Brodsky B, Zagari A, Berman HM. X-ray crystallographic determination of a collagen-like peptide with a repeating sequence (Pro-Pro-Gly). *J. Mol. Biol.* **1998**; 280: 623-638.
30. Kramer RZ, Bella J, Mayville P, Brodsky B, Berman HM. Sequence dependent conformational variations of collagen triple-helical structure. *Nat. Struct. Biol.* **1999**; 6: 454-457.
31. Miles CA, Bailey AJ. Thermally labile domains in the collagen molecule. *Micron* **2001**; 32: 325-332.

32. Rosenblo J, Harsch M, Jimenez S. Hydroxyproline content determines the denaturation tmeperature of chick tendon collagen. *Arch. Biochem. Biophys.* **1973**; 158: 478-484.
33. Kramer RZ, Venugopal MG, Bella J, Mayville P, Brodsky B, Berman HM. Staggered molecular packing in crystals of a collagen-like peptide with a single charged pair. *J. Mol. Biol.* **2000**; 301: 1191-1205.
34. Hulmes DJS, Wess TJ, Prockop DJ, Fratzl P. Radial packing, order, and disorder in collagen fibrils. *Biophys. J.* **1995**; 68: 1661-1670.
35. Hodge AJ, Petruska JA. Recent studies with the electron microscope on ordered aggregates of the tropocollagen macromolecules. In *Aspects of protein structure. Academic Press, New York, 1963.*
36. Wess TJ, Hammersley AP, Wess L, Miller A. A consensus model for molecular packing of type I collagen. *J. Struct. Biol.* **1998**; 122: 92-100.
37. Smith JW. Molecular pattern in native collagen. *Nature* **1968**; 219: 157-158.
38. Piez KA, Trus BL. A new model for packing of type-I collagen molecules in the native fibril. *Bioscience Rep.* **1981**; 1: 801-810.
39. Wess TJ, Hammersley AP, Wess L, Miller A. Molecular packing of type I collagen in tendon. *J. Mol. Biol.* **1998**; 275: 255-267.
40. Hulmes DJS, Miller A. Quasi-hexagonal molecular packing in collagen fibrils. *Nature* **1979**; 282: 878-880.
41. Silver D, Miller J, Harrison R, Prockop DJ. Helical model of nucleation and propagation to account for the growth of type I collagen fibrils from the symmetrical pointed tips: a special example of self assembly of rod like monomers. *Proc. Natl. Acad. Sci. USA* **1992**; 89: 9860-9864.
42. Baselt DR, Revel JP, Baldschwieler JD. Subfibrillar structure of type I collagen observed by atomic force microscopy. *Biophys. J.* **1993**; 65: 2644-2655.
43. Raspanti M, Congiu T, Guizzardi S. Tapping-mode atomic force microscopy in fluid of hydrated extracellular matrix. *Matrix Biol.* **2001**; 20: 601-604.
44. Habelitz S, Balooch M, Marshall SJ, Balooch G, Marshall GW. In situ force microscopy of partially demineralized human dentin collagen fibrils. *J. Struct. Biol.* **2002**; 138: 227-236.
45. Holmes DF, Gilpin CJ, Baldock C, Ziese U, Koster AJ, Kadler KE. Corneal collagen fibril structure in three dimensions: structural insights into fibril assembly, mechanical properties, and tissue organization. *Proc. Natl. Acad. Sci. USA* **2001**; 98: 7307-7312.
46. Orgel JPRO, Irving TC, Miller A, Wess TJ. Microfibrillar structure of type I collagen in situ. *Proc. Natl. Acad. Sci. USA* **2006**; 103: 9001-9005.
47. Vidal BD. Image analysis of tendon helical superstructure using interference and polarized light microscopy. *Micron* **2003**; 34: 423-432.
48. Yamamoto E, Hayashi K, Yamamoto N. Mechanical properties of collagen fascicles from stress-shielded patellar tendons in the rabbit. *Clin. Biomech.* **1999**; 14: 418-425.

49. Fratzl P, Misof K, Zizak I, Rapp G, Amenitsch H, Bernstorff S. Fibrillar structure and mechanical properties of collagen. *J. Struct. Biol.* **1998**; 122: 119-122.
50. Diamant J, Arridge RGC, Baer E, Litt M, Keller A. Collagen: Ultrastructure and its relation to mechanical properties as a function of aging. *Proc. R. Soc. Lon. B.* **1972**; 180: 293-315.
51. Cribb AM, Scott JE. Tendon response to tensile stress: an ultrastructural investigation of collagen: proteoglycan interactions in stressed tendons. *J. Anat.* **1995**; 187: 423-428.
52. Misof K, Rapp G, Fratzl P. A new molecular model for collagen elasticity based on synchrotron X-ray scattering evidence. *Biophys. J.* **1997**; 72: 1376-1381.
53. Folkhard W, Mosler E, Geercken W, Knorz E, Nemetschek-Gansler H, Nemetschek T, Koch MHJ. Quantitative analysis of the molecular sliding mechanism in native tendon collagen-time-resolved dynamic studies using synchrotron radiation. *Int. J. Biol. Macromol.* **1987**; 9: 169-175.
54. Folkhard W, Geercken W, Knorz E, Mosler E, Nemetschek-Gansler H, Nemetschek T, Koch MHJ. Structural dynamic of native tendon collagen. *J. Mol. Biol.* **1987**; 193: 405-407.
55. An KN, Sun YL, Luo ZP. Flexibility of type I collagen and mechanical properties of connective tissue. *Biorheology* **2004**; 41: 239-246.
56. Takaku K, Ogawa T, Kuriyama T, Narisawa I. Fracture behavior and morphology of spun collagen fibers. *J Appl. Polym. Sci.* **1996**; 59: 887-896.
57. Pins GD, Silver FH. A self-assembled collagen scaffold suitable for use in soft and hard tissue replacement. *Mater. Sci. Eng. C-Biomim. Mater. Sensors. Syst.* **1995**; 3: 101-107.
58. Kato YP, Christiansen DL, Hahn RA, Shieh SJ, Goldstein JD, Silver FH. Mechanical properties of collagen fibers: a comparison of reconstituted and rat tail tendon fibers. *Biomaterials* **1989**; 10: 38-41.
59. Purslow PP, Wess TJ, Hukins DWL. Collagen orientation and molecular spacing during creep and stress-relaxation in soft connective tissues. *J. Exp. Biol.* **1998**; 201: 135-142.
60. Pradas MM, Calleja RD. Nonlinear viscoelastic behavior of the flexor tendon of the human hand. *J. Biomech.* **1990**; 23: 773-781.
61. Haut TL, Haut RC. The state of tissue hydration determines the strain-rate sensitive stiffness of human patellar tendon. *J. Biomech.* **1997**; 30: 79-81.
62. Robinson PS, Lin TW, Reynolds PR, Derwin KA, Iozzo RV, Soslowsky LJ. Strain-rate sensitive mechanical properties of tendon fascicles from mice with genetically engineered alterations in collagen and decorin. *J. Biomech. Eng-T ASME* **2004**; 126: 252-257.
63. Wu JJ. Quantitative constitutive behavior and viscoelastic properties of fresh flexor tendons. *Int. J. Artif. Organs* **2006**; 29: 852-857.

64. Lynch HA, Johannessen W, Wu JP, Jawa A, Elliott DM. Effect of fiber orientation and strain rate on the nonlinear uniaxial tensile material properties of tendon. *J. Biomech. Eng-T ASME* **2003**; 125: 726-731.
65. Wu JZ, Cutlip RG, Welcome D, Dong RG. Estimation of the viscous properties of skin and subcutaneous tissue in uniaxial stress relaxation tests. *Bio-Med. Mater. Eng.* **2006**; 16: 53-66.
66. Usha R, Subramanian V, Ramasami T. Role of secondary structure on the stress relaxation processes in rat tail tendon (RTT) collagen fibre. *Macromol. Biosci.* **2001**; 1: 100-107.
67. Silver FH, Christiansen DL, Snowhill PB, Chen Y. Transition from viscous to elastic-based dependency of mechanical properties of self-assembled type I collagen fibers. *J. Appl. Polym. Sci.* **2001**; 79: 134-142.
68. Screen HRC, Lee DA, Bader DL, Shelton JC. An investigation into the effects of the hierarchical structure of tendon fascicles on micromechanical properties. *Proc. Instn. Mech. Engrs H: Engineering in Medicine* **2004**; 218: 109-119.
69. Provenzano PP, Vanderby R. Collagen fibril morphology and organization: Implications for force transmission in ligament and tendon. *Matrix Biol.* **2006**; 25: 71-84.
70. Lam TC, Frank CB, Shrive NG. Changes in the cyclic and static relaxations of the rabbit medial collateral ligament complex during maturation. *J. Biomech.* **1993**; 26: 9-17.
71. Yamamoto E, Hayashi K, Yamamoto N. Mechanical properties of collagen fascicles from the rabbit patellar tendon. *J. Biomech. Eng-T ASME* **1999**; 121: 124-131.
72. Wineman AS, Rajagopal KR. *In Mechanical response of polymers: an introduction. Cambridge University Press, New York, 2000.*
73. Gutsman T, Fantner GE, Kindt JH, Venturoni M, Danielsen S, Hansma PK. Force spectroscopy of collagen fibers to investigate their mechanical properties and structural organization. *Biophys. J.* **2004**; 86: 3186-3193.
74. Wang XN, Li XD, Yost MJ. Microtensile testing of collagen fibril for cardiovascular tissue engineering. *J. Biomed. Mater. Res.A* **2005**; 74: 263-268.
75. van der Rijt JAJ, van der Werf KO, Bennink ML, Dijkstra PJ, Feijen J. Micromechanical testing of individual collagen fibrils. *Macromol. Biosci.* **2006**; 6: 697-702.
76. Yang L, van der Werf KO, Koopman BFJM, Subramaniam V, Bennink ML, Dijkstra PJ, Feijen J. Micromechanical bending of single collagen fibrils using atomic force microscopy. *J. Biomed. Mater. Res.A* **2007**; 82: 160-168. (Chapter 3 of this thesis)
77. Graham JS, Vomund AN, Phillips CL, Grandbois M. Structural changes in human type I collagen fibrils investigated by force spectroscopy. *Exp. Cell Res.* **2004**; 299: 335-342.
78. Wenger MPE, Bozec L, Horton MA, Mesquida P. Mechanical properties of collagen fibrils. *Biophys. J.* **2007**; 93: 1255-1263.

79. Strasser S, Zink A, Janko M, Heckl WM, Thalhammer S. Structural investigations on native collagen type I fibrils using AFM. *Biochem. Biophys. Res. Co.* **2007**; 354: 27-32.
80. Eppell SJ, Smith BN, Kahn H, Ballarini R. Nano measurements with micro-devices: mechanical properties of hydrated collagen fibrils. *J. R. Soc. Interface* **2006**; 3: 117-121.
81. Losic D, Short K, Mitchell JG, Lal R, Voelcker NH. AFM nanoindentations of diatom biosilica surfaces. *Langmuir* **2007**; 23: 5014-5021.
82. Radmacher M, Fritz M, Cleveland JP, Walters DA, Hansma PK. Imaging adhesion forces and elasticity of lysozyme adsorbed on mica with the atomic force microscope. *Langmuir* **1994**; 10: 3809-3814.
83. Weisenhorn AL, Khorsandi M, Kasas S, Gotzos V, Butt HJ. Deformation and height anomaly of soft surfaces studied with an AFM. *Nanotechnology* **1993**; 4: 106-113.
84. Crick SL, Yin FCP. Assessing micromechanical properties of cells with atomic force microscopy: importance of the contact point. *Biomechan. Model Mechanobiol.* **2007**; 6: 199-210.
85. Gutsman T, Fantner GE, Venturoni M, Ekani-Nkodo A, Thompson JB, Kindt JH, Morse DE, Fygenon DK, Hansma PK. Evidence that collagen fibrils in tendon are inhomogeneously structured in tubelike manner. *Biophys. J.* **2003**; 84: 2593-2598.
86. Engel J. Biochemistry: Versatile collagens in invertebrates. *Science* **1997**; 277: 1785-1786.
87. Sasaki N, Odajima S. Stress-strain curve and Young's modulus of a collagen molecule as determined by the X-ray diffraction technique. *J. Biomech.* **1996**; 29: 655-658.
88. Thompson JB, Kindt JH, Drake B, Hansma HG, Morse DE, Hansma PK. Bone indentation recovery time correlates with bond reforming time. *Nature* **2001**; 414: 773-776.
89. Bozec L, Horton M. Topography and mechanical properties of single molecules of type I collagen using atomic force microscopy. *Biophys. J.* **2005**; 88: 4223-4231.
90. Namazu T, Isono Y, Tanaka T. Evaluation of size effect on mechanical properties of single crystal silicon by nanoscale bending test using AFM. *J. Microelectromech. Syst.* **2000**; 9: 450-459.
91. Ni H, Li XO. Young's modulus of ZnO nanobelts measured using atomic force microscopy and nanoindentation techniques. *Nanotechnology* **2006**; 17: 3591-3597.
92. Xiong QH, Duarte N, Tadigadapa S, Eklund PC. Force-deflection spectroscopy: a new method to determine the Young's modulus of nanofilaments. *Nano. Lett.* **2006**; 6: 1904-1909.
93. Jeng YR, Tsai PC, Fang TH. Molecular-dynamics studies of bending mechanical properties of empty and C60-filled carbon nanotubes under nanoindentation. *J. Chem. Phys.* **2005**; 122: 224713-1-8.

94. Ni H, Li XD, Gao HS. Elastic modulus of amorphous SiO₂ nanowires. *Appl. Phys. Lett.* **2006**; 88: 043108-1-3.
95. Lee SH, Tekmen C, Sigmund WM. Three-point bending of electrospun TiO₂ nanofibers. *Mat. Sci. Eng. A-Struct.* **2005**; 398: 77-81.
96. Salvetat JP, Briggs GAD, Bonard JM, Bacsá RR, Kulik AJ, Stöckli T, Burnham NA, Forró L. Elastic and shear moduli of single-walled carbon nanotube ropes. *Phys. Rev. Lett.* **1999**; 82: 944-947.
97. Niu LJ, Chen XY, Allen S, Tandler SJB. Using the bending model to estimate the elasticity of diphenylalanine nanotubes. *Langmuir* **2007**; 23: 7443-7446.
98. Sneddon IN. The relation between load and penetration in the axisymmetric boussinesq problem for a punch of arbitrary profile. *Int. J. Engng. Sci.* **1965**; 3: 47-57.
99. Radmacher M, Fritz M, Kacher CM, Cleveland JP, Hansma PK. Measuring the viscoelastic properties of human platelets with the atomic force microscope. *Biophys. J.* **1996**; 70: 556-567.
100. Shroff SG, Saner DR, Lal R. Dynamic micromechanical properties of cultured rat atrial myocytes measured by atomic-force microscopy. *Am. J. Physiol.-Cell Ph.* **1995**; 269: C286-292.
101. Goldmann WH, Ezzell RM. Viscoelasticity in wild-type and vinculin-deficient (5.51) mouse F9 embryonic carcinoma cells examined by atomic force microscopy and rheology. *Exp. Cell Res.* **1996**; 226: 234-237.
102. Vinckier A, Dumortier C, Engelborghs Y, Hellemans L. Dynamical and mechanical study of immobilized microtubules with atomic force microscopy. *J. Vac. Sci. Technol. B* **1996**; 14: 1427-1431.
103. Chothia C, Jones EY. The molecular structure of cell adhesion molecules. *Annu. Rev. Biochem.* **1997**; 66: 823-862.
104. Chicurel ME, Chen CS, Ingber DE. Cellular control lies in the balance of forces. *Curr. Opin. Cell Biol.* **1998**; 10: 232-239.
105. Zhang W, Zhang X. Single molecule mechanochemistry of macromolecules. *Prog. Polym. Sci.* **2003**; 28: 1271-1295.
106. Hugel T, Seitz M. The study of molecular interactions by AFM force spectroscopy. *Macromol. Rapid Comm.* **2001**; 22: 989-1016.
107. Janshoff A, Neitzert M, Oberdorfer Y, Fuchs H. Force spectroscopy of molecular system - single molecule spectroscopy of polymers and biomolecules. *Angew. Chem. Int. Edit.* **2000**; 39: 3213-3237.
108. Oberhauser AF, Marszalek PE, Carrion-Vazquez M, Fernandez JM. Single protein misfolding events captured by atomic force microscopy. *Nat. Struct. Biol.* **1999**; 6: 1025-1028.
109. Rief M, Gautel M, Oesterhelt F, Fernandez JM, Gaub HE. Reversible unfolding of individual titin immunoglobulin domains by AFM. *Science* **1997**; 276: 1109-1112.

Micromechanical Bending of Single Collagen Fibrils using AFM*

Lanti Yang¹, Kees O. van der Werf², Bart F. J. M. Koopman³, Vinod Subramaniam², Martin L. Bennink², Pieter J. Dijkstra¹, Jan Feijen¹

¹ *Polymer Chemistry and Biomaterials, Faculty of Science & Technology and Institute for Biomedical Technology (BMTI), University of Twente, P.O. Box 217, 7500 AE, Enschede, The Netherlands*

² *Biophysical Engineering, Faculty of Science & Technology and MESA+ Institute for Nanotechnology, University of Twente, P.O. Box 217, 7500 AE, Enschede, The Netherlands*

³ *Biomechanical Engineering, Faculty of Engineering Technology, University of Twente, P. O. Box 217, 7500 AE, Enschede, The Netherlands*

Abstract

A new micromechanical technique was developed to study the mechanical properties of single collagen fibrils. Single collagen fibrils, the basic components of the collagen fiber, have a characteristic highly organized structure. Fibrils were isolated from collagenous materials and their mechanical properties were studied with atomic force microscopy (AFM). In this study, we determined the Young's modulus of single collagen fibrils at ambient conditions from bending tests after depositing the fibrils on a poly(dimethyl siloxane) (PDMS) substrate containing micro-channels. Force-displacement relationships of freely suspended collagen fibrils were determined by loading them with a tip-less cantilever. From the deflection-piezo displacement curve, force-displacement curves could be deduced. With the assumption that the behavior of collagen fibrils follows the model describing the bending of isotropic materials and that the fibrils were freely supported at the rims, a Young's modulus of 5.4 ± 1.2 GPa was determined. After cross-linking with glutaraldehyde, the Young's modulus of a single fibril increased to 14.7 ± 2.7 GPa. When it

* This chapter has been published in *J. Biomed. Mater. Res. A* **2007**; 82: 160-168.

was assumed that the fibril was fixed at the rims of the channel the Young's moduli of native and cross-linked collagen fibrils were calculated to be 1.4 ± 0.3 GPa and 3.8 ± 0.8 GPa, respectively. The minimum and maximum values determined for native and glutaraldehyde cross-linked collagen fibrils represent the boundaries of the Young's modulus.

3.1 Introduction

Collagen is the principal, tensile stress-bearing component of connective tissue. Over the past decade, several studies have been directed toward the elucidation of the substructures present in collagen in order to relate the structure to its function and mechanical properties [1-5]. In summary, the hierarchical structure can be described as follows: 5 tropocollagen molecules (collagen triple helices from which the propeptides are enzymatically removed) assemble into microfibrils. These microfibrils aggregate in the lateral and longitudinal direction to form fibrils [6-9]. The collagen fibrils have a diameter between 10 - 500 nm and further assemble into fibers. It must be noted that microfibrils have never been isolated but researchers nowadays agree on this microfibrillar structure based mainly on X-ray data [10], three-dimensional imaging using automated electron tomography [11] and AFM imaging [12,13].

The macro-mechanical properties of collagenous materials were studied extensively in the past decades. Due to the hierarchical structure of collagen material, the contribution of the different substructures to the mechanical behavior appears complicated. With macro-tensile testing, the data presented in the literature on the modulus of elasticity (Young's modulus) of dry collagen tissue and collagen fibers range from 1 to 8 GPa [14-17]. Based on X-ray diffraction studies, Puxkandl *et al.* reported that the overall strain of the tendon was always larger than the strain in the individual fibrils [18]. In addition, Sasaki and co-researchers [19,20] reported different values of Young's modulus by testing collagen molecules, fibrils and tendons. It was found that intermolecular cross-links have a great influence on the mechanical behavior of collagen.

Recently, some studies on the micro-mechanical properties of collagen fibrils and molecules using micromanipulation techniques such as AFM and optical tweezers have been reported [21-25]. Thompson *et al.* used an AFM to perform pulling experiments on collagen molecules exposed on the surface of a polished bone. They reported that there are 'sacrificial bonds' within and between collagen molecules. The force versus extension curves show that these sacrificial bonds can be broken, and prevent the force increasing to a

value that may break the collagen backbone. The time needed for these sacrificial bonds to reform after pulling correlates with the time needed for bone to recover its toughness [21]. Later in 2003, Gutschmann in the same group [23] investigated the correlation between periodic patterns in the topography of tendon collagen fibrils and the force-extension curves observed in the force spectroscopy measurements on the sub-units of collagen fibers. They found two different periodic rupture events with a periodicity of 78 nm and 22 nm. The periodic rupture found by force spectroscopy was consistent with their previous results on the 65 nm D-period and small 23 nm spacing of collagen fibrils [26]. Very recently, Graham *et al.* [24] measured the force-elongation profiles of single collagen fibrils to investigate the structural changes in single fibrils during elongation. They concluded that the major reorganization of the collagen fibril structure occurs in the 1.5 to 4.5 nN range. Sun *et al.* [27] studied the flexibility of individual type I procollagen by stretching the procollagen using optical tweezers. The persistence length, which relates to the flexibility of the collagen molecule, was determined to be 14.5 nm and the contour length to be 309 nm. Comparable results were obtained by Bozec *et al.* with an AFM imaging and force spectroscopy study on single collagen molecules. They found that the contour length of single collagen molecules is 287 ± 35 nm [25].

Besides the tensile tests as described above, bending tests form another method to determine the mechanical properties of a specimen [28,29]. In this paper we describe for the first time the use of an atomic force microscope (AFM) for bending measurements of collagen fibrils that freely span the micro-channels in a polymeric substrate. The force needed to bend a suspended fibril at the center point was determined and fitted to elasticity models to deduce the Young's modulus of a collagen fibril. Similar experiments were performed on collagen fibrils cross-linked with glutaraldehyde, a commonly used cross-linking agent to increase the stability of collagen-based biomaterials [30,31]. The results are discussed in relation to the collagen mechanical properties and its hierarchical structure.

3.2 Materials and Methods

3.2.1 Preparation of PDMS substrates

Poly(dimethyl siloxane) (PDMS) molds were prepared using Sylgard 184 silicone elastomer (Dow Corning, Wiesbaden, Germany). The prepolymer was mixed with the curing agent in a 10:1 weight ratio as specified by the manufacturer. After 10 min stirring and 40 min degassing in a vacuum oven the mixture was poured onto a pre-patterned silicon wafer with parallel channels and cured at 70°C overnight. The width and depth of the

channels on the pre-patterned silicon wafer were approximately 5 μm and 1 μm , respectively. After curing, the PDMS layer was peeled off the silicon wafer. The width and depth of the channels in the PDMS were determined by AFM measurements.

3.2.2 Deposition of collagen fibrils

Bovine Achilles tendon collagen type I from Sigma-Aldrich (Steinheim, Germany) was swollen in hydrochloric acid (0.01 M) overnight at 0°C. The resulting slurry was shredded for 10 min at 9500 rpm using a Braun MR 500 HC blender (Braun, Kronberg, Germany). The temperature was kept below 5°C. The resulting mixture was filtered using a 74 μm filter (Bellco Glass Inc., collector screen 200 mesh, Vineland, NJ, USA). The helical content of the collagen suspension after filtration was determined by FTIR (Biorad, FTS-60) according to a method described by Friess *et al.* [32] To 1 ml of the filtrate, mainly containing collagen fibrils, 150 ml of PBS (pH = 7.4) was added. Deposition of the collagen fibrils on the PDMS substrates was done by incubating the substrates for 10 min in the diluted fibril dispersion. Subsequently, the collagen deposited PDMS substrates were washed with PBS for 10 min and three times for 10 min each with demineralized water and finally dried under ambient conditions for at least 24 h. Cross-linked collagen fibrils were prepared by mixing 1 ml of the non-diluted fibrillar dispersion with 5 ml of a 10 wt % glutaraldehyde solution and 195 ml phosphate buffer (pH = 7.4) for 2 h. The resulting cross-linked fibrils were deposited on the PDMS substrates as described above.

Single collagen fibrils deposited on the PDMS surface were imaged by tapping mode AFM (home-built instrument) and SEM (LEO Gemini 1550 FEG-SEM, Oberkochen, Germany). The characteristic D-period of the fibril was characterized by TEM (Philips CM30 Twin/STEM, Eindhoven, the Netherlands).

3.2.3 Denaturation temperature and free amino group content

The diluted fibril dispersion was centrifuged for 15 min at 4500 rpm (Hettich Mikco Rapid/k, Depex, De Bilt, the Netherlands). The solution was removed and the collagen was washed with MilliQ water twice for 30 min each. Similarly, the diluted cross-linked collagen fibril dispersion was centrifuged as described above and then washed twice with 4M NaCl for 30 min each and four times with MilliQ water for 30 min each. After the washing steps, both native and cross-linked collagen samples were frozen in liquid nitrogen and subsequently freeze-dried for 24 h.

The degree of cross-linking of the collagen fibrils is related to the increase of the

denaturation (shrinkage) temperature (T_d) after cross-linking. The T_d values were determined by means of DSC (DSC 7, Perkin Elmer, Norwalk, CT, USA). Freeze-dried native and cross-linked collagen fibril samples of 3-5 mg were swollen in 50 μ l of PBS (pH = 7.4) in high-pressure pans overnight. Samples were heated from 20°C to 90°C at a heating rate of 5 °C/min. A sample containing 50 μ l of PBS (pH = 7.4) was used as a reference. The onset of the endothermic peak was recorded as the T_d .

The free amino group content of native and cross-linked samples was determined using the 2,4,6-trinitrobenzenesulfonic acid (TNBS) assay. Collagen fibril samples of 3-5 mg were incubated for 30 min in 1 ml of a 4 wt % solution of NaHCO_3 . To this mixture 1 ml of a freshly prepared solution of TNBS (0.5 wt %) in 4 wt % NaHCO_3 was added. The resulting mixture was left for 2 h at 40°C. After the addition of HCl (3 ml, 6 M), the temperature was raised to 60°C. Solubilization of collagen was achieved within 90 min. The resulting solution was diluted with 5.0 ml MilliQ water and cooled to room temperature. The absorbance at 420 nm was measured using a Varian Cary 300 Bio spectrophotometer (Varian Inc., Middelburg, the Netherlands). A blank was prepared applying the same procedure, except that HCl was added before the addition of TNBS. The absorbance was correlated to the concentration of free amino groups using a calibration curve obtained with glycine. The free amino group content was expressed as the number of free amino groups per 1000 amino acids (n/1000).

3.2.4 Single collagen fibril bending tests

A home-built AFM combined with an optical microscope was used for the bending tests. Bending experiments were performed using modified triangular silicon nitride cantilevers (coated sharp microlevers MSCT-AUHW, type F, spring constant $k = 0.5$ N/m, Veeco, Cambridge, UK). The tip on the AFM cantilever was removed using focused ion beam (FIB) (FEI, NOVALAB 600 dual beam machine, Eindhoven, the Netherlands) to prevent damaging of the collagen fibril surface during the bending tests. Also, the width of the cantilever is wider than the fibril diameter, which facilitated the positioning of the cantilever above the fibril. After cutting, the modified cantilevers (Fig. 3.1) were inspected using the built-in SEM. The spring constant of each tipless cantilever was calibrated by pushing on a pre-calibrated cantilever as described elsewhere [33,34].

The sensitivity (S) of the applied method, i.e. the ratio between the bending of the cantilever and the deflection as measured by the quadrant detector, was derived from the force-indentation curve measured on a glass surface. During bending tests, an AFM piezo

displacement of 1.5 μm and a frequency of 10 Hz were applied. At different positions on the PDMS surface and on the collagen fibrils (Fig. 3.2), bending experiments using the AFM cantilever afforded deflection versus piezo displacement curves. From the results force-displacement curves were derived. At least three deflection versus piezo displacement curves were recorded at every position.

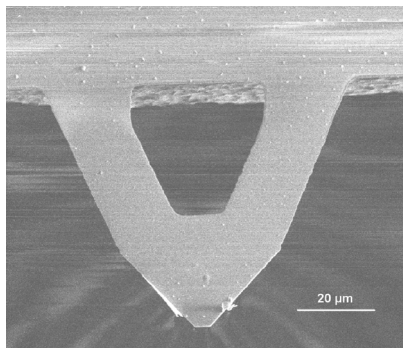


Figure 3.1 SEM image of an AFM cantilever from which the tip has been removed by FIB.

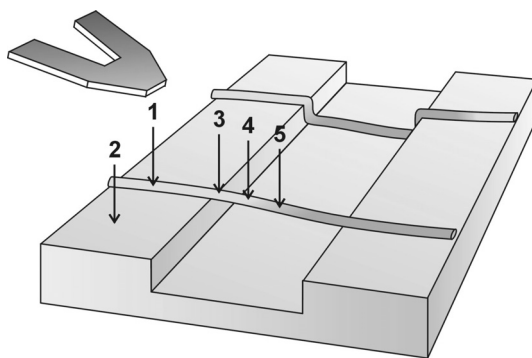


Figure 3.2 Schematic drawing of collagen fibrils crossing the micrometer-sized channel in PDMS and locations where deflection versus piezo displacement curves were obtained. 1: collagen fibril on PDMS surface; 2: PDMS surface; 3: fibril at the edge of the channel; 4: fibril between the edge and middle point of the channel; 5: fibril at the middle point of the channel.

3.3 Results and Discussion

3.3.1 Collagen fibril deposition

For the mechanical tests an experimental set-up was prepared consisting of a PDMS surface containing micro-channels. The rims of the channels support deposited collagen fibrils and thus allow bending experiments by pushing with an AFM cantilever. AFM images of the

prepared PDMS substrates showed that the width and depth of the channels are $5.5 \pm 0.5 \mu\text{m}$ and $0.7 \pm 0.3 \mu\text{m}$, respectively. Due to the transparency of the PDMS, the top surface can be imaged using an inverted optical microscope positioned below the sample plate. In this way the position of the AFM cantilever and collagen fibrils deposited on top of the surface can be visualized simultaneously.

Type I collagen fibrils were conveniently obtained through homogenization and filtering bovine Achilles tendon in diluted acetic acid. The helical content of the collagen in the fibrillar suspension was determined with FTIR and revealed a maximum percentage of helicity [32]. The filtrate, a dispersion of fibrils, was subsequently highly diluted. Incubating the PDMS substrate in the diluted dispersion afforded many free single fibrils not interacting with other fibrils on the surface. Both SEM (Fig. 3.3) and AFM images showed that the diameter of fibrils ranged from ~ 200 to ~ 350 nm and the length of the fibril ranged from $\sim 20 \mu\text{m}$ to $\sim 200 \mu\text{m}$. The characteristic D-period of a single collagen fibril was visualized by TEM (inserted image in Fig. 3.3) and phase imaging using tapping mode AFM. The visualized D-period ensures that the bending tests (vide supra) were performed on intact single collagen fibrils. Moreover, the denaturation temperature (T_d) and the number of free amino groups ($n/1000$) of the native and cross-linked collagen fibrils were determined. The T_d of the native fibrils was 57°C and increased to 76°C after cross-linking with glutaraldehyde. The free amino group content of the native collagen fibrils of 28 per 1000 amino acids decreased to a value of 8 after cross-linking which was in line with previous reported data [31].

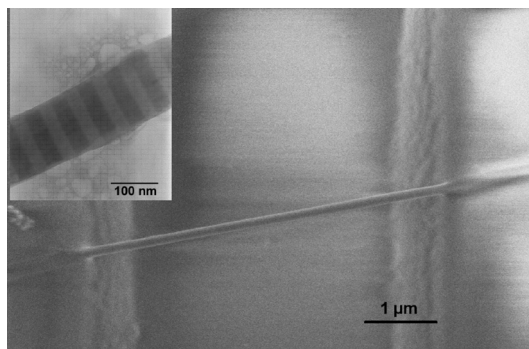


Figure 3.3 SEM image of a single collagen fibril spanning a channel. Insert: TEM image showing the characteristic D-period of the fibril.

Tapping mode AFM revealed that the collagen fibrils were deposited in either of two ways (Fig. 3.4A and Fig. 3.4B). Fig. 3.4A shows that above the channel the collagen fibril

appears thicker when compared to the fibril on the PDMS surface. This is most probably due to the interaction of the AFM tip with the freely suspended part of the collagen fibril. In Fig. 3.4B, it is shown that the height of the collagen fibril on the channel is much lower than the other parts of the fibril, which indicated that the collagen fibril was attached to the rims and bottom of the channel. Only collagen fibrils with a minimum length of 50 μm and spanning multiple channels were used for bending experiments.

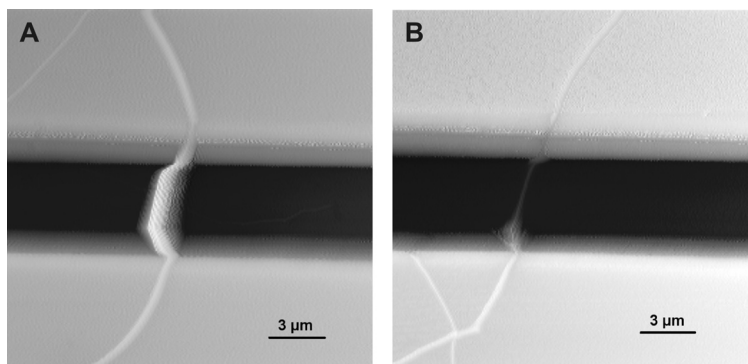


Figure 3.4 Tapping mode AFM image of two types of collagen fibril deposition on a PDMS surface with micro channels: (A) Collagen fibril spanning a channel; (B) Collagen fibril attached to the bottom of a channel. The scan size of both images is $20 \times 20 \mu\text{m}$ and the scan direction is from left to right in both images. The z-scale is $2.2 \mu\text{m}$ for (A) and $1.6 \mu\text{m}$ for (B).

3.3.2 Bending tests

Collagen fibrils spanning the channels were bent with a tip-less cantilever. The deflection-piezo displacement curves obtained from these bending tests on different points at the PDMS surface and collagen fibrils as indicated in Fig. 3.2 are shown in Fig. 3.5A. In the experiments, no difference was found in the deflection-piezo displacement curves after bending the same position 3 times, which ensures the reproducibility of the test and that no permanent deformation of the collagen fibril occurred. As a reference material and for calibration, deflection-piezo displacement curves on a glass surface were recorded. Due to its high stiffness a large slope was found. Mechanical tests on the PDMS surface and on the fibril supported by the PDMS also showed a large slope. Moving to the centre point of the fibril above the channel the slope of the curve resulting from bending of the fibril decreases. The smallest slope of the deflection-piezo displacement curves was found at the centre point above the channel. As a control the same measurement was performed on a collagen fibril adhered at the rims and bottom of the channel. In this case all curves showed an almost similar slope (Fig. 3.5B). The mechanical properties of a collagen fibril were derived from the deflection-piezo displacement curve at the center of the fibril above the channel.

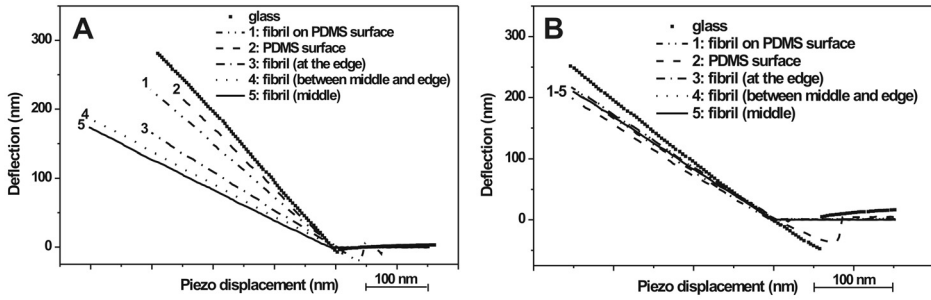


Figure 3.5 Two examples of deflection–piezo displacement curves of bending tests on different points of the surface; (A) Collagen fibril spanning the channel (B) Collagen fibril attached to the bottom of the channel. The numbers on the curves indicate different bending positions as shown in Fig. 3.2.

Every measured point of the approaching part of the deflection versus piezo displacement curve was used for calculating a force-displacement curve. The force (F) and the displacement (z) in the z -direction were calculated using the following equations:

$$z = A - D \times S \tag{3.1}$$

$$F = D \times S \times k \tag{3.2}$$

in which A is the piezo displacement in the z -direction, D is the deflection measured (in Volts), S is the sensitivity of the cantilever and k is the calibrated spring constant of the cantilever. A linear relationship between the force and the displacement for bending the collagen fibril at different positions above the channel was found (Fig. 3.6).

Following the same procedure as described above, bending tests were also performed using collagen fibrils cross-linked with glutaraldehyde. The gradient of the force-displacement curve on bending the collagen fibril at its middle point (dF/dz) was obtained in the same way. After every experiment, the radius of the collagen fibril was measured by SEM. In Fig. 3.7, every point represents the results of a single bending test. Because one collagen fibril which can be 100 μm in length can span more than one channel with a width of 5 μm , bending tests were also performed with the same fibril on different channels. The values of dF/dz for the same fibril are similar which illustrates the reproducibility of the tests. Also, some overlapping fibrils were found from high resolution SEM measurements. The gradient of force-displacement for the overlapping fibrils was not included in the results. The results revealed that single collagen fibrils became stiffer after cross-linking with glutaraldehyde.

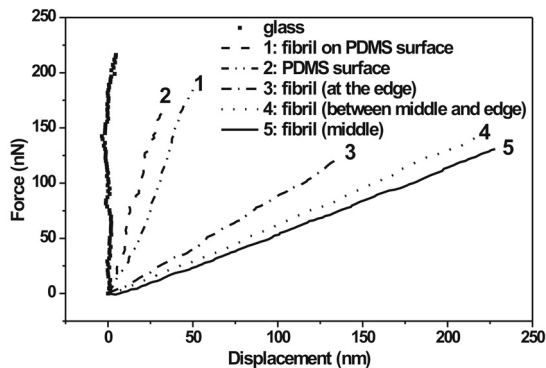


Figure 3.6 A typical example of a set of force-displacement curves derived from the deflection-piezo displacement curves. The numbers on the curves indicate different bending positions as shown in Fig. 3.2.

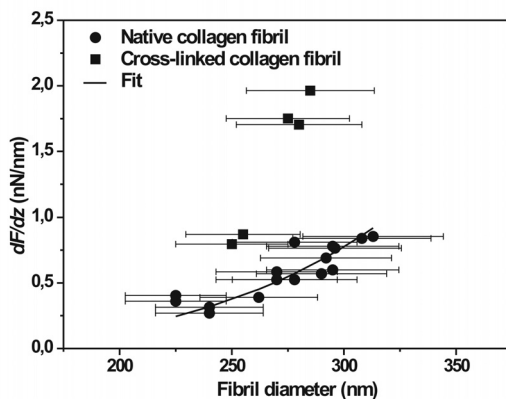


Figure 3.7 The slope of the force-displacement curve (dF/dz) obtained in different experiments on collagen fibrils as a function of the diameter of the fibril. Filled dots are results from experiments performed on native collagen fibrils. Filled squares are derived from experiments on cross-linked fibrils. dF/dz of native collagen fibrils were fitted with $C \times d^4$, d is the diameter of the fibril and C is a constant. The error bars in the figure are S.D. derived from the accuracy of SEM measurements of the diameter of each tested fibril.

However, applying a force on the fibril may cause a deformation of the PDMS at the supporting edges which would obscure the results. Using the force-displacement curves, the indentation of the PDMS substrate resulting from the bending of a collagen fibril was estimated. As shown in Fig. 3.8, the largest force upon bending collagen fibrils is ~ 120 nN at a displacement of the fibril of ~ 200 nm. As schematically shown in Fig. 3.8A, the force on the fibril at the end of channel is ~ 60 nN in a vertical direction. According to the force-displacement curve of the PDMS surface as shown in Fig. 3.6 line 2, the maximum deformation of the PDMS can be estimated to be about 10 nm in the bending direction at a

loading force of 60 nN. The deformation of the PDMS surface thus appears only 5% of the displacement of the collagen fibril at the center point, which is regarded negligible.

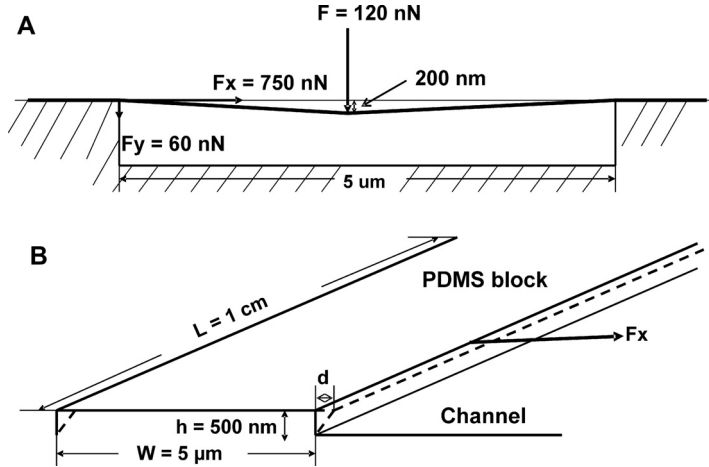


Figure 3.8 (A) Maximum forces on the centre of a collagen fibril and on the PDMS surface during bending. F : the maximum force applied at the center of the collagen fibril with 200 nm displacement; F_x : the force on the fibril at the end of the channel in horizontal direction; F_y : the force on the fibril at the end of the channel in vertical direction (B) The dimensions of the PDMS block and deformation in horizontal direction. L : the length of the PDMS block; w : the width of the PDMS block; h : the height of the channel; d : deformation in the horizontal direction.

The gradient (dF/dz) of the force-displacement curve was used to calculate the Young's modulus. Because of the high length to diameter ratio of the collagen fibril and the fact that the force was applied perpendicular to the fibril axis, it is assumed that the mechanical properties of the collagen fibrils can be described by the model describing the bending of isotropic materials. The Young's modulus of a single collagen fibril can be calculated from the measured force on the middle point of the collagen fibril spanning a channel (Fig. 3.2) using the expressions [35]:

$$E = \frac{l^3}{48I} \times \frac{dF}{dz} \quad (3.3)$$

$$E = \frac{l^3}{192I} \times \frac{dF}{dz} \quad (3.4)$$

In which I is the moment of inertia and is equal to $\frac{1}{4}\pi R^4$ (the fibril is considered a rod with

a circular cross-section with radius R), l is the length of the collagen fibril spanning the channel and dF/dz is the slope of the force-displacement curve obtained from bending the middle point of the collagen fibrils.

Eq. 3.3 represents the condition that the fibril is freely supported by the two ends of the channel. However, because collagen is well known for its surface adhesive properties, the fibril is expected to be strongly adhered to the PDMS and then Eq. 3.4 has to be used. The Young's modulus of the collagen fibril was calculated from Eq. 3.3 and Eq. 3.4 to set the maximum and minimum values of the Young's modulus.

The Young's modulus of single native collagen fibrils was calculated and the results are summarized in Fig. 3.9. The absolute error in the Young's modulus of every individual fibril is derived from the fibril diameter (SEM measurements), the accuracy in determining the length of the fibril spanning the channel and the error in determining the spring constant of the cantilever. Because the force-displacement curves were well fitted with a linear function, the error in the dF/dz can be neglected. For the native fibrils, the Young's moduli are constant at the measured fibril diameter range. An average Young's modulus of 5.4 ± 1.2 GPa from Eq. 3.3 and 1.4 ± 0.3 GPa from Eq. 3.4 were obtained from the bending tests. Because the two models represent extremely different supporting conditions, the real Young's modulus determined from our tests is expected to fit within the range of these two values. The Young's moduli are comparable to those of dry collagen (1 - 8 GPa) presented in literature [14-17]. After cross-linking with glutaraldehyde, an average Young's modulus value of 14.7 ± 2.7 GPa from Eq. 3.3 or 3.8 ± 0.8 GPa from Eq. 3.4 was obtained. Reaction of free amine groups in the collagen with glutaraldehyde results in the formation of different type of cross-links. Most characteristic is the occurrence of short or longer chain cross-links through the possibility of generated intermediates to further polymerize. This will result in bridging collagen molecules as well as microfibrils in the collagen fibril. The increase in the stiffness of collagenous materials on the macro-level is regarded as a result of restriction of the viscous sliding of collagen molecules and fibrils with respect to each other [36]. Here, the increase of the Young's modulus compared to non-crosslinked collagen fibrils is also detected within the single collagen fibril and is ascribed to the reduced possibility of slippage of collagen molecules or segments like microfibrils. However, the Young's modulus of cross-linked fibrils seems to increase with an increase in the fibril diameter. One possible reason is that cross-linking does not occur homogeneously within the fibril. Further investigation is needed to determine the distribution of crosslinks and its relation to the fibril mechanical properties.

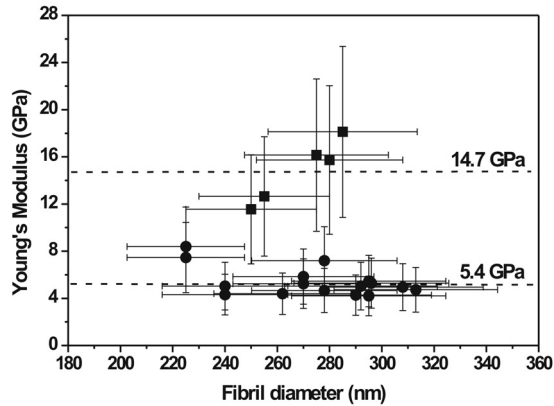


Figure 3.9 Young's modulus of fibrils with different diameters calculated with the model assuming the fibril is simply supported at the rims of the channel. Filled dots are results from experiments performed on native collagen fibrils. Filled squares are derived from experiments on cross-linked fibrils. (Young's modulus calculated with the model assuming the fibril was fixed at the ends of the channel was $\frac{1}{4}$ of the corresponding values presented in the figure.) The absolute error in the Young's modulus of every individual fibril was derived from the fibril diameter (SEM measurements), the accuracy in determining the length of the fibril spanning the channel, and the error in determining the spring constant of the cantilever.

Using an average value of the Young's modulus of 2.0 ± 0.2 MPa as determined by tensile testing and a shear modulus of PDMS of 0.67 ± 0.07 MPa from literature [37] the maximum deformation of PDMS in a horizontal direction was calculated to be 0.7×10^{-12} m assuming the shear force is distributed along the whole PDMS block. As shown in Fig. 3.8B, the dimensions of the PDMS block are much larger than the collagen fibril. Therefore, the deformation in the horizontal direction of the PDMS block, which is in the order of 10^{-12} m, can be ignored compared with the displacement of the collagen fibril (2×10^{-7} m). It has been reported in the literature that the movement of the supporting points or load point during the bending tests would result in a non-linear force-displacement relationship [28,38]. This non-linearity was not observed in our experiments. Therefore, it can be assumed that in the experiments, the slippage of the collagen fibril on the supporting PDMS surface can be ignored in the calculation of the Young's modulus.

3.4 Conclusions

In the present study, we developed a method and determined the mechanical properties of single collagen fibrils by bending tests using AFM. PDMS substrates with a micro-channel structure could be well used to support single collagen fibrils. Fibrils spanning multiple PDMS channels were subjected to bending tests using an AFM cantilever without a tip.

From the deflection-piezo displacement curve, force-displacement curves were deduced and with the assumption that the deformation of collagen fibrils follows the model describing the bending of isotropic materials, a Young's modulus of 5.4 GPa was calculated. After cross-linking with glutaraldehyde, the Young's modulus of a single fibril increases to 14.7 GPa. Because glutaraldehyde cross-linking enables binding of amine groups of (hydroxy)-lysine residues over distances of at least 1.3 nm it can be estimated that crosslinks are generated between collagen molecules as well as microfibrils. Further investigations will focus on single collagen fibrils cross-linked with different types of cross-linking agents to study the relationship between mechanical properties and collagen structure, also in an aqueous environment.

Acknowledgement

This research is financially supported by the Softlink program of ZonMw. Project number: 01SL056.

References

1. Silver FH, Freeman JW, Seehra GP. Collagen self-assembly and the development of tendon mechanical properties. *J. Biomech.* **2003**; 36: 1529-1553.
2. Fratzl P, Misof K, Zizak I, Rapp G, Amenitsch H, Bernstorff S. Fibrillar structure and mechanical properties of collagen. *J. Struct. Biol.* **1997**; 122: 119-122.
3. Silver FH, Freeman JW, Horvath I, Landis WJ. Molecular basis for elastic energy storage in mineralized tendon. *Biomacromolecules* **2001**; 2: 750-756.
4. Redaelli A, Vesentini S, Soncini M, Vena P, Mantero S, Montevercchi FM. Possible role of decorin glycosaminoglycans in fibril to fibril force transfer in relative mature tendons—a computational study from molecular to microstructural level. *J. Biomech.* **2003**; 36: 1555-1569.
5. Scott JE. Extracellular-matrix, supramolecular organization and shape. *J. Anat.* **1995**; 187: 259-269.
6. Ottani V, Martini D, Franchi M, Ruggeri A, Raspanti M. Hierarchical structures in fibrillar collagens. *Micron* **2002**; 33: 587-596.
7. Hulmes DJS. Building collagen molecules, fibrils, and suprafibrillar structures. *J. Struct. Biol.* **2002**; 137: 2-10.
8. Wess TJ, Hammersley AP, Wess L, Miller A. Molecular packing of type I collagen in tendon. *J. Mol. Biol.* **1998**; 275: 255-267.
9. Prockop DJ, Fertala A. The collagen fibril: the almost crystalline structure. *J. Struct. Biol.* **1998**; 122: 111-118.

10. Orgel JP, Miller A, Irving TC, Fischetti RF, Hammersley AP, Wess TJ. The in situ supermolecular structure of type I collagen. *Structure* **2001**; 9: 1061-1069.
11. Holmes DF, Gilpin CJ, Baldock C, Ziese U, Koster AJ, Kadler KE. Corneal collagen fibril structure in three dimensions: structural insights into fibril assembly, mechanical properties, and tissue organization. *Proc. Natl. Acad. Sci. USA* **2001**; 98: 7307-7312.
12. Habelitz S, Balooch M, Marshall SJ, Balooch G, Marshall GW. In situ atomic force microscopy of partially demineralized human dentin collagen fibrils. *J. Struct. Biol.* **2002**; 138: 227-236.
13. Baselt D, Revel J, Baldeschwieler J. Subfibrillar structure of type I collagen observed by atomic force microscopy. *Biophys. J.* **1993**; 65: 2644-2655.
14. An K, Sun Y, Luo Z. Flexibility of type I collagen and mechanical property of connective tissue. *Biorheology* **2004**; 41: 239-246.
15. Takaku K, Ogawa T, Kuriyama T, Narisawa I. Fracture behavior and morphology of spun collagen fibers. *J. Appl. Polym. Sci.* **1996**; 59: 887-896.
16. Pins GD, Silver FH. A self-assembled collagen scaffold suitable for use in soft and hard tissue replacement. *Mater. Sci. Eng. C-Biomim. Mater. Sensors Syst.* **1995**; 3: 101-107.
17. Silver FH, Christiansen D, Snowhill PB, Chen Y, Landis WJ. The Role of mineral in the storage of elastic energy in turkey tendons. *Biomacromolecules* **2000**; 1: 180-185.
18. Puxkandl R, Zizak I, Paris O, Keckes J, Tesch W, Bernstorff S, Purslow P, Fratzl P. Viscoelastic properties of collagen: synchrotron radiation investigations and structural model. *Phil. Trans. R. Soc. Lond. B* **2002**; 357: 191-197.
19. Sasaki N, Odajima S. Elongation mechanism of collagen fibrils and force-strain relations of tendon at each level of structural hierarchy. *J. Biomech.* **1996**; 29: 1131-1136.
20. Sasaki N, Odajima S. Stress-strain curve and young's modulus of a collagen molecule as determined by the x-ray diffraction technique. *J. Biomech.* **1996**; 29: 655-658.
21. Thompson JB, Kindt JH, Drake B, Hansma HG, Morse DE, Hansma PK. Bone indentation recovery time correlates with bond reforming time. *Nature* **2001**; 414: 773-776.
22. Wang X, Li X, Yost M. Microtensile testing of collagen fibril for cardiovascular tissue engineering. *J. Biomed. Mater. Res. A* **2005**; 74: 263-268.
23. Gutschmann T, Fantner GE, Kindt JH, Venturoni M, Danielsen S, Hansma PK. Force spectroscopy of collagen fibers to investigate their mechanical properties and structural organization. *Biophys. J.* **2004**; 86: 3186-3193.
24. Graham JS, Vomund AN, Phillips CL, Grandbois M. Structural changes in human type I collagen fibrils investigated by force spectroscopy. *Exp. Cell. Res.* **2004**; 299: 335-342.

25. Bozec L, Horton M. Topography and mechanical properties of single molecules of type I collagen using atomic force microscopy. *Biophys. J.* **2005**; 88: 4223-4231.
26. Venturoni M, Gutschmann T, Fantner GE, Kindt JH, Hansma PK. Investigations into the polymorphism of rat tail tendon fibrils using atomic force microscopy. *Biochem. Biophys. Res. Co.* **2003**; 303: 508-513.
27. Sun Y, Luo Z, Fertala A, An K. Direct quantification of the flexibility of type I collagen monomer. *Biochem. Biophys. Res. Co.* **2002**; 295: 382-386.
28. Namazu T, Isono Y, Tanaka T. Evaluation of size effect on mechanical properties of single crystal silicon by nanoscale bending test using AFM. *J. Microelectromech. Syst.* **2000**; 9: 450-459.
29. Salvetat JP, Briggs GAD, Bonard JM, Bacsá RR, Kulik AJ, Stöckli T, Burnham NA, Forró L. Elastic and shear moduli of single-walled carbon nanotube ropes. *Phys. Rev. Lett.* **1999**; 82: 944-947.
30. Gratzner PF, Lee JM. Altered mechanical properties in aortic elastic tissue using glutaraldehyde/solvent solutions of various dielectric constant. *J. Biomed. Mater. Res. A* **1997**; 37: 497-507.
31. Olde Damink LHH, Dijkstra PJ, van Luyn MJA, van Wachem PB, Nieuwenhuis P, Feijen J. Glutaraldehyde as a crosslinking agent for collagen-based biomaterials. *J. Mater. Sci. Mater. M* **1995**; 6: 460-472.
32. Friess W, Lee G. Basic thermoanalytical studies of insoluble collagen matrices. *Biomaterials* **1996**; 17: 2289-2294.
33. Torii A, Sasaki M, Hane K, Okuma S. A method for determining the spring constant of cantilevers for atomic force microscopy. *Meas. Sci. Technol.* **1996**; 7: 179-184.
34. Serre C, Pérez-Rodríguez A, Morante JR, Gorostiza P, Esteve J. Determination of micromechanical properties of thin films by beam bending measurements with an atomic force microscope. *Sensor. Actuator.* **1999**; 74: 134-138.
35. Gere JM, Timoshenko SP. *In Mechanics of materials 4th edition.* Stanley Thornes, Cheltenham, **1999**.
36. Silver FH, Christiansen. DL, Snowhill PB, Chen Y. Transition from viscous to elastic-based dependency of mechanical properties of self-assembled type I collagen fibers. *J. Appl. Polym. Sci.* **2001**; 79: 134-142.
37. Mele E, Benedetto F, Persano L, Pisignano D, Cingolani R. Combined capillary force and step and flash lithography. *Nanotechnology* **2005**; 16: 391-395.
38. Ljungcrantz H, Hultman L, Sundgren J, Johansson S, Kristensen N, Schweitz J. Residual stresses and fracture properties of magnetron sputtered Ti films on Si microelements. *J. Vac. Sci. Technol. A* **1993**; 11: 543-553.

Mechanical Properties of Native and Cross-linked Type I Collagen Fibrils*

Lanti Yang¹, Kees O. van der Werf², Carel F. C. Fitié¹, Martin L. Bennink², Pieter J. Dijkstra¹, Jan Feijen¹

¹ *Polymer Chemistry and Biomaterials, Faculty of Science & Technology and Institute for Biomedical Technology (BMTI), University of Twente, P.O. Box 217, 7500 AE, Enschede, The Netherlands*

² *Biophysical Engineering, Faculty of Science & Technology and MESA+ Institute for Nanotechnology, University of Twente, P.O. Box 217, 7500 AE, Enschede, The Netherlands*

Abstract

Micromechanical bending experiments using AFM were performed to study the mechanical properties of native and carbodiimide cross-linked single collagen fibrils. Fibrils obtained from a suspension of insoluble collagen type I isolated from bovine Achilles tendon were deposited on a glass substrate containing micro-channels. Force-displacement curves recorded at multiple positions along the collagen fibril were used to assess the bending modulus. By fitting the slope of the force-displacement curves recorded at ambient conditions to a model describing the bending of a rod, bending moduli ranging from 1.0 GPa to 3.9 GPa were determined. Using a model for anisotropic materials the shear modulus of the fibril was calculated to be 33 ± 2 MPa at ambient conditions. When immersed in PBS buffer, the bending and shear modulus of fibrils decreased to 0.07-0.17 GPa and 2.9 ± 0.3 MPa, respectively. The two orders of magnitude lower shear modulus compared with the Young's modulus confirms the mechanical anisotropy of the collagen single fibrils. Cross-linking the collagen fibrils with a water soluble carbodiimide, did not significantly affect the bending modulus. The shear modulus of these fibrils however changed to 74 ± 7 MPa at ambient conditions and to 3.4 ± 0.2 MPa in PBS buffer.

* This chapter has been accepted for publication in *Biophys. J.* **2007**. In press (online published).

4.1 Introduction

Collagen, the most abundant protein in the human body, provides structural stability and strength to various tissues. About 25 types of collagen have been identified, of which collagen type I is the major component of the fibrous structure of skin, tendon and bone in the human body [1].

Studies on the collagen type I structure have shown a complex hierarchical arrangement of collagen subunits. In this hierarchical arrangement, it is widely accepted that 5 tropocollagen molecules assemble into microfibrils [2-4]. Of the various hypothesized models, the compressed microfibril model [2] and the supertwisted right-handed microfibril model [3] most closely fit to the X-ray diffraction data. Recently, the structure of microfibrils has been visualized using AFM imaging [5]. These microfibrils aggregate in lateral and longitudinal direction to form fibrils. The collagen fibrils with diameters between 10 and 500 nm further assemble into fibers that become part of the structural skeleton of tissues. Due to the highly organized way of self-assembly, a single collagen fibril is regarded as homogenous which means it has the same composition throughout the fibril. However, the alignment of collagen molecules and microfibrils in the longitudinal fibril direction may induce mechanical anisotropy of the single collagen fibrils. The packing of these structural components and the organization of the collagen fibrous structure are crucial to the mechanical function of tissues. Mechanical anisotropy of tissues such as tendon, bone and cartilage have been studied with different techniques [6-9] and using theoretical modeling [10-12]. It is suggested that the mechanical anisotropy at the fibril level and the highly ordered parallel packing of fibrils result in mechanical anisotropy of most tissues [13,14]. However, current mechanical approaches cannot easily separate the contribution of mechanical anisotropy as a result of the hierarchical arrangement of collagen molecules in the fibril and/or parallel packing of the fibrils.

Efforts have been made to determine the mechanical properties of collagen single fibrils using different micro-mechanical techniques. Graham *et al.* [15] stretched in vitro-assembled type I collagen fibrils obtained from human fibroblasts using AFM and obtained a Young's modulus of 32 MPa. Eppell *et al.* [16] studied the stress-strain relationship of single type I collagen fibrils isolated from the sea cucumber and found a Young's modulus of 550 MPa in hydrated state. Also, in our lab, we used a home-built AFM system to perform tensile tests on single collagen type I fibrils isolated from bovine Achilles tendon [17]. A Young's modulus of 5 ± 2 GPa for dry collagen type I fibrils was found and when immersed in PBS buffer the Young's moduli range from 0.2 to 0.5 GPa.

Very recently, the reduced modulus of collagen single fibrils isolated from rat tail tendons was determined by nano-indentation using AFM [18] in air at room temperature and ranged from 5 to 11 GPa. These results support the hypothesis that the anisotropy of collagen results from the alignment of subfibrils along the fibril axis. However, current methods to investigate the mechanical properties of single collagen fibrils are limited as no shear related mechanical properties are measured.

Recently an AFM-based three-point bending technique has been developed by different groups to measure the mechanical properties of nanoscale beams and wires [19-22]. This method has been applied to silicon beams [19], ZnS nanowires [21], SiO₂ nanowires [23], and recently to electrospun polymer-ceramic composites [24] and individual amyloid fibrils [25]. Using the same principle, bending of single-walled carbon nanotubes [26] and microtubules [27] has been performed with contact-mode AFM. In their measurements, the bending modulus (E_{bending}) related to the bending stiffness ($E_{\text{bending}}I$) representing the resistance of the material upon bending was determined (I is the second moment of area of the beam or tube). Using the unit-load equation, the shear moduli of tested materials were determined by bending the materials with different length to diameter ratios. The determined shear moduli of single-wall carbon nanotubes and microtubules were two or three orders of magnitude lower than the Young's modulus, which confirms the mechanical anisotropy of the materials. Adapting the same technique, mechanical anisotropy in single vimentin intermediate filaments (IFs) was determined. This experimental approach offers new insights in separating the contribution of the actin filaments, microtubules and vimentin IFs networks to the stiffness of the cytoskeleton [28].

In order to get more insight into the mechanical behavior of tissues, an AFM-based bending technique was developed to study the mechanical behavior of single collagen type I fibrils isolated from bovine Achilles tendon. Using a home-built AFM system and a glass substrate with microchannels, fibril bending by cantilever movement in the z-direction was combined with a continuous scanning motion along the fibril. In this way, the slope of the force-displacement curve (dF/dz) at different positions along the fibril spanning a channel can be obtained. The bending moduli of tested single collagen fibrils were determined by fitting the slope (dF/dz) of multiple individual bending experiments to well-established mechanical models. This method allows a more accurate determination of the bending modulus and allowed for the first time the calculation of the shear modulus of a collagen fibril. Chemical cross-linking is often necessary to improve the stability of

collagen based biomaterials. Therefore, the change of the mechanical properties upon cross-linking the fibrils was investigated.

4.2 Materials and Methods

Quartz glass substrates with parallel micro-channels were prepared by reactive ion etching using a RIE Elektrotech system (Elektrotech Twin PF 340, UK). The width and depth of the channels were determined by AFM (home-built instrument) and SEM (LEO Gemini 1550 FEG-SEM, Oberkochen, Germany) measurements.

4.2.1 Isolation and deposition of single collagen fibrils

Insoluble bovine Achilles tendon collagen type I from Sigma-Aldrich (Steinheim, Germany) was swollen in hydrochloric acid (0.01 M) overnight at 0°C. The resulting slurry was homogenized for 10 min at 9500 rpm using a Braun MR 500 HC blender (Braun, Kronberg, Germany). The temperature was kept below 5°C. The resulting mixture was filtered using a 74 µm filter (Bellco Glass Inc., collector screen 200 mesh, Vineland, NJ, USA). The helical content of the collagen suspension after filtration was determined by FTIR (Biorad, FTS-60) according to a method described by Friess *et al.* [29]. After filtration, 1 ml of the collagen dispersion was diluted with 150 ml of PBS (pH = 7.4). Deposition of the collagen fibrils on the quartz glass substrates was done by incubating the substrates for 10 min in the diluted collagen dispersion. Subsequently, the substrates were washed with PBS for 10 min and three times with demineralized water for 10 min each and finally dried at ambient conditions for at least 24 h. The bending tests of collagen fibrils in PBS buffer were carried out after equilibrating the fibrils for 15 min in PBS at room temperature. Longer equilibration times did not lead to changes in the results of the bending tests.

Cross-linked collagen fibrils were prepared by mixing 2 ml of the non-diluted collagen dispersion with a solution of 1.73 g 1-ethyl-3-(3-dimethyl aminopropyl)carbodiimide hydrochloride (EDC) and 0.45 g N-hydroxysuccinimide (NHS) in 215 ml 2-morpholinoethane sulfonic acid (MES) (0.05 M, pH = 5.4) for 2 h. The resulting cross-linked fibrils were deposited on the quartz glass substrates and washed as described above.

4.2.2 Collagen denaturation temperature and free amino group content

The diluted native collagen fibril dispersion was centrifuged for 15 min at 4500 rpm (Hettich Mikco Rapid/k, Depex, De Bilt, the Netherlands). The solution was removed and the collagen was washed twice with MilliQ water for 30 min each. Similarly, a diluted

cross-linked collagen fibril dispersion was centrifuged as described above and then washed twice with PBS buffer for 30 min each and four times with MilliQ water for 30 min each. After the washing steps, both native and cross-linked collagen samples were frozen in liquid nitrogen and subsequently freeze-dried for 24 h.

The degree of cross-linking of the collagen samples is related to the increase of the denaturation (shrinkage) temperature (T_d) after cross-linking. The T_d values were determined by DSC (DSC 7, Perkin Elmer, Norwalk, CT, USA). Freeze-dried native and cross-linked collagen samples of 3-5 mg were swollen in 50 μ l of PBS (pH = 7.4) in high-pressure pans overnight. Samples were heated from 20°C to 90°C at a heating rate of 5 °C/min. A sample containing 50 μ l of PBS (pH = 7.4) was used as a reference. The onset of the endothermic peak was taken as the T_d .

The free amino group content of native and cross-linked samples was determined using the 2,4,6-trinitrobenzenesulfonic acid (TNBS) assay. Collagen samples of 3 - 5 mg were incubated for 30 min in 1 ml of a 4 wt % solution of NaHCO_3 . To this mixture 1 ml of a freshly prepared solution of TNBS (0.5 wt %) in 4 wt % NaHCO_3 was added. The resulting mixture was left for 2 h at 40°C. After the addition of HCl (3 ml, 6 M), the temperature was raised to 60°C. Degradation of collagen was achieved within 90 min. The resulting solution was diluted with 5.0 ml MilliQ water and cooled to room temperature. The absorbance at 420 nm was measured using a Varian Cary 300 Bio spectrophotometer (Middelburg, the Netherlands). A blank was prepared applying the same procedure, except that HCl was added before the addition of TNBS. The absorbance was correlated to the concentration of free amino groups using a calibration curve obtained with glycine. The free amino group content was expressed as the number of free amino groups per 1000 amino acids (n/1000).

4.2.3 Micromechanical bending in scanning mode using AFM

Modified triangular silicon nitride cantilevers (coated sharp microlevers MSCT-AUHW, type F, spring constant $k = 0.5$ N/m, Veeco, Cambridge, UK) were used in the bending test. The tip on the AFM cantilever was removed using a focused ion beam (FIB) (FEI, NOVALAB 600 dual beam machine). After cutting, the modified cantilevers were inspected using the built-in SEM [30]. The spring constant of each tip-less cantilever was calibrated by pushing on a pre-calibrated cantilever as described elsewhere [31]. The sensitivity (S) of the AFM system with the cantilever, i.e. the ratio between the bending of the cantilever and the deflection as measured by the quadrant detector, was derived from a

force-indentation curve measured on a glass surface with an identical scan rate and amplitude as used in the bending experiments.

4.3 Results and Discussion

4.3.1 Sample preparation and characterization

AFM images of the quartz glass substrates (Fig. 4.1A) show that ion etching allows the preparation of a substrate with well defined micro channels with a width of $\sim 3 \mu\text{m}$. The depth of the channels is approximately 600 nm which is sufficient for the intended bending experiments of collagen fibrils spanning these channels and supported by the glass rims.

The glass substrates were incubated in a freshly prepared and highly diluted suspension of collagen fibrils. After washing and drying the samples, single fibrils perpendicularly spanning the micro-channels were selected and used in the scanning mode mechanical bending tests (vide supra). The characteristic 67 nm D-period of the collagen fibrils deposited on the glass surface was visualized by AFM images both for fibrils at ambient conditions (Fig. 4.1C) and in PBS buffer (Fig. 4.1D). Collagen fibrils with at least 50 μm in length crossed more than 3 channels on the glass substrate (Fig. 4.1B). The diameters of all tested fibrils were determined by high magnification SEM images.

The helical content of the collagen in the fibrillar suspension was determined with FTIR and revealed a maximum percentage of helicity [29]. The single collagen fibrils used were also characterized by determining their characteristic denaturation temperature (T_d) and number of free amino groups (n/1000). The T_d of the native fibrils was 55.0°C and increased to 74.5°C after cross-linking with the water-soluble carbodiimide 1-ethyl-3-(3-dimethyl aminopropyl)carbodiimide hydrochloride (EDC) in the presence of N-hydroxysuccinimide (NHS). The free amino group content decreased from 28 per 1000 amino acids to a value of 8 which was in line with previously reported data [32]. These results reveal a high degree of cross-linking.

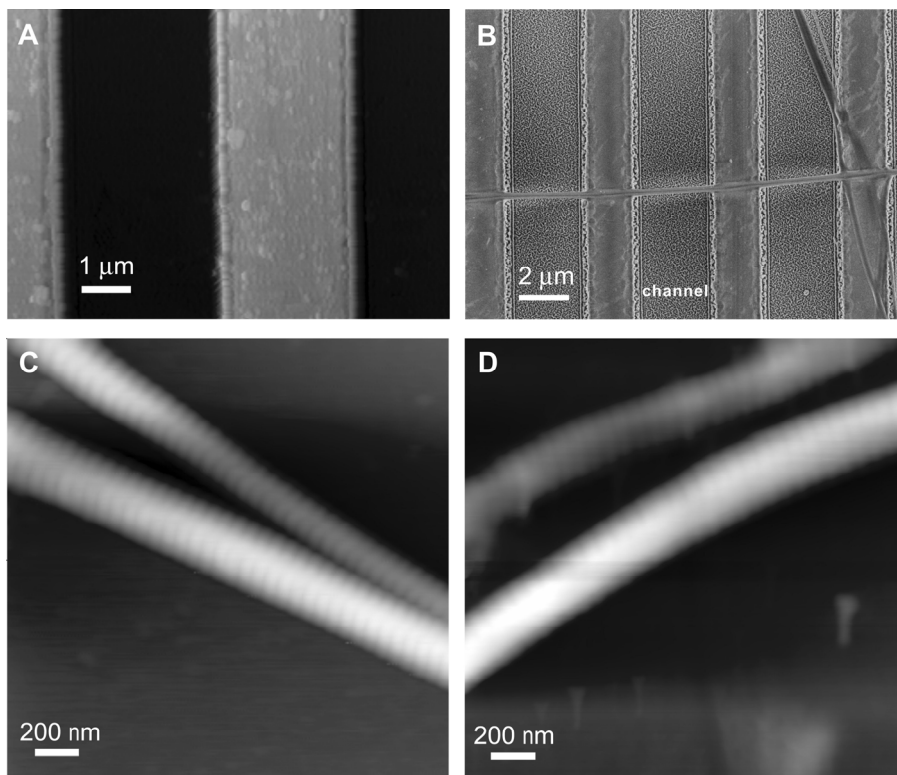


Figure 4.1 (A) Tapping mode AFM height image of a glass surface patterned with channels, the full z-range of the image is 1 μm ; (B) SEM image of a single collagen fibril spanning multiple channels. The width of the channel is $3.0 \pm 0.2 \mu\text{m}$; (C) Tapping mode AFM height image of single collagen fibrils on a glass surface at ambient conditions, the full z-range of the image is 250 nm; (D) Tapping mode AFM height image of single collagen fibrils on a glass surface in PBS buffer, the full z-range of the image is 225 nm.

4.3.2 Micromechanical bending of native and cross-linked collagen type I fibrils

Using an optical microscope, collagen fibrils that freely and perpendicularly span multiple channels of the glass substrate were selected for the bending tests. The actual scanning bending procedure was started after a successful approach of the AFM tip-less cantilever above the fibril. In scanning mode, fibril bending by cantilever movement in the z-direction was combined with a continuous scanning motion along the fibril. To achieve this, the output signal for the fast scanning direction as used in AFM scanning was used to drive the piezo movement in the z-direction while the one for the slow scanning direction was used to move the cantilever along the fibril (Fig. 4.2). During the bending tests, the total scanning distance was chosen to be 4 - 5 μm which was slightly larger than the channel width. A typical piezo movement of 1.5 - 3.0 μm with a frequency of 1.3 Hz in

the z-direction was applied. In each step, one cycle (approach and retraction) of the cantilever deflection and piezo movement was recorded. After every step, the tip was moved one step further along the fibril. A complete scan consists of 256 steps with a total measuring time of 200 s.

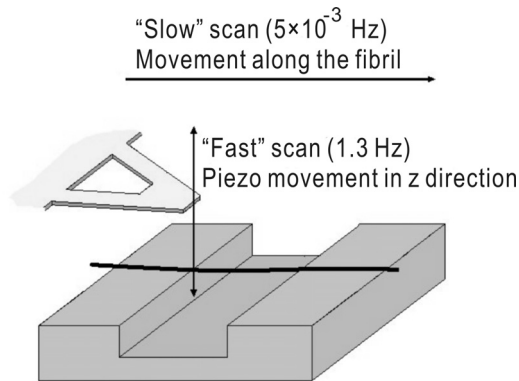


Figure 4.2 Schematic representation of the cantilever movement over a single collagen type I fibril during the scanning mode bending experiments. Each cycle (approach and retraction) of the cantilever movement in the z direction gives a piezo movement-deflection curve. After each cycle, the cantilever moves one step further along the fibril. In total, 256 steps along the fibril gave 256 piezo movement-deflection curves.

Four of the individual piezo movement-deflection curves obtained from bending the fibril at the middle point of the channel (a), between the middle and edge of the channel (b) and at the edge of the channel (c) and indenting the fibril on the glass surface (d) are presented in Fig. 4.3. During the first part of the approach there is no deflection, indicating that the cantilever is not interacting with the collagen fibril. As the cantilever moves closer, a snap-in point can be observed (negative deflection). After this point a linear relationship between the piezo movement and deflection of the fibril is found for all individual bending measurements. The slope of the piezo movement-deflection curve differs from one position to the next.

A custom computer program, written in Labview (version 6.1, National Instruments, Austin, Texas, USA) was used to analyze the data. A force-displacement curve of every 256 bending measurements was obtained using the following equations:

$$z = A - D \quad (4.1)$$

$$F = D \times k \quad (4.2)$$

in which z is the displacement of the fibril in the z -direction during bending, A is the piezo movement in the z -direction and D is the calibrated deflection signal of the cantilever in nm. F is the force applied to the fibril and k is the calibrated spring constant of the cantilever.

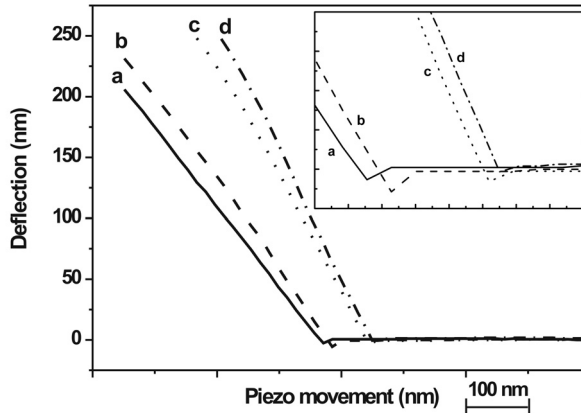


Figure 4.3 Four individual piezo movement versus deflection curves obtained at different positions along the fibril (diameter 240 nm); (a) at the middle of the channel; (b) between the middle and edge of the channel; (c) at the edge of the channel; (d) on the glass surface. Insert: Enlargement of the snap-in points in the same piezo movement versus deflection curves. The scale units are 10 nm and 5 nm for horizontal axis and vertical axis, respectively.

The slope of each force-displacement curve of the tested fibril was determined by linear fit and the obtained data are presented in Fig. 4.4. A decrease in the slope (dF/dz) was found during scanning from the edge up to the middle of the channel which clearly proves that the fibril is freely suspending the micro-channel. In all experiments, no difference was found in the force-displacement curves upon bending the same collagen fibril multiple times, which ensures the reproducibility of the test and confirms that no permanent deformation of the collagen fibrils occurred. It has to be noted that in the measurements near the edges of the channel the cantilever can touch the glass surface upon bending the fibril and those data were omitted from analysis.

When a force is applied to the suspended part of the fibril a possible displacement in the z -direction at both rims of the channel has to be taken into account. Due to the strong surface adhesion properties of collagen to glass [15] and the fact that each collagen fibril crosses at least 3 channels (the length of the fibril is more than 50 μm), it is assumed that the fibril is firmly attached to the surface at the supporting rims and that the rim behaves as a stiff material and thus the displacement can be neglected. Also, it has been reported that

slippage of a collagen fibril on the supporting points or loading points during the bending tests will result in a non-linear force-displacement curve [33]. This nonlinearity was not observed in our experiments.

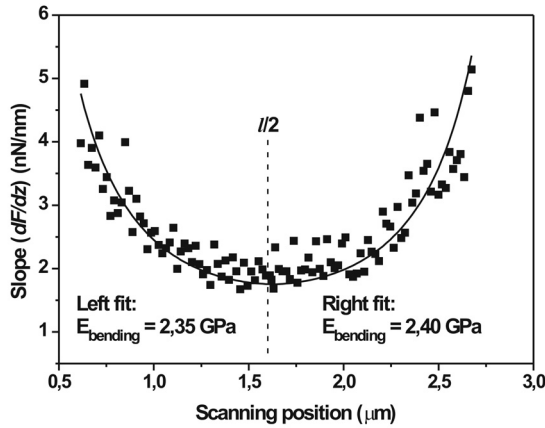


Figure 4.4 Slope of the force versus displacement curve of a collagen type I fibril (diameter 240 nm) as a function of the scanning position along the channel. The dashed line in the image indicates the middle point of the channel (channel width is $\sim 3.2 \mu\text{m}$). The dF/dz data at the left half and right half of the channel are fitted to Eq. 4.3 separately.

4.3.3 Determining the mechanical properties of native and cross-linked single collagen fibrils

Deflections of a rod induce both bending and shear deformation. A bending modulus E_{bending} as previously defined by Kis, *et al.*[27] equals the Young's modulus (E) if the rod is isotropic or the length to diameter ratio fulfills the following requirement: ($l/R \geq 4\sqrt{E/G}$) (G is the shear modulus). The E_{bending} of the suspended fibril can be obtained by fitting the measured slope of the force-displacement curves at all positions to Eq. 4.3 [34],

$$\frac{dF}{dz} = \frac{3 \times l^3 \times E_{\text{bending}} \times I}{(1 - x)^3 \times x^3} \quad (4.3)$$

in which x is the relative position along the fibril ($0 \leq x \leq l/2$), l is the length of the fibril spanning the channel, I is the moment of inertia ($I = \frac{1}{4}\pi R^4$), and dF/dz is the slope deduced from the force-displacement curve obtained during bending of the collagen fibril. The fibril is considered a rod with a circular cross-section with radius R .

As shown in Fig. 4.4 the dF/dz data do fit to Eq. 4.3. The standard error in the least squares fit parameter is 2-6% and values obtained from the left and right half of the fibril are similar (average difference 3-4%).

In Chapter 3, we reported on the determination of the Young's modulus of dry collagen fibrils by single point bending tests [30]. The Young's modulus of a fibril crossing a channel in a poly(dimethyl siloxane) (PDMS) substrate was determined close to its middle point using Eq. 4.4 which is derived from Eq. 4.3 by substituting $x = l/2$

$$E_{bending} = \frac{l^3}{192I} \times \frac{dF}{dz} \quad (4.4)$$

Compared to a single point bending procedure the scanning mode bending allows a more accurate determination of the bending modulus (equals the Young's modulus for isotropic materials or high length to diameter ratio) since it results from fitting multiple individual bending experiments. Furthermore, data generated from multiple bending experiments of the suspended fibril and fitted to the model of bending a rod reveals that no permanent deformation of the collagen fibril occurred during the bending tests. The relative error (~ 23%) in the bending modulus using the applied scanning mode bending method is derived from the error (S.E.M.) of the diameter (~ 3%), the width of the channel (~ 3%), the spring constant of the cantilever (~ 5%) and the fitting (~ 3%). The largest contribution to the error of the bending modulus is due to the error in the diameter of the fibril (~ 3%). This leads to a 12% error in the bending modulus. Improvement of the accuracy in the fibril diameter determination is critical for further reducing the error.

The ranges of the bending modulus values that were obtained from the scanning mode bending tests are presented in Table 4.1. Typically the bending modulus of a collagen fibril with a diameter of 240 nm is ~ 2.4 GPa (Fig. 4.4) at ambient conditions. The bending modulus of such a fibril decreased with a factor of ~ 20 to 120 MPa when immersed in PBS buffer. Introducing cross-links between collagen molecules by activation of carboxylic acid groups of glutamic or aspartic acid residues with a carbodiimide, which subsequently react with amine groups with the formation of amide bonds [32] and with hydroxyl groups with the formation of ester bonds [35], did not significantly affect the bending modulus of the fibril.

For isotropic rods or rods with high length to diameter ratio, the bending modulus is equal to the Young's modulus and is independent of the rod diameter. Otherwise, the

contribution of shear in the deflection of the rod can not be ignored. The deflection from bending and shear deformation when a force is applied at the middle of the channel can be written as [34]:

$$\begin{aligned}
 z &= z_B + z_S \\
 &= Fl^3/192EI + f_s Fl/4GA \\
 &= Fl^3/192E_{bending}l
 \end{aligned} \tag{4.5}$$

In Eq. 4.5, z is the total displacement of the fibril in the z -direction, z_B is the deflection resulting from bending, z_S is the deflection resulting from shearing, E is the Young's modulus, G is the shear modulus, f_s is the form factor of shear and A is the cross-sectional area of the rod. For a rod with a circular cross-sectional area, the form factor of shear f_s equals 10/9 [34].

Equation 4.5 can be converted into Eq. 4.6 using $A = \pi R^2$, $f_s = 10/9$ and $I = \pi R^4/4$.

$$\frac{1}{E_{bending}} = \frac{1}{E} + \frac{120}{9G} \times \left(\frac{R^2}{l^2}\right) \tag{4.6}$$

From Eq. 4.6, a diameter dependent bending modulus is expected. Such a diameter dependent bending modulus was observed before in microtubules [27] and single-wall nanotube ropes [26] with relatively weak bonds between the subunits in the lateral direction. Here, a large number of fibrils were tested and we found that the bending modulus increased with decreasing fibril diameter at both ambient conditions and in PBS buffer (Fig. 4.5, A and B).

Using Eq. 4.6, the shear modulus of the tested collagen fibrils can be determined from the slope of the linear relationship between $1/E_{bending}$ and (R^2/l^2) . A similar equation has been used by Kis *et al.* [27] for studying the bending and shear modulus of microtubules. With the linear fit as shown in Fig. 4.6 A, the shear modulus of native single collagen fibrils at ambient conditions is 33 ± 2 MPa. After cross-linking with EDC/NHS, the shear modulus increases to 74 ± 7 MPa. Also as shown in Fig. 4.6 B, the shear modulus of the collagen fibrils placed in PBS buffer can be estimated from the linear plot. The values of the shear moduli are 2.9 ± 0.3 MPa and 3.4 ± 0.2 MPa for native and EDC/NHS cross-linked fibrils, respectively, which are not statistically different. The differences in the increase of the shear modulus for fibrils at ambient conditions and placed in PBS buffer before and after

cross-linking may relate to the different hydration states of the fibrils. Intermolecular cross-links in collagen fibrils are mainly present in the telopeptide regions. Cross-linking using a carbodiimide like EDC involves the formation of additional amide bonds by reaction of free amine groups (lysine residues) and activated carboxylic acid groups (glutamic- and aspartic acid) and ester bonds by reaction of hydroxyl groups (serine, hydroxyproline, and hydroxylysine residues) and activated carboxylic acid groups as well, which results in additional inter- and intra-molecular cross-links in the collagen fibrils. It is not expected that cross-links can be formed between microfibrils for the distance is too long. However, displacement of microfibrils with respect to each other at ambient conditions may be hampered due to the friction resulting from the surface decoration by activated carboxylic acid groups. In PBS buffer, the surface decoration does not hamper the displacement of microfibrils with respect to each other. It is expected that after cross-linking the displacement of collagen molecules with respect to each other becomes more difficult. However, the similar shear moduli for native and cross-linked collagen fibrils placed in buffer indicate that the displacement of microfibrils with respect to each other is probably the main factor influencing the shear modulus of single collagen fibrils.

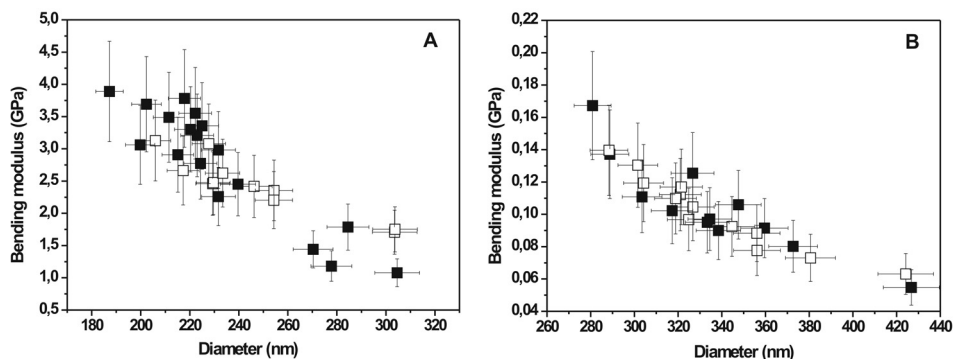


Figure 4.5 Bending moduli of collagen type I fibrils as a function of diameter at ambient conditions (A) and in PBS buffer (B). Data points are of native collagen fibrils (filled squares) and collagen fibrils cross-linked by EDC/NHS (open squares). N = 18 for native collagen (at ambient conditions); N = 11 for cross-linked collagen (at ambient conditions); N = 12 for native collagen (in PBS buffer); and N = 13 for cross-linked collagen (in PBS buffer). The relative error in the bending modulus of every individual fibril is derived from the errors in fibril diameter (SEM measurements), the length of the fibril spanning the channel and the spring constant of the cantilever.

The values of shear moduli for different collagen fibrils at different conditions are listed in Table 4.1. In Chapter 3 [30], the diameter dependent bending modulus was not observed because we used channels with a larger width resulting in a higher length to diameter ratio

($l/R \geq 4\sqrt{E/G}$), therefore, the E_{bending} corresponds more closely with the Young's modulus.

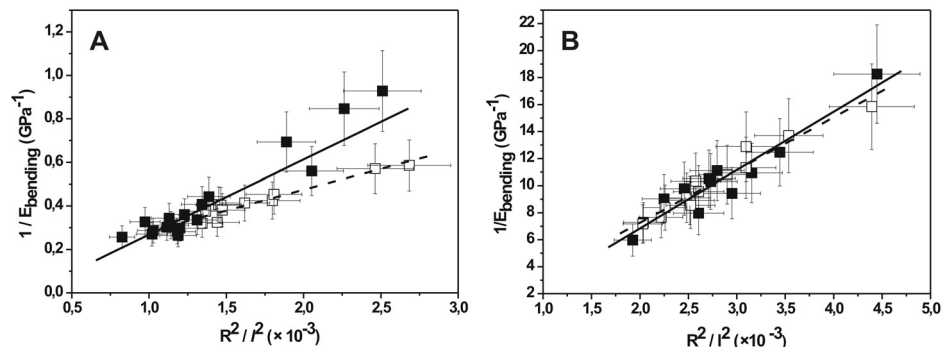


Figure 4.6 Reciprocal bending modulus (E_{bending}) as a function of R^2/l^2 of collagen type I fibrils at ambient conditions (A) and in PBS buffer (B). R is the collagen fibril radius and l is the suspended length of the fibril over the channel. Data points and linear fit are of native collagen type I fibrils (filled squares, fit: solid line) and collagen type I fibrils cross-linked by EDC/NHS (open squares, fit: dashed line). $N = 18$ for native collagen (at ambient conditions); $N = 11$ for cross-linked collagen (at ambient conditions); $N = 12$ for native collagen (in PBS buffer); and $N = 13$ for cross-linked collagen (in PBS buffer).

Table 4.1 Bending and shear moduli of collagen type I fibrils obtained from scanning bending measurements

Collagen type I fibril	Conditions	Number of samples	Range of Diameters ^c (nm)	Bending moduli ^d (GPa)	Shear modulus ^e (MPa)
Native	Dry	18	187 ~ 305	3.9 ~ 1.0	33 ± 2
Cross-linked ^a	Dry	11	205 ~ 303	3.1 ~ 1.7	74 ± 7
Native	PBS buffer ^b	12	280 ~ 426	0.17 ~ 0.07	2.9 ± 0.3
Cross-linked ^a	PBS buffer ^b	13	287 ~ 424	0.14 ~ 0.06	3.4 ± 0.2

a. Cross-linking was performed with EDC and NHS in MES buffer.

b. PBS: phosphate buffered saline pH = 7.4

c. Ranges of diameters of different fibrils used in the mechanical tests. The error in the diameter of individual fibrils is ~ 3% (S.E.M.) calculated from multiple measurements on the same fibril.

d. Ranges of bending moduli determined from fibrils with different diameters. A 23% relative error is estimated for the value of the bending modulus determined for individual fibrils.

e. The error in the shear modulus is the standard error of the weighted least squares fit parameter.

According to current models described in literature [2,3,36,37], collagen molecules and microfibrils are arranged parallel to the fibril axis. Intermolecular cross-linking for native collagen is believed to occur only via lysine and hydroxyl-lysine groups within the

telopeptide regions [3]. The interaction between the collagen subunits in the parallel direction will be different than in the lateral direction leading to mechanical anisotropy. Previously, micro-tensile tests of single collagen fibrils have been performed in our group. The Young's modulus of single collagen fibrils was determined to be 5 ± 2 GPa and 0.2 - 0.5 GPa at ambient conditions and in PBS buffer, respectively [17]. The shear modulus of the single collagen fibrils determined from the bending experiments is 2 orders of magnitude lower than the Young's modulus, which confirms anisotropy at the single collagen fibril level.

4.4 Conclusions

To summarize, in the present study, the mechanical properties of insoluble collagen type I fibrils isolated from tendon were investigated using scanning mode bending tests with a home-built AFM. Single fibrils perpendicularly spanning multiple channels in a glass substrate were subjected to bending tests using an AFM cantilever without a tip.

Subjecting a single collagen fibril to the scanning mode bending test afforded multiple force-displacement curves at different positions across the channel. From the slope of these curves (dF/dz) the bending modulus of the fibrils could be determined using a model describing the bending of a rod. For single collagen type I fibrils immersed in buffer, the bending modulus decreased a factor of 20 compared to fibrils at ambient conditions. Cross-links introduced upon reaction with a carbodiimide did not change the bending modulus of the fibril.

The dependence of the bending modulus on the collagen fibril diameter allowed for the first time an estimation of the shear modulus. The calculated shear modulus indicates that the collagen fibrils are mechanically anisotropic. For collagen fibrils in PBS buffer, it is shown that cross-linking through amide bond formation between amine and carboxylic acid groups and ester bond formation between hydroxyl and carboxylic acid groups does not affect the shear modulus of the fibril. These results provide new insight on the mechanical behavior of collagen based tissues.

Acknowledgement

This research was financially supported by the Softlink program of ZonMw. Project number: 01SL056.

References

1. Veis A. Collagen fibrillar structure in mineralized and nonmineralized tissues. *Curr. Opin. Solid St. M.* **1997**; 2: 370-378.
2. Piez KA, Trus BL. A new model for packing of type-I collagen molecules in the native fibril. *Bioscience Rep.* **1981**; 1: 801-810.
3. Orgel JPRO, Irving TC, Miller A, Wess TJ. Microfibrillar structure of type I collagen in situ. *Proc. Natl. Acad. Sci. USA* **2006**; 103: 9001-9005.
4. Wess TJ, Hammersley AP, Wess L, Miller A. Molecular packing of type I collagen in tendon. *J. Mol. Biol.* **1998**; 275: 255-267.
5. Habelitz S, Balooch M, Marshall SJ, Balooch G, Marshall GW. In situ atomic force microscopy of partially demineralized human dentin collagen fibrils. *J. Struct. Biol.* **2002**; 138: 227-236.
6. Hoffmeister BK, Handley SM, Wickline SA, Miller JG. Ultrasonic determination of the anisotropy of Young's modulus of fixed tendon and fixed myocardium. *J. Acoust. Soc. Am.* **1996**; 100: 3933-3940.
7. Kostyuk O, Birch HL, Mudera V, Brown RA. Structural changes in loaded equine tendons can be monitored by a novel spectroscopic technique. *J. Physiol.* **2003**; 554: 791-801.
8. Fan Z, Smith PA, Eckstein EC, Harris GF. Mechanical properties of OI type III bone tissue measured by nanoindentation. *J. Biomed. Mater. Res. A* **2006**; 79: 71-77.
9. Elliott DM, Narmoneva DA, Setton LA. Direct measurement of the Poisson's ratio of human patella cartilage in tension. *J. Biomech. Eng-T ASME* **2002**; 124: 223-228.
10. Akkus O. Elastic deformation of mineralized collagen fibrils: an equivalent inclusion based composite model. *J. Biomech. Eng-T ASME* **2005**; 127: 383-390.
11. Natali AN, Pavan PG, Carniel EL, Lucisano ME, Tagliavero G. Anisotropic elasto-damage constitutive model for the biomechanical analysis of tendons. *Med. Eng. Phys.* **2005**; 27: 209-214.
12. Bischoff JE. Reduced parameter formulation for incorporating fiber level viscoelasticity into tissue level biomechanical models. *Ann. Biomed. Eng.* **2006**; 34: 1164-1172.
13. Wu JZ, Herzog W. Elastic anisotropy of articular cartilage is associated with the microstructures of collagen fibers and chondrocytes. *J. Biomech.* **2002**; 35: 931-942.
14. Hellmich C, Barthélémy JF, Dormieux L. Mineral-collagen interactions in elasticity of bone ultrastructure-a continuum micromechanics approach. *Eur. J. Mech. A-Solid* **2004**; 23: 783-810.
15. Graham J S, Vomund AN, Phillips CL, Grandbois M. Structural changes in human type I collagen fibrils investigated by force spectroscopy. *Exp. Cell Res.* **2004**; 299: 335-342.
16. Eppell SJ, Smith BN, Kahn H, Ballarini R. Nano measurements with micro-devices: mechanical properties of hydrated collagen fibrils. *J. R. Soc. Interface* **2006**; 3:

- 117-121.
17. van der Rijt JAJ, van der Werf KO, Bennink ML, Dijkstra PJ, Feijen J. Micromechanical testing of individual collagen fibrils. *Macromol. Biosci.* **2006**; 6: 697-702.
 18. Wenger MPE, Bozec L, Horton MA, Mesquida P. Mechanical properties of collagen fibrils. *Biophys. J.* **2007**; 93: 1255-1263.
 19. Namazu T, Isono Y, Tanaka T. Evaluation of size effect on mechanical properties of single crystal silicon by nanoscale bending test using AFM. *J. Microelectromech. Syst.* **2000**; 9: 450-459.
 20. Ni H, Li X. Young's modulus of ZnO nanobelts measured using atomic force microscopy and nanoindentation techniques. *Nanotechnology* **2006**; 17: 3591-3597.
 21. Xiong Q, Duarte N, Tadigadapa S, Eklund PC. Force-deflection spectroscopy: a new method to determine the Young's modulus of nanofilaments. *Nano. Lett.* **2006**; 6: 1904-1909.
 22. Jeng YR, Tsai PC. Molecular-dynamics studies of bending mechanical properties of empty and C₆₀-filled carbon nanotubes under nanoindentation. *J. Chem. Phys.* **2005**; 122: 224713-1-8.
 23. Ni H, Li X, Gao H. Elastic modulus of amorphous SiO₂ nanowires. *Appl. Phys. Lett.* **2006**; 88: 043108-1-3.
 24. Lee SH, Tekmen C, Sigmund WM. Three-point bending of electrospun TiO₂ nanofibers. *Mat. Sci. Eng. A-Struct.* **2005**; 398: 77-81.
 25. Smith JF, Knowles TPJ, Dobson CM, MacPhee CE, Welland ME. Characterization of the nanoscale properties of individual amyloid fibrils. *Proc. Natl. Acad. Sci. USA* **2006**; 103: 15806-15811.
 26. Salvetat JP, Briggs GAD, Bonard JM, Bacsá RR, Kulik AJ, Stöckli T, Burnham NA, Forró L. Elastic and shear moduli of single-walled carbon nanotube ropes. *Phys. Rev. Lett.* **1999**; 82: 944-947.
 27. Kis A, Kasas S, Babić B, Kulik AJ, Benoît W, Briggs GAD, Schönenberger C, Catsicas S, Forró L. Nanomechanics of microtubules. *Phys. Rev. Lett.* **2002**; 89: 248101-1-4.
 28. Guzmán C, Jeney S, Kreplak L, Kasas S, Kulik AJ, Aebi U, Forró L. Exploring the mechanical properties of single vimentin intermediate filaments by atomic force microscopy. *J. Mol. Biol.* **2006**; 360: 623-630.
 29. Friess W, Lee G. Basic thermoanalytical studies of insoluble collagen matrices. *Biomaterials* **1996**; 17: 2289-2294.
 30. Yang L, van der Werf KO, Koopman BFJM, Subramaniam V, Bennink ML, Dijkstra PJ, Feijen J. Micromechanical bending of single collagen fibrils using atomic force microscopy. *J. Biomed. Mater. Res. A* **2007**; 82: 160-168 (chapter 3 of this thesis).
 31. Torii A, Sasaki M, Hane K, Okuma S. A method for determining the spring constant of cantilevers for atomic force microscopy. *Meas. Sci. Technol.* **1996**; 7: 179-184.

32. Olde Damink LHH, Dijkstra PJ, van Luyn MJA, van Wachem PB, Nieuwenhuis P, Feijen J. Cross-linking of dermal sheep collagen using a water-soluble carbodiimide. *Biomaterials* **1996**; 17: 765-773.
33. Ljungcrantz H, Hultman L, Sundgren J, Johansson S, Kristensen N, Schweitz J. Residual stresses and fracture properties of magnetron sputtered Ti films on Si. microelements. *J. Vac. Sci. Technol.* **1993**; A 11: 543-553.
34. Gere JM, Timoshenko SP. *In Mechanics of materials* 3rd edition. *Chapman & Hall*, London, **1993**.
35. Everaerts F, Torrianni M, Hendriks M, Feijen J. Quantification of carboxyl groups in carbodi- imide cross-linked collagen sponges. *J. Biomed. Mater. Res. A* **2007**; 83: 1176-1183.
36. Buehler MJ. Nature designs tough collagen: Explaining the nanostructure of collagen fibrils. *Proc. Natl. Acad. Sci. USA* **2006**; 103: 12285-12290.
37. Prockop DJ, Fertala A. The collagen fibril: the almost crystalline structure. *J. Struct. Biol.* **1998**; 122: 111-118.

Mechanical Properties of Single Electrospun Collagen Type I Fibers*

Lanti Yang¹, Carel F. C. Fitié¹, Kees O. van der Werf², Martin L. Bennink², Pieter J. Dijkstra¹, Jan Feijen¹

¹ *Polymer Chemistry and Biomaterials, Faculty of Science & Technology and Institute for Biomedical Technology (BMTI), University of Twente, P.O. Box 217, 7500 AE, Enschede, The Netherlands*

² *Biophysical Engineering, Faculty of Science & Technology and MESA+ Institute for Nanotechnology, University of Twente, P.O. Box 217, 7500 AE, Enschede, The Netherlands*

Abstract

The mechanical properties of single electrospun collagen fibers were investigated using scanning mode bending tests performed with an AFM. Electrospun collagen fibers with diameters ranging from 100 to 600 nm were successfully produced by electrospinning of an 8% w/v solution of acid soluble collagen in 1,1,1,3,3,3-hexafluoro-2-propanol (HFP). Circular Dichroism (CD) spectroscopy showed that 45% of the triple helical structure of collagen molecules was denatured in the electrospun fibers. The electrospun fibers are water soluble and became insoluble after cross-linking with glutaraldehyde vapor for 24 hours. The bending moduli and shear moduli of both non- and cross-linked single electrospun collagen fibers were determined by scanning mode bending tests after depositing the fibers on glass substrates containing micro-channels. The bending moduli of the electrospun fibers at ambient conditions ranged from 1.3 to 7.8 GPa and ranged from 0.07 to 0.26 MPa for fibers immersed in PBS buffer. As the diameter of the fibrils increased, a decrease in bending modulus was measured clearly indicating mechanical anisotropy of the fiber. Cross-linking of the electrospun fibers with glutaraldehyde vapor increased the shear modulus of the fiber from ~ 30 MPa to ~ 50 MPa at ambient conditions.

* This chapter has been published in *Biomaterials* **2008**; 29: 955-962.

5.1 Introduction

Fibers with diameters ranging from a few to hundreds of nanometers have found a broad range of applications in different areas, such as reinforcement in composite materials, highly porous membrane supports and electronics [1-3]. Both synthetic and natural polymer fibers have been extensively studied for the preparation of scaffolds for tissue engineering applications [4-6]. It is envisaged that the high surface to volume ratio of fiber meshes enhances the efficiency of mass transport and cell attachment to scaffolds [5,7].

Electrospinning is a suitable technique for the production of fibers with diameters smaller than 1 μm and has a number of advantages. By applying a high voltage to a polymer solution, polymer fibers can be produced in a continuous and relatively easy way. Also, electrospinning allows control over the fiber diameter and orientation of the fibers in a mesh [8]. Many biodegradable synthetic polymers have been electrospun into fibrous meshes and successfully used in cell culture systems for tissue engineering [9-11]. Recently, several studies have been performed using natural polymer fibers as scaffolding materials because of their biocompatibility and resorbability [12-14]. Electrospinning was used to prepare tubular scaffolds of soluble collagen type I for tissue engineering of blood vessels [15]. These electrospun collagen fibers had diameters ranging from 100 to 700 nm. Preliminary cell culture experiments have been performed successfully with the obtained collagen tubular scaffolds.

In order to mimic the physical and chemical structure of the native extracellular matrix, understanding of the material properties is important for an optimal scaffold design. The mechanical properties of the scaffold must be taken into account because the scaffold must be able to withstand the forces exerted by e.g. pulsed blood flow [7]. Also, different types of cells may require different mechanical properties of the scaffolds. Therefore, understanding the mechanical behavior of the single fibers in a scaffold is essential in optimizing the scaffold design.

Although polymer fibers have been successfully used in the preparation of scaffolds, only recently a few studies have focused on the mechanical properties of single fibers in the sub-micron range [7,16,17]. By performing tensile tests with single polymer fibers, the Young's modulus, tensile strength and the strain at break of the tested fibers were determined. These studies however only allow the assessment of properties in the longitudinal direction. Alignment and reorientation of molecules is known to occur during

electrospinning [18,19]. Knowing the shear modulus of electrospun fibers is also important in investigating their effect on cellular activities.

In this paper we present a study on the mechanical properties of single electrospun collagen fibers. Micromechanical bending tests were performed on native and glutaraldehyde cross-linked single electrospun fibers using atomic force microscopy. Both bending moduli and shear moduli of the electrospun collagen fibers were determined. The mechanical anisotropy of the electrospun fibers was investigated and related to the structure of the fibers.

5.2 Materials and Methods

5.2.1 Electrospinning of collagen

All electrospinning experiments were performed using a setup schematically depicted in Fig. 5.1. An 8% w/v solution of acid soluble collagen type I from calf skin (Elastin Products Company Inc., Owensville, MO, USA) in 1,1,1,3,3,3-hexafluoro-2-propanol (HFP) was prepared for electrospinning [15]. The spinning solution was transferred to a 50 ml syringe (Perfusor-Spritze OPS, B-Brain, Melsungen, Switzerland) which was connected to a syringe pump (Perfusor E segura, B-Braun, Melsungen, Switzerland). The spinning solution was pushed through a silicon tube (Nalgene 50, 1.6 mm ID \times 3.1 mm OD, Rochester, NY, USA) into a blunt steel needle (22G 1 $\frac{1}{4}$ ", 0.7 mm ID \times 30 mm length) at a constant speed of 80 μ l/min. The needle was attached to the electrode of a high voltage supply (Bertan Associates Inc., 230R, Hicksville, NY, USA). A stainless steel ring was connected to the same electrode and placed just under the needle tip to stabilize the jet and direct it downwards. A grounded piece of aluminum foil (12 \times 12 cm²) was placed at a 15 - 20 cm distance from the needle tip to collect the fibers. A continuous production of collagen electrospun fibers was obtained at 19 - 21 kV.

During the electrospinning Quartz glass substrates containing micro-channels with a depth of 600 nm and width of 3 μ m were placed on the aluminum foil for 30 s to collect a suitable amount of electrospun fibers for the micromechanical bending tests. Electrospun fibers were also collected on a rotating rectangular stainless steel wire frame (wire diameter 0.5 mm, 12 \times 3 cm²) placed just above the collecting aluminum plate in order to collect samples for determining the primary amino group content and the denaturation temperature of the collagen fibers. The collecting time was varied between 30 and 180 min.

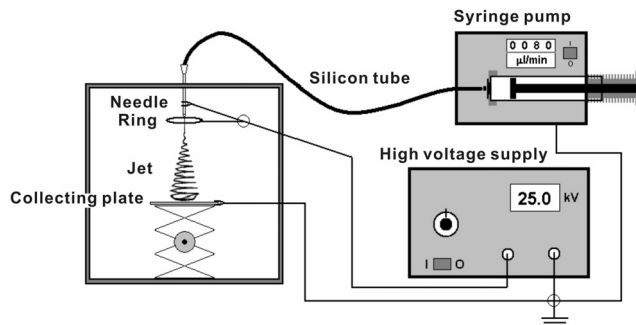


Figure 5.1 Schematic representation of the electrospinning set-up.

5.2.2 Cross-linking of the electrospun fibers

Electrospun collagen fibers cut from the wire frame and deposited on the glass substrate containing microchannels were cross-linked using glutaraldehyde vapor [15,20,21]. Cross-linking was carried out by placing the substrate with the electrospun collagen fibers above 20 ml of 25 wt% glutaraldehyde solution (grade I, Sigma, Zwijndrecht, the Netherlands) in a sealed beaker for 24 h at room temperature. After the cross-linking reaction, the samples were left to dry at ambient conditions for at least 24 hours under a glass cover. The cross-linked and non-crosslinked electrospun collagen fibers were immersed in MilliQ water for 4 h to test their solubility.

5.2.3 Determination of the primary amino group content

The primary amino group content of non- and cross-linked electrospun collagen fibers was determined using the 2,4,6-trinitrobenzenesulfonic acid (TNBS) assay. Electrospun collagen fibers (3-5 mg) cut from the wire frame were incubated for 30 min in 1 ml of a 4 wt % solution of NaHCO_3 . To this mixture 1 ml of a freshly prepared solution of TNBS (0.5 wt %) in 4 wt % NaHCO_3 was added. The resulting mixture was left for 2 h at 40°C. After the addition of HCl (3 ml, 6 M), the temperature was raised to 60°C. Hydrolyzation of collagen was achieved within 90 min. The resulting solution was diluted with 5 ml MilliQ water and cooled to room temperature. The absorbance at 420 nm was measured using a Varian Cary 300 Bio spectrophotometer (Middelburg, the Netherlands). A blank was prepared applying the same procedure, except that HCl was added before the addition of TNBS. The absorbance was correlated to the concentration of free amino groups using a calibration curve obtained with glycine. The primary amino group content was expressed as the number of primary amino groups per 1000 amino acids (n/1000).

5.2.4 Circular Dichroism (CD)

Solutions of untreated acid soluble collagen and electrospun collagen fibers were prepared by dissolving 5 mg dry material in 5 ml acetic acid (0.1 M) and stirring for 3 h at room temperature. Subsequently, the clear solutions were equilibrated overnight at 4°C. A solution prepared from untreated acid soluble collagen was placed in an oven at 95°C for 20 min to obtain thermally denatured acid soluble collagen [22,23]. CD spectra (Jasco J-715 spectropolarimeter) were recorded at 25°C over the wavelength interval 180 to 260 nm at a scan speed of 20 nm/min and data were averaged from 5 scans. A bandwidth of 1 nm and a time constant of 1 s were used in the measurements. The path length of the cylindrical sample cell was 0.1 mm. A reference spectrum of 0.1 M acetic acid was recorded, and subtracted from the sample spectra. The circular dichroism of the collagen is expressed as mean molar residual ellipticity.

The fraction of triple helical collagen in the samples was calculated using Eq. 5.1 assuming a linear dependence of the individual data [23,24].

$$f_{TH} = \frac{[\theta]_E - [\theta]_{DN}}{[\theta]_C - [\theta]_{DN}} \times 100 \quad (5.1)$$

Where:

- f_{TH} = fraction triple helices in the electrospun fibers determined at wavelength λ (%)
- $[\theta]_E$ = ellipticity of electrospun collagen at wavelength λ ($\text{deg}\cdot\text{cm}^2\cdot\text{dmol}^{-1}$)
- $[\theta]_{DN}$ = ellipticity of denatured soluble collagen at wavelength λ ($\text{deg}\cdot\text{cm}^2\cdot\text{dmol}^{-1}$)
- $[\theta]_C$ = ellipticity of soluble collagen at wavelength λ ($\text{deg}\cdot\text{cm}^2\cdot\text{dmol}^{-1}$)

5.2.5 Micromechanical tests of electrospun collagen fibers using AFM

Micromechanical bending tests were performed as described in Chapter 4 [25]. In brief, triangular silicon nitride cantilevers (coated sharp microlevers MSCT-AUHW, type F, spring constant $k = 0.5$ N/m, Veeco, Cambridge, UK) of which the tips were removed were used in the bending tests. The spring constant of each tip-less cantilever was calibrated by pushing on a pre-calibrated cantilever as described elsewhere [26]. Single electrospun collagen fibers freely and perpendicularly spanning multiple channels of the glass substrate were selected for the bending tests in scanning mode. The electrospun collagen fiber was bent by pushing with the AFM cantilever in the z-direction. A typical piezo movement of 1.5 - 3.0 μm with a frequency of 1.3 Hz in the z-direction was applied. In the scanning mode bending test, after every step of bending, the tip is moved one step further along the fiber. A complete scan consists of 256 steps, the total measuring time is

200 s, and the total scanning distance was chosen to be slightly larger than the channel width. The mechanical properties of the electrospun collagen fibers were investigated both at ambient conditions and in PBS buffer (pH = 7.4).

5.2.6 Data analysis

A custom computer program, written in Labview (version 6.1, National Instruments, Austin, Texas, USA) was used to analyze the data. A force-displacement curve of every 256 bending measurements was obtained using the following equations:

$$z = A - D \quad (5.2)$$

$$F = D \times k \quad (5.3)$$

in which z is the displacement of the fiber in the z -direction during bending, A is the piezo movement in the z -direction and D is the deflection of the cantilever in nm. F is the force applied to the fiber and k is the calibrated spring constant of the cantilever.

The bending modulus (E_{bending}) of the single electrospun fibers was deduced by fitting the slope of the force-displacement curve at different positions (x) of the suspended fiber to the following equation [27]:

$$\frac{dF}{dz} = \frac{3 \times l^3 \times E_{\text{bending}} \times I}{(1 - x)^3 \times x^3} \quad (5.4)$$

In which x is the relative position along the fiber ($0 \leq x \leq l/2$), l is the length of the fiber spanning the channel, I is the moment of inertia ($I = \frac{1}{4} \pi R^4$), dF/dz is the slope of the force-displacement curve obtained during bending of the electrospun fibers. The fiber is considered to be a rod with a circular cross-section with radius R .

5.2.7 Morphology

The morphology and diameter of all micromechanically tested electrospun collagen fibers was determined from SEM measurements (Leo Gemini 1550 FEG-SEM, Oberkochen, Germany). No sputter coating was applied on the sample before imaging.

5.3 Results and Discussion

5.3.1 Electrospun collagen fibers

Electrospinning of soluble collagen into meshes that can be applied for tissue engineering applications is not possible using aqueous solutions but was recently accomplished by Matthews *et al.* [15] using HFP. The viscosity and conductivity of the solution, the spinning voltage, the flow rate and the collecting distance were adjusted in preliminary experiments to optimize the electrospinning conditions. During electrospinning of an 8% w/v collagen solution in HFP, jet formation was first observed at 12 kV. Increasing the voltage to values between 19 - 21 kV offered operating conditions to electrospin continuously for more than 3 h. Due to evaporation of HFP, dry collagen fibers could be collected at a distance of 15 - 20 cm on a grounded plate. A deposition rate of ~ 22 mg/h was obtained using a wire frame collector placed just above the grounded plate. It is noted that the collagen fibers produced by this method using the mentioned parameters have similar dimensions as native collagen fibrils and range from 100 to 600 nm.

In the electrospinning process, the morphology of the resulting electrospun fiber was influenced by many parameters, [2,28,29] and was analyzed by SEM. As shown in Fig. 5.2A, at above mentioned electrospinning condition, most fibers have a smooth surface. Some split and ribbon-type fibers were also observed. High resolution SEM measurements showed that the characteristic D-period found in native collagen fibrils was not present (Fig. 5.2B). It is known that soluble collagen molecules assemble in a structure similar to native collagen fibrils depending on the pH and electrolytes [30,31]. The absence of a D-period indicates that the structure is different from that of native collagen. Moreover, it is known that aliphatic alcohols affect the secondary structure of proteins [32,33]. Also, in the specific case of collagen, it has been reported that HFP as a highly fluorinated alcohol destabilizes the native triple helical structure of the protein although the exact mechanism of the process is not completely understood yet [34,35].

Electrospun collagen fibers were collected on glass substrates containing micro-channels during electrospinning for the micromechanical tests. The diameter and suspended length of every tested fiber was determined from a SEM image (Fig. 5.2C) after the bending measurements.

5.3.2 Collagen CD spectral analysis

To gain information on the fraction of the triple helical secondary structure present in the electrospun collagen fibers, CD measurements were performed. The triple helical

secondary structure found in native collagen gives rise to a characteristic positive peak at around 220 nm in the CD spectrum which decreases upon denaturation. It was reported that complete denaturation results in the total disappearance of the positive peak at 220 nm [22,23]. The CD spectra of the electrospun collagen fiber, untreated acid soluble collagen and thermally denatured acid soluble collagen have been measured and are shown in Fig. 5.3. The general shape and peaks of the spectrum change when the collagen is denatured and are in agreement with literature data [22,23]. The spectrum of the resolubilized electrospun collagen fibers displays positive and negative peaks with lower intensity compared to the native soluble collagen, which implies that the electrospun collagen was partly denatured. As mentioned above, using HFP as a solvent may destabilise the native helical structure of the collagen. The triple helical fraction of the partly denatured electrospun collagen fibers is approximately 45% calculated from the positive peak using Eq. 5.1. The lower triple helical content might alter or disturb the hierarchical order as seen in native soluble collagen, and explain the absence of any periodicity in the structure.

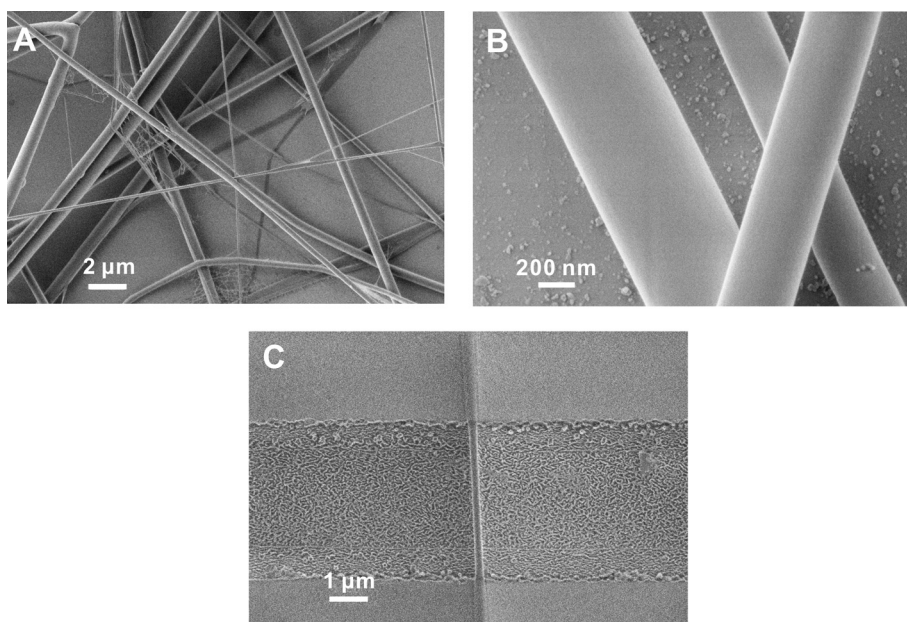


Figure 5.2 (A) SEM image of collagen fibers electrospun from an 8% w/v solution of acid soluble collagen type I from calf skin in HFP. (B) High resolution SEM image of electrospun collagen fibers showing a smooth surface. (C) SEM image of an electrospun collagen fiber spanning a microchannel in the glass substrate. The channel width is $\sim 4 \mu\text{m}$ and the diameter of this electrospun fiber is $\sim 190 \text{ nm}$.

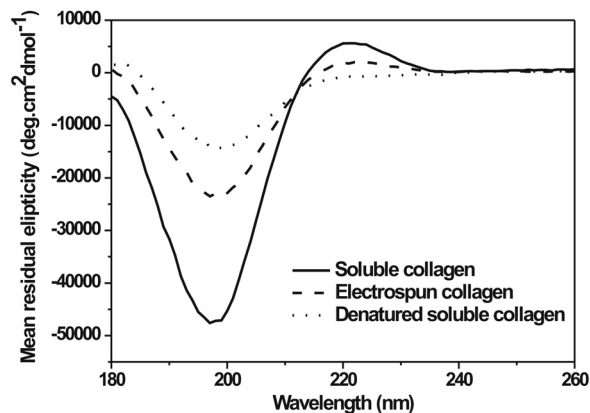


Figure 5.3 Circular dichroism (CD) spectra of solutions containing electrospun collagen, soluble collagen, and denatured soluble collagen in 0.1 M acetic acid at 25 °C. All spectra shown were obtained after subtraction of baseline spectrum for the acetic acid.

5.3.3 Fiber stability in aqueous solution before and after cross-linking

Non-crosslinked electrospun fibers (Fig. 5.4A) were soluble in water. After 4 hours immersion in MilliQ water, the fibers appear to flatten (Fig. 5.4B). Thus, to potentially use electrospun collagen fibers for biomedical applications, like a scaffold material, cross-linking of the collagen is necessary. Cross-linking was performed by placing the electrospun fibers in a sealed beaker filled with glutaraldehyde (GA) vapor. The stability of the cross-linked fibers was subsequently tested by incubating the samples in water for 4 hours. SEM pictures as represented in Fig. 5.4C and Fig. 5.4D show that these fibers cross-linked with GA preserve their fibrous structure on the supporting glass surface.

The degree of crosslinking was estimated from the decrease in primary amino groups when compared to non-crosslinked collagen. The primary amino group content decreased from 36 to 4 per 1000 amino acids and was comparable to previously reported data on GA crosslinking [36].

5.3.4 Micromechanical properties of electrospun collagen fibers

After a fiber that perpendicularly crossed a channel in the glass substrate was selected, the cantilever was positioned above the fiber at the edge of the channel. Bending experiments were then performed by recording 256 force-distance curves along the suspended fiber. The vertical piezo movement was between 1.5 μm and 3.0 μm and adjusted in such a way that the maximum displacement of the fiber was ~ 200 nm. As shown in Fig. 5.5(A), a linear increase of force was found from bending the electrospun fibers. The slope (dF/dz)

of each force-displacement curve of the tested electrospun fibers was determined by a linear fit. Fitting the data as a function of the scanning position to Eq. 5.4, afforded the E_{bending} of the single electrospun collagen fiber. As shown by the curve fit (Eq. 5.4) in Fig. 5.5(B), the experimental data do fit to Eq. 5.4 with a standard error of 2-6% in the least squares fit parameter.

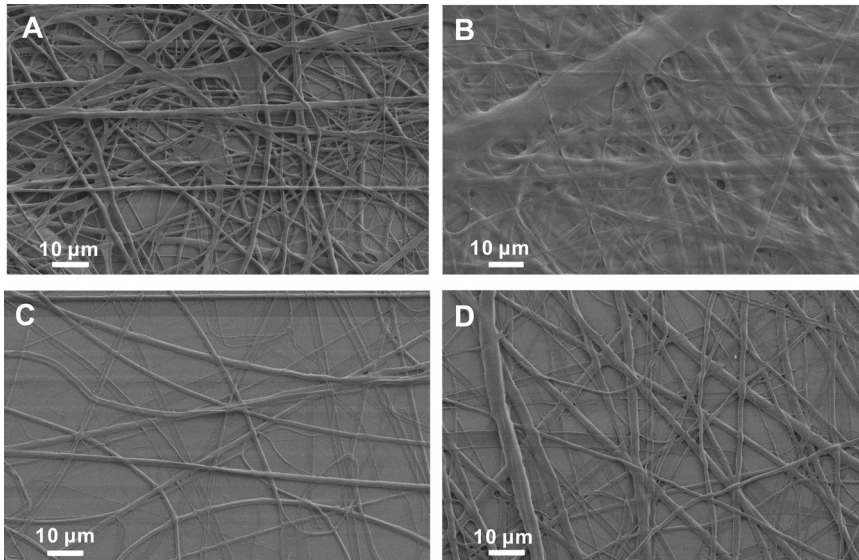


Figure 5.4 SEM images of electrospun collagen fibers. (A) without cross-linking before immersion in MilliQ water; (B) without cross-linking after immersion in MilliQ water at room temperature for 4 h. (C) cross-linked with glutaraldehyde before immersion in MilliQ water (D) cross-linked with glutaraldehyde after immersion in MilliQ water at room temperature for 4 h.

The bending moduli of several electrospun fibers determined at ambient conditions with diameters ranging from 150 to 450 nm are presented in Fig. 5.6(A). The bending modulus decreases from 7.5 ± 1.6 GPa to 1.4 ± 0.2 GPa with increasing fiber diameter up to ~ 250 nm and remains at a constant value of ~ 1.4 GPa for fibers with larger diameters. It is interesting to note that the bending modulus of the fibers is comparable to the modulus of native collagen fibrils with similar diameters as reported in Chapter 4 [25] although the electrospun fibers are partly denatured. This can be explained by the alignment of individual molecules preferably in the axial direction during the spinning process [18,19]. The alignment of the collagen molecules may enhance intermolecular interactions and result in a bending modulus of the electrospun collagen fibers, similar to that of native collagen fibrils.

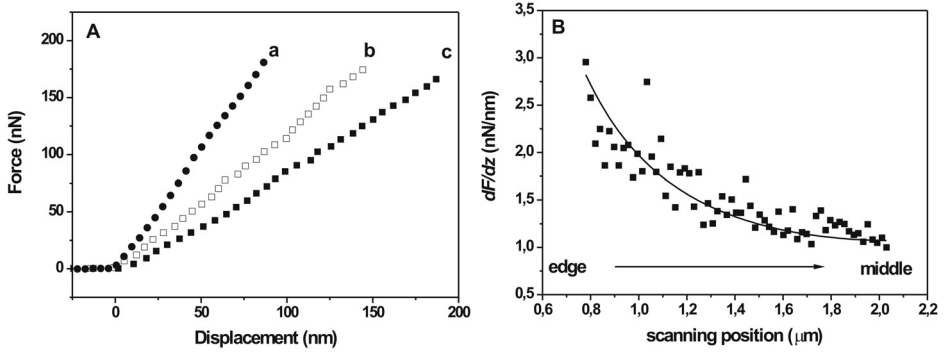


Figure 5.5 (A) Three force-displacement curves obtained from bending the electrospun collagen fiber at different positions: a: at the edge of the channel; b: between the edge and middle of the channel; c: at the middle of the channel. (B) Graph showing the slope (dF/dz) of the force displacement curves as a function of the scanning position. A curve fit using Eq. 5.4 is shown as a solid line.

For glutaraldehyde cross-linked electrospun collagen fibers the mechanical properties were measured both for fibers at ambient conditions and for fibers in PBS buffer. The bending modulus of the fibers was not affected by the cross-linking process. The same values and dependency on the fiber diameter were observed (Fig. 5.6A). When immersed in PBS buffer lower E_{bending} values were obtained but the moduli show a similar dependency on the fiber diameter (Fig. 5.6C). The dependence of the bending modulus on the diameter indicates the presence of shearing between segments in the electrospun collagen fibers [37,38]. Using the applied force and the displacement of the fiber at the middle of the channel, the shear modulus can be calculated from the following equations [27]:

$$z = z_B + z_S = Fl^3/192EI + f_S Fl/4GA = Fl^3/192E_{\text{bending}}I \quad (5.5)$$

And therefore:

$$\frac{1}{E_{\text{bending}}} = \frac{1}{E} + \frac{12f_S}{G} \times \left(\frac{R^2}{l^2}\right) \quad (5.6)$$

In which, z is the total displacement of the fiber in the z -direction, z_B is the deflection from bending, z_S is the deflection from shearing, E is the Young's modulus, G is the shear modulus, f_S is the form factor of shear which equals 10/9 for a cylinder and A is the cross-sectional area of the fiber.

Plotting $1/E_{\text{bending}}$ versus (R^2/l^2) , the shear modulus (G) of the (non-) cross-linked fibers at ambient conditions was determined from the slope using a linear fit as shown in Fig. 5.6B. The shear modulus of the electrospun collagen fibers was 29.4 ± 2.6 MPa, which was approximately two magnitudes lower than the bending modulus and increased to 48.0 ± 6.0 MPa for cross-linked fibers. As shown above, the primary amino group content decreased upon glutaraldehyde cross-linking from 35 to 4. The intra- and inter-molecular covalent bonds formed between glutaraldehyde and the amine groups of collagen are responsible for the improved mechanical strength in the lateral direction. The shear modulus of the cross-linked electrospun collagen fibers in PBS buffer was found to be 5 MPa (Fig. 5.6D) which was 20 - 50 times lower than the bending modulus.

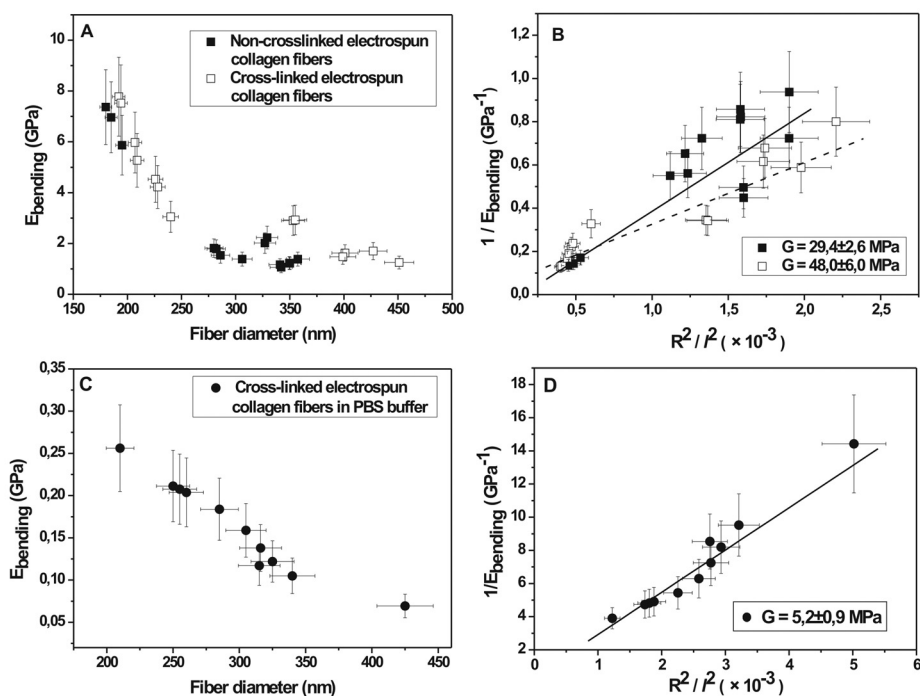


Figure 5.6 (A) Bending modulus as a function of the diameter of non-crosslinked electrospun collagen fibers (filled squares) and cross-linked electrospun fibers (open squares) at ambient conditions. (B) Reciprocal bending modulus (E_{bending}) as a function of R^2/l^2 of non-crosslinked electrospun collagen fibers (filled squares) and cross-linked electrospun fibers (open squares) at ambient conditions. The slope of the linear fit (solid line: non-crosslinked electrospun fibers; dotted line: cross-linked electrospun fibers) equals to $120/(9 \times G)$, from which the shear modulus (G) was calculated. (C) Bending modulus as a function of the diameter of cross-linked electrospun fibers (filled circles) in PBS buffer. (D) Reciprocal bending modulus (E_{bending}) as a function of R^2/l^2 of cross-linked electrospun fibers (filled circle) in PBS buffer. The shear modulus (G) was calculated as in (B).

The fact that the shear modulus of the fiber is one to two magnitudes lower than the bending modulus indicates that the single electrospun fibers are mechanically anisotropic. From the CD results, it was shown that a high percentage of the collagen triple helical structure has been changed to random coil in the electrospun fibers. Therefore, the shearing could result from displacement between collagen molecules and individual α -chains with respect to each other.

From the micromechanical tests, the bending and shear moduli of single electrospun collagen fibers were calculated (results summarized in Table 5.1). The results indicate that the mechanical properties of single electrospun collagen fibers are comparable to the mechanical properties of native collagen fibrils, a principal structural element of fiber forming collagens. The resemblance of the mechanical properties makes electrospun collagen fibers and also collagen-polymer composites promising materials to be applied as scaffolds materials in tissue engineering.

Table 5.1 Bending and shear moduli of electrospun collagen fibers obtained from scanning bending measurements

Electrospun collagen fibers	Conditions	Range of Diameters (nm) ^c	Bending moduli (GPa) ^d	Shear modulus ^e (MPa)
Non-cross-linked	Dry	179 ~ 356	7.5 ~ 1.4	29.4 ± 2.6
Cross-linked ^a	Dry	191 ~ 450	7.8 ~ 1.3	48.0 ± 6.0
Cross-linked ^a	PBS buffer ^b	210 ~ 425	0.26 ~ 0.07	5.2 ± 0.9

a. Cross-linking was performed with glutaraldehyde vapor.

b. PBS: phosphate buffered saline pH = 7.4

c. Range of diameters: the ranges of the diameter from different electrospun fibers used in the mechanical tests. The error (S.E.M.) of the diameter of individual fiber is ~ 3% calculated from multiple measurements on the same fiber.

d. Ranges of bending moduli: the range of bending moduli determined from electrospun fibers with different diameters. A 23% relative error is estimated for the bending modulus of individual fibers [25].

e. The error in the shear modulus is the standard error of the weighted least squares fit parameter.

5.4 Conclusions

By electrospinning soluble collagen in HFP, it was possible to obtain collagen fibers with diameters between 100 nm and 600 nm. Cross-linking in glutaraldehyde vapour for 24 hours introduced a high degree of cross-linking in the electrospun fibers and afforded water-resistant fibers. The CD spectrum of electrospun collagen fibers indicates that the fibers were partly denatured.

The mechanical properties of single electrospun collagen type I fibers were investigated by micromechanical bending tests in scanning mode. The bending moduli were derived from the slopes of force-displacement curves. The bending moduli of the cross-linked electrospun collagen fibers at ambient conditions range from 1.3 GPa to 7.8 GPa with diameters decreasing from 450 to 190 nm and decrease ~ 20 times when the fibers are immersed in PBS buffer. A high degree of alignment of the collagen molecules in the electrospun collagen fibres can explain the bending moduli observed similar to that of native collagen fibrils. By testing fibers with different diameters, the shear modulus of the tested collagen fibers was estimated from the relationship between bending modulus and the length to diameter ratio. The electrospun fibers showed anisotropic mechanical properties with a two orders of magnitude lower shear modulus compared to the bending modulus. Cross-linking with glutaraldehyde increased the shear modulus and the water insolubility of the electrospun fibers. Evaluation of the mechanical properties of single electrospun collagen fibers results in a better understanding of the potential use of the electrospun fibers as scaffolds for e.g. tissue engineering.

Acknowledgement

This research is financially supported by the Softlink program of ZonMw. Project number: 01SL056.

References

1. Frenot A, Chronakis IS. Polymer nanofibers assembled by electrospinning. *Curr. Opin. Colloid Interface Sci.* **2003**; 8: 64-75.
2. Li D, Xia Y. Electrospinning of nanofibers: Reinventing the wheel? *Adv. Mater.* **2004**; 16: 1151- 1170.
3. Bognitzki M, Czado W, Frese T, Schaper A, Hellwig M, Steinhart M, Greiner A, Wendorff JH. Nanostructured fibers via electrospinning. *Adv. Mater.* **2001**; 13: 70-72.
4. Xu CY, Inai R, Kotaki M, Ramakrishna S. Aligned biodegradable nanofibrous structure: a potential scaffold for blood vessel engineering. *Biomaterials* **2004**; 25: 877-886.
5. Buttafoco L, Kolkman N, Engbers-Buijtenhuijs P, Poot A, Dijkstra PJ, Vermes I, Feijen J. Electro-spinning of collagen and elastin for tissue engineering applications. *Biomaterials* **2006**; 27: 724-734.
6. Khil MS, Kim HY, Kim MS, Park SY, Lee DR. Nanofibrous mats of poly-(trimethylene terephthalate) via electrospinning. *Polymer* **2004**; 45: 295-301.
7. Chew SY, Hufnagel TC, Lim CT, Leong KW. Mechanical properties of single

- electrospun drug encapsulated nanofibres. *Nanotechnology* **2006**; 17: 3880-3891.
8. Teo WE, Ramakrishna S. A review on electrospinning design and nanofibre assemblies. *Nano-technology* **2006**; 17: R89-106.
 9. Zhang YZ, Venugopal J, Huang ZM, Lim CT, Ramakrishna S. Characterization of the surface biocompatibility of the electrospun PCL-collagen nanofibers using fibroblasts. *Biomacromolecules* **2005**; 6: 2583-2589.
 10. Zhong S, Teo WE, Zhu X, Beuerman R, Ramakrishna S, Yung LYL. Formation of Collagen-glycosaminoglycan blended nanofibrous scaffolds and their biological properties. *Biomacromolecules* **2005**; 6: 2998-3004.
 11. He W, Yong T, Ma ZW, Inai R, Teo WE, Ramakrishna S. Biodegradable polymer nanofiber mesh to maintain functions of endothelial cells. *Tissue Eng.* **2006**; 12: 2457-2466.
 12. Zhang YZ, Venugopal J, Huang ZM, Lim CT, Ramakrishna S. Crosslinking of the electrospun gelatin nanofibers. *Polymer* **2006**; 47: 2911-2917.
 13. Ayres C, Bowlin GL, Henderson SC, Taylor L, Shultz J, Alexander J, Telemeco TA, Simpson DG. Modulation of anisotropy in electrospun tissue-engineering scaffolds: Analysis of fiber alignment by the fast fourier transform. *Biomaterials* **2006**; 27: 5524-5534.
 14. Bhattarai N, Li Z, Edmondson D, Zhang M. Alginate-based nanofibrous scaffolds: structural, mechanical, and biological properties. *Adv. Mater.* **2006**; 18: 1463-1467.
 15. Matthews JA, Wnek GE, Simpson DG, Bowlin GL. Electrospinning of collagen nanofibers. *Biomacromolecules* **2002**; 3: 232-238.
 16. Inai R, Kotaki M, Ramakrishna S. Structure and properties of electrospun PLLA single nanofibres. *Nanotechnology* **2005**; 16: 208-213.
 17. Tan EPS, Goh CN, Sow CH, Lim CT. Tensile test of a single nanofiber using an atomic force microscope tip. *Appl. Phys. Lett.* **2005**; 86: 073115-1-3.
 18. Gu SY, Wu QL, Ren J, Vancso GJ. Mechanical properties of a single electrospun fiber and its structures. *Macromol. Rapid. Commun.* **2005**; 26: 716-720.
 19. Reneker DH, Chun I. Nanometre diameter fibers of polymer, produced by electrospinning. *Nanotechnology* **1996**; 7: 216-223.
 20. Ramires PA, Milella E. Biocompatibility of poly(vinyl alcohol)-hyaluronic acid and poly(vinyl alcohol)-gellan membranes crosslinked by glutaraldehyde vapors. *J. Mater. Sci.: Mater. in Med.* **2002**; 13: 119-123.
 21. Chen GP, Ushida T, Tateishi T. A hybrid network of synthetic polymer mesh and collagen sponge. *Chem. Commun.* **2000**; 16: 1505-1506.
 22. Usha R, Ramasami T. The effects of urea and n-propanol on collagen denaturation: using DSC, circular dichroism and viscosity. *Thermo.chim. Acta.* **2004**; 409: 201-206.
 23. Long CG, Braswell E, Zhu D, Apigo J, Baum J, Brodsky B. Characterization of collagen-like peptides containing interruptions in the repeating Gly-X-Y sequence. *Biochemistry* **1993**; 32: 11688-11695.
 24. Holmgren SK, Bretscher LE, Taylor KM, Raines RT. A hyperstable collagen mimic.

- Chem. Biol.* **1999**; 6: 63-70.
25. Yang L, van der Werf KO, Fitié CFC, Bennink ML, Dijkstra PJ, Feijen J. Mechanical properties of native and cross-linked type I collagen fibrils. *Biophys. J.* **2007**; Online.
 26. Torii A, Sasaki M, Hane K, Okuma S. A method for determining the spring constant of cantilevers for atomic force microscopy. *Meas. Sci. Technol.* **1996**; 7: 179-184.
 27. Gere J, Timoshenko SP. *In Mechanics of materials.* Chapman & Hall, London, **1991**.
 28. Huang ZM, Zhang YZ, Kotaki M, Ramakrishna S. A review on polymer nanofibers by electro- spinning and their applications in nanocomposites. *Compos. Sci. Technol.* **2003**; 63: 2223-2253.
 29. Doshi J, Reneker DH. Electrospinning process and applications of electrospun fibers. *J. Electrostat.* **1995**; 35: 151-160.
 30. Goh MC, Paige MF, Gale MA, Yadegari I, Edirisinghe M, Strzelczyk J. Fibril formation in collagen. *Physica A* **1997**; 239: 95-102.
 31. Jiang F, Hörber H, Howard J, Müller DJ. Assembly of collagen into microribbons: effects of pH and electrolytes. *J. Struct. Biol.* **2004**; 148: 268-278.
 32. Konno T, Iwashita J, Nagayama K. Fluorinated alcohol, the third group of cosolvents that stabilize the molten-globule state relative to a highly denatured state of cytochrome c. *Protein. Sci.* **2000**; 9: 564-569.
 33. Hirota N, Mizuno K, Goto Y. Cooperative α -helix formation of β -lactoglobulin and melittin induced by hexafluoroisopropanol. *Protein. Sci.* **1997**; 6: 416-421.
 34. Bianchi E, Rampone R, Tealdi A, Ciferri A. The role of aliphatic alcohols on the stability of collagen and tropocollagen. *J. Biol. Chem.* **1970**; 245: 3341-3345.
 35. Doillon CJ, Drouin R, Côte MF, Dallaire N, Pageau JF, Laroche G. Chemical inactivators as sterilization agents for bovine collagen materials. *J. Biomed. Mater. Res.* **1997**; 37: 212-221.
 36. Olde Damink LHH, Dijkstra PJ, van Luyn MJA, van Wachem PB, Nieuwenhuis P, Feijen J. Glutaraldehyde as a cross-linking agent for collagen-based biomaterials. *J. Mater. Sci.: Mater. in Med.* **1995**; 6: 460-472.
 37. Kis A, Kasas S, Babić B, Kulik AJ, Benoît W, Briggs GAD, Schönenberger C, Catsicas S, Forró L. Nanomechanics of microtubules. *Phys. Rev. Lett.* **2002**; 89: 248101-1-4.
 38. Salvétat JP, Briggs GAD, Bonard JM, Bacsá RR, Kulik AJ, Stöckli T, Burnham NA, Forró L. Elastic and shear moduli of single-walled carbon nanotube ropes. *Phys. Rev. Lett.* **1999**; 82: 944-947.

Micro-tensile Testing of Individual Native and Cross-linked Collagen Type I Fibrils*

Lanti Yang¹, Kees O. van der Werf², Martin L. Bennink², Pieter J. Dijkstra¹, Jan Feijen¹

¹ *Polymer Chemistry and Biomaterials, Faculty of Science & Technology and Institute for Biomedical Technology (BMTI), University of Twente, P.O. Box 217, 7500 AE, Enschede, The Netherlands*

² *Biophysical Engineering, Faculty of Science & Technology and MESA+ Institute for Nanotechnology, University of Twente, P.O. Box 217, 7500 AE, Enschede, The Netherlands*

Abstract

Tensile properties of individual collagen fibrils of approximately 200 nm in diameter were determined using a slightly adapted AFM system. After depositing fibrils from a dilute suspension on glass substrates which were partially coated with Teflon, an individual collagen fibril was selected and fixed between the AFM cantilever and the glass substrate for tensile testing. An additional calibrated piezo tube which can extend up to 400 μm was added to allow stretching of collagen fibrils up to failure. At ambient conditions a linear stress-strain behavior of the collagen fibrils was found. The mechanical behavior was reversible up to a maximum stress of 80 ± 20 MPa, and a Young's modulus of 2.5 ± 0.9 GPa was determined from the stress-strain curve. When fibrils were loaded at higher stresses, hysteresis resulting from the viscoelastic properties of collagen was observed. Subsequent loading and unloading cycles revealed a permanent lengthening of the fibril after each cycle. When performing tensile tests of fibrils immersed in PBS buffer, a non-linear stress-strain behavior was found up to a stress of 5 MPa. At higher stresses, the stress-strain curve became linear and a Young's modulus of 0.6 GPa was calculated. For the first time a failure stress of 0.06 ± 0.01 GPa and a strain at break of 13 ± 2 % of individual collagen fibrils in PBS buffer could be determined. These values are similar to

* This chapter is to be submitted for publication.

the mechanical properties of tendon and collagen type I fibers. Furthermore, the influence of cross-linking, a method widely used for stabilizing collagen in biomedical applications, on the mechanical properties was determined. Both carbodiimide cross-linking and glutaraldehyde cross-linking resulted in an increase of the failure stress and strain at break of collagen fibrils. Compared to native collagen fibrils, an increase of the Young's modulus was only found for collagen fibrils cross-linked with glutaraldehyde. This may be related to cross-links formed between micro-fibrils by glutaraldehyde, which is not possible upon cross-linking with a carbodiimide.

6.1 Introduction

Of the at least 25 types of collagen proteins known, fibril forming collagen is an important component in many tissues [1]. The fibril-forming collagens provide the structural framework and are largely responsible for the biomechanical properties of tissues [2]. Collagen-based tissues show mechanical properties [3] which are related to their hierarchical structure. A typical example is tendon tissue consisting mostly of collagen type I. The collagen structure in tendon is organized in a hierarchical manner comprising collagen molecules, micro-fibrils, fibrils, fibers, fiber bundles, fascicles and tendon units [4].

The outstanding mechanical properties of tendon are due to this specific hierarchical structure. One of the challenges is to understand the respective influence of each level to the overall mechanical properties of tendon. The stress-strain behavior at the tendon level has been a subject of several studies in the past decades [2-9]. A typical tendon stress-strain behavior in the hydrated state comprises an initial toe region up to a strain of 2%. This toe region represents the removal of the collagen fiber "crimp" [10]. The toe region is followed by the heel region where the slope increases due to stretching of the gap region in the fibrils. Further increasing the stress leads to a linear stress-strain behavior of the tendon (start at ~ 3% strain) where molecular stretching and sliding of molecules with respect to each other are the main mechanisms for the tendon deformation [11]. The slope of the linear region is referred to as the Young's modulus of the tendon. Beyond 8-10% strain, macroscopic failure occurs and further stretch causes the tendon to rupture [4].

The mechanical properties of collagen subunits like fibrils only received attention during the past years although the collagen fibril was considered the basic force-transmitting unit of tendon [6]. Synchrotron X-ray diffraction and simultaneous tensile testing has revealed

different strains at different hierarchical levels of the tendon [3,11,12]. Among them, Sasaki and Odajima [12] studied the force-strain relation of collagen fibrils in bovine Achilles tendon. In their measurements, X-ray diffractometry was performed on a loaded tendon sample to measure the strain at the fibril level. Using the force applied to the bulk tendon, they found a linear force-strain relationship at the fibril level with a Young's modulus of 400 MPa for the fibril in the hydrated state.

With the development of micro-manipulation techniques combined with force measurements, force spectroscopy measurements on subunits of collagen [13-15] especially tensile tests of individual collagen fibrils became possible. Graham *et al.* [16] stretched in vitro-assembled type I collagen fibrils cultured from human fibroblasts using AFM. A highly jagged pattern in the 1.5 to 4.5 nN force range was observed in the stretching part of the force profile, which the authors proposed to relate to the unfolding of the triple-helical polypeptides in the gap region. Eppell *et al.* [17] studied the stress-strain relationship of single hydrated type I collagen fibrils isolated from sea cucumber using an electrostatic actuator and found a Young's modulus of 0.3 - 0.4 MPa at the toe region and 6 GPa at the linear region of the stress-strain curves. With the device they used, it is possible to perform cyclic loading of a fibril. A decrease in the modulus of the fibril after larger numbers of cyclic loading was determined. In our previous work, we showed the possibility of performing tensile tests on single collagen fibrils using a home-built AFM system [18]. However, due to the limitation of the micro-tensile techniques used, the tests could only be performed up to a limited strain. The fibrils failure stress and strain at break, and the stress-strain behavior at higher strains of single collagen fibrils, which are essential in understanding the contribution of each level of the hierarchical structure to the overall mechanical properties of tissue, have still not been measured.

Here, we report on the stress-strain behavior of single collagen fibrils using a modified home-built AFM system which allows an increased strain range for testing. A calibrated piezo tube which can extend up to 400 μm in the z direction at a preset rate was connected to the sample holder of the AFM system. The increased strain range allowed for the first time the recording of the stress-strain behavior of individual collagen fibrils up to the point of failure.

In the biomedical field collagen-based biomaterials received considerable attention [19,20]. For the application of collagen-based materials chemical cross-linking of collagen is often needed. Chemical cross-linking is an efficient method to retard the degradation of

collagen by collagenase and also to inhibit immunological reactions. Cross-linking alters the mechanical properties of collagen-based materials and these properties mainly have been studied at a macroscopic level [21-23]. In general, cross-linking appears to increase the elastic modulus and the failure stress of collagen. However, only initial studies of the effects of cross-linking on the stress-strain behavior of single collagen fibrils were carried out [24]. The influence of different chemical cross-linking agents on the tensile properties of single collagen fibrils was therefore studied in detail.

6.2 Materials and Methods

6.2.1 Preparation of partly Teflon coated glass substrates

Glass substrates (Microscope cover glasses, $\text{\O} = 15$ mm, Marlenfeld GmbH, Germany) were cleaned in piranha solution (3:1 H_2SO_4 : H_2O_2 (30%) by v/v), then rinsed with MilliQ water and ethanol and finally stored in ethanol. Prior to use, the substrates were dried for 4 h at ambient conditions under a cover. Then, the substrates were manually partly dip-coated in a 6 wt% solution of Teflon AF (1601S Dupont, Wilmington, DE, USA) and dried overnight at ambient conditions under a cover.

6.2.2 Deposition of collagen fibrils on the substrates

Bovine Achilles tendon collagen type I from Sigma-Aldrich (Steinheim, Germany) was swollen in hydrochloric acid (0.01 M) overnight at 0°C . The resulting slurry was homogenized and filtered to give a suspension of collagen fibrils [25]. To 1 ml of the suspension, 150 ml of PBS (pH = 7.4) was added. Deposition of the collagen fibrils on the partly Teflon coated glass substrates was done by incubating the substrates for 10 min in the diluted fibril suspension. Subsequently, the substrates were washed with PBS for 10 min and three times for 10 min each with MilliQ water and finally dried at ambient conditions for at least 24 h.

6.2.3 Collagen cross-linking

Collagen fibrils cross-linked with glutaraldehyde were prepared by mixing 1 ml of the non-diluted fibrillar suspension with 5 ml of a 10 wt % glutaraldehyde solution (Sigma-Aldrich, Steinheim, Germany) and 195 ml phosphate buffer (pH = 7.4). The resulting mixture was kept at room temperature for 2 h. The cross-linked fibrils were deposited on the partly Teflon coated glass substrates and washed as described above.

Cross-linking of the collagen fibrils by 1-ethyl-3-(3-dimethylaminopropyl)carbodiimide hydrochloride (EDC) (Sigma-Aldrich, Steinheim, Germany) and N-hydroxysuccinimide

(NHS) (Fluka, Buchs, Germany) was performed by mixing 2 ml of the non-diluted collagen suspension with a freshly prepared solution of 1.73 g EDC and 0.45 g NHS in 215 ml 2-morpholinoethane sulfonic acid (MES) (0.05 M, pH = 5.4) and kept at room temperature for 2 h [26]. The resulting cross-linked fibrils were deposited on the glass substrates and washed as described above.

The degree of cross-linking of the collagen samples is related to the increase of the denaturation (shrinkage) temperature (T_d) after cross-linking and the residual amount of free amino groups. The T_d values were determined by DSC (DSC 7, Perkin Elmer, Norwalk, CT, USA). The free amino group content of native and cross-linked samples were determined using the 2,4,6-trinitrobenzenesulfonic acid (TNBS) assay [25].

6.2.4 Fixation of the collagen fibril between the surface and AFM cantilever

Using an optical microscope, individual collagen fibrils with a minimal length of 40 μm and crossing the Teflon-glass boundary were selected for fixation and tensile testing. A collagen fibril was fixed to the surface of the glass substrate and AFM cantilever (Multi 130A, $k = 35 \text{ N/m}$ Veeco, Dourdan, France) using two component epoxy glue (Araldite 2011, Vantico, Basel, Switzerland) [18]. The tip on the AFM cantilever was removed using a focused ion beam (FIB) (FEI, NOVALAB 600 dual beam machine, Eindhoven, the Netherlands). The gluing procedure is shown in detail in Fig. 6.1.

6.2.5 Micro-tensile tests of individual collagen fibrils

After fixation of the collagen fibril between the AFM cantilever and the glass surface, the AFM head was slowly raised from the surface by manually adjusting the fine-adjustment spindle in the AFM setup [27]. The cantilever was moved above the glue droplet on the glass surface in order to ensure that the stretching of the fibril will be in a vertical direction. A calibrated piezo tube (Micros, Piezosystem Jena, Jena, Germany) was connected to the sample plate. After positioning the AFM cantilever, the sample plate was moved downward by the piezo tube until a $\sim 4 \text{ nN}$ deflection signal of the AFM cantilever was reached. The distance between the AFM cantilever and the glass surface at this point was defined as the initial length of the fibril.

The piezo tube connected to the sample plate can extend in the z-direction over a maximum distance of 400 μm at a preset rate. After a force of $\sim 4 \text{ nN}$ was recorded, a saw-tooth loading pattern with variable extension between 1% and 30% of the fibril initial length was used to determine the tensile properties of the non- and cross-linked collagen

fibrils at ambient conditions. For the tensile tests of fibrils in PBS buffer, the collagen fibrils fixed between the AFM cantilever and the glass surface were immersed in ~ 1 ml PBS buffer and left to equilibrate for 15 min. Longer equilibration times did not lead to changes in the results of the micro-tensile tests. Then, micro-tensile tests as described above were performed to determine the tensile properties of non- and cross-linked collagen fibrils. All the tested fibrils were loaded cyclically from low strain to high strain with a strain rate of $4 \mu\text{m/s}$. The Young's moduli of the tested fibrils were determined from the maximum slope of the stress-strain curves.

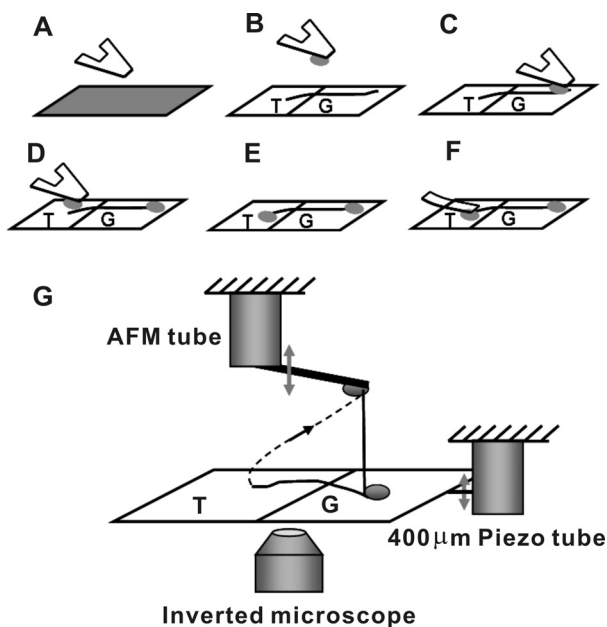


Figure 6.1 Schematic drawing of the procedure of attaching an individual collagen fibril between the AFM cantilever and the partly Teflon (T) coated glass surface. (A) Two component epoxy glue was mixed and spread onto a microscope glass surface. A triangular AFM cantilever was dipped into the layer of the glue to get a droplet at the end of the cantilever. (B) Using an optical microscope, a collagen fibril crossing the glass-Teflon boundary was selected. (C) The triangular AFM cantilever with a glue droplet attached was moved to the glass surface, and the droplet was deposited on the end of the collagen fibril. (D) Using the same procedure, a small glue droplet was put on the end of the collagen fibril on the Teflon surface. (E) The triangular cantilever was replaced by a tipless rectangular cantilever with a higher spring constant. (F) The rectangular cantilever was brought into contact with the glue droplet at the end of the collagen fibril at the Teflon surface and left for 12 h. (G) The AFM cantilever was carefully raised from the surface. Because of the non-sticking properties of the glue to the Teflon surface, the collagen fibril was attached between the AFM cantilever and the glass surface and was ready for micro-tensile testing. A $400 \mu\text{m}$ piezo tube connected to the sample holder was used in the tensile tests.

6.2.6 AFM imaging

Before attachment of the selected fibril, several tapping mode AFM images at different positions along the fibril were made to determine the diameter and morphology of the fibril both at ambient conditions and in aqueous media. The measurements were carried out with the same AFM in tapping mode using V-shaped Si₃N₄ cantilevers (coated sharp micro-levers MSCT-AUHW, type F, spring constant $k = 0.5$ N/m, Veeco, Cambridge, UK). At ambient conditions, a tapping frequency of ~ 120 kHz and a tapping amplitude of $\sim 400 - 600$ nm were used. In aqueous media, the resonance frequency of the cantilever was shifted to ~ 33 kHz. The tapping amplitude used in aqueous media varied from 50 to 250 nm. The height of the collagen fibrils measured on the Teflon coated glass substrates was used as a measure of the fibril diameter.

6.3 Results and Discussion

6.3.1 Sample preparation and characterization

Incubating partly Teflon coated glass substrates in a highly diluted collagen suspension gave several isolated collagen fibrils that cross the Teflon-glass boundary. Using the inverted optical microscope, sufficiently long (40 - 100 μm) and uniformly shaped fibrils were selected, and these fibrils were used for tensile testing.

An AFM image of an individual collagen fibril crossing the Teflon-glass boundary is presented in Fig. 6.2A. This image shows the distinct Teflon-glass boundary. The Teflon layer has a thickness of 500 ± 200 nm. The selected collagen fibrils were then imaged using tapping mode AFM along its length in order to verify the uniformity of the structure and the presence of the characteristic D-period of 67 nm (Fig. 6.2B). The diameters of the fibrils selected for tensile tests ranged from 180 to 250 nm.

Applying collagen-based materials as biomaterials requires chemical cross-linking to avoid possible immunogenic and allergic reactions. Cross-linking affects the mechanical properties of collagen-based materials but its effect on single collagen fibrils has not been studied in detail. Therefore the collagen fibrils were cross-linked with two commonly applied methods. Glutaraldehyde cross-linking has been widely applied e.g. for the stabilization of tissue heart valves and activation methods used in the polypeptide chemistry like EDC/NHS are well known as an alternative to overcome problems associated with glutaraldehyde toxicity. Both methods were used to cross-link collagen fibrils and both of the cross-linked fibrils still showed the D-period of 67 nm. Furthermore the changes in denaturation temperature (T_d) and free amino group content ($n/1000$) were determined to

relate the changes in mechanical properties to the different structural changes introduced by these cross-linking methods.

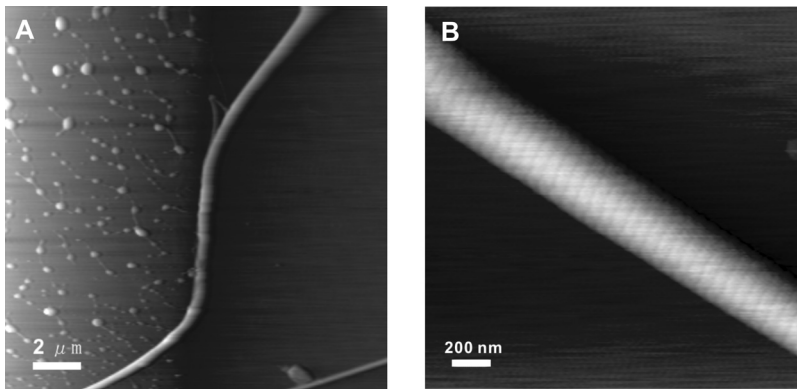


Figure 6.2 (A) AFM image of a collagen type I single fibril deposited on a Teflon/glass interface. The surface of the left part of the image is glass coated with Teflon. (B) AFM image of a collagen type I single fibril. The D-period of the collagen fibril is clearly visible in the image.

The T_d of the native fibrils was 55.0°C and increased to 75.0°C after cross-linking with the water-soluble carbodiimide 1-ethyl-3-(3-dimethyl aminopropyl)carbodiimide hydrochloride (EDC) in the presence of N-hydroxysuccinimide (NHS). The free amino group content decreased from 28 per 1000 amino acids to a value of 9 which was in line with previously reported data [23]. After cross-linking with glutaraldehyde, the denaturation temperature increased to 76.0°C and the primary amino group content decreased to a value of 8 per 1000. These results reveal a high degree of cross-linking with both cross-linking methods.

6.3.2 Stress-strain curves of individual native collagen fibrils

After fixation between the AFM cantilever and the glass surface, the collagen fibril was straightened to its initial length by adjusting the position of the AFM cantilever and the height of the sample plate manually. The length of the collagen fibrils used was always in between 40 and 100 μm. A calibrated piezo tube with a maximum extension distance of 400 μm was fixed to the sample plate allowing the collagen fibril to be stretched to different percentages of strain and even to failure. In the experiments, the fibril was loaded cyclically with a strain rate of 4 μm/s. The force-length curves of cyclically loading of a fibril with initial length of 70 μm are shown in Fig. 6.3.

Measuring the force applied on the cantilever, and knowing the length and the cross-sectional area of the fibril, stress-strain relationships of individual collagen fibrils

could be derived. As shown in Fig. 6.3, irreversible lengthening of the fibril was observed after each cycle of loading when a force higher than 1000 nN was applied. Therefore, the length (L) and the cross-sectional area (A) of the fibrils were corrected after each cycle of loading in order to correctly calculate the stress-strain behavior.

$$L = L_0 + \Delta L \quad (6.1)$$

$$A = A_0 \times L_0 / L \quad (6.2)$$

Where L is the length of the fibril, L_0 is the initial length of the fibril, ΔL is the irreversible lengthening of the fibril. A and A_0 are the cross-sectional area and initial cross-sectional area of the fibril, respectively.

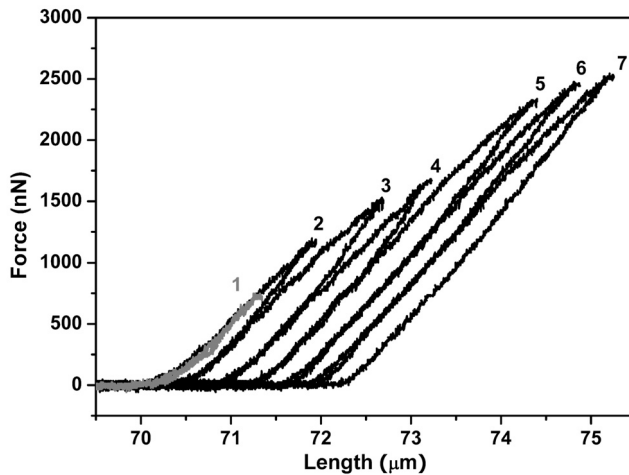


Figure 6.3 Force-length curves of cyclically loading a native collagen fibril with initial length of 70 μm at ambient conditions. Curves indicated with different numbers represent subsequent cycles (1 to 7) of stretching the fibril up to different lengths. After each cycle, irreversible lengthening of the fibril was observed, except the first cycle (gray line).

More than 10 fibrils were tested at ambient conditions and all of them showed a linear stress-strain behavior. The Young's modulus, as determined from the maximum slope of the stress-strain curves, was 2.5 ± 0.9 GPa. As shown in Fig. 6.4A, the stretching and relaxation part in the stress-strain curve fully overlap, revealing reversible mechanical behavior up to 3.5% strain with a maximum stress of 90 MPa. At higher strains hysteresis and an irreversible lengthening of the fibril were observed (Fig. 6.4B). As shown in Fig. 6.4A and B, the Young's modulus of the fibril did not change after cyclic loading although there was irreversible lengthening of the fibril. These stress-strain curves revealed that

individual collagen fibrils like collagen tissue and collagen fibers demonstrate viscoelastic behavior. The viscoelastic properties of collagen-based tissues have been the subject of several studies [3]. A mechanical model was postulated which relates the mechanical properties of collagen fibers or the interface between fiber and matrix to the viscoelastic behavior of tissue. Our results indicate that collagen fibrils, the subunits of a collagen fiber, show viscoelastic properties which may contribute to the overall viscoelastic behavior of tissues.

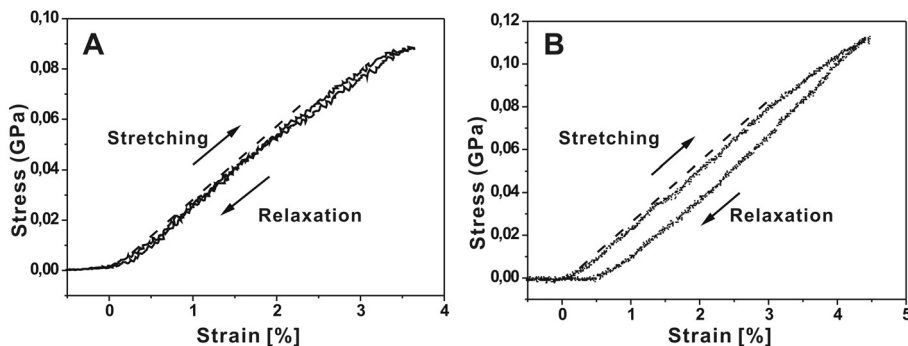


Figure 6.4 (A) Stress-strain curve revealing the reversible behavior of a collagen fibril when stretched to 3.5% strain and then relaxed at ambient conditions. A Young's modulus of 2.9 ± 0.1 GPa is calculated from the maximum slope of the curve as indicated with dashed line. (B) Stress-strain curve of the same collagen fibril stretched to 4.5% strain showing hysteresis. A Young's modulus of 2.9 ± 0.1 GPa is calculated from the maximum slope of the curve as indicated with dashed line. For both (A) and (B) the strain rate for a stretching-relaxation cycle is $4 \mu\text{m/s}$. The tested fibril is $60 \pm 2 \mu\text{m}$ in length and $210 \pm 10 \text{ nm}$ in diameter.

To mechanically test a fibril in the hydrated state, a collagen fibril fixed between the AFM cantilever and the glass surface was fully immersed in PBS buffer. After equilibration, the swelling of the fibril was measured using AFM tapping mode imaging [18]. The diameter of the fibrils increased by $\sim 50\%$ upon hydration in PBS buffer. Stress-strain curves obtained from measurements at different percentages of strain are presented in Fig. 6.5. Instead of the linear stress-strain behavior observed at ambient conditions, a toe region at low strain was found, followed by a heel region and then by a linear region at higher strain. These stress-strain curves reflect the typical stress-strain behavior of collagen-based tissues and fibers [4]. In the toe and heel region, the slope of the stress-strain curves increased continuously up to $\sim 3\%$ strain. From this point on, the stress-strain behavior of the fibril was linear and a Young's modulus of 0.6 ± 0.2 GPa was calculated. The difference in the stress-strain behavior for fibrils at ambient conditions and in PBS buffer has been ascribed to the straightening of kinks in the collagen molecules caused by

hydration [28]. Several native collagen fibrils were tested and the failure of all fibrils occurred at 11-15% strain with a stress at break of 60 ± 10 MPa. It should be noted that the fibrils never failed at the glue fixation points. Similarly as in stretching the fibril at ambient conditions, the mechanical behavior of the fibril was reversible below $\sim 6\%$ strain (Fig. 6.5A). At higher strain levels hysteresis and irreversible lengthening of the fibril were found (Fig. 6.5B).

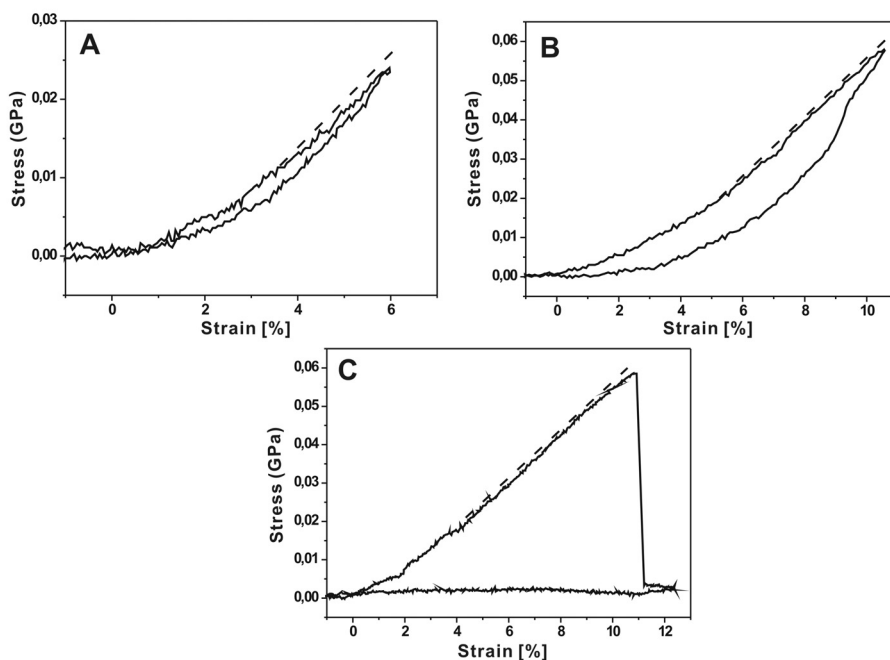


Figure 6.5 Representative stress-strain responses of an individual collagen type I fibril in PBS buffer up to 6% (A), 10% (B) and 11% (C) of strain. The strain rate in all stretching-relaxation cycles was $4 \mu\text{m/s}$. The Young's modulus of the fibril was determined from the maximum slope of the stress-strain curve as indicated with dashed line. The stress-strain behavior was fully reversible at low strain levels (below 6%) (A). Hysteresis and irreversible lengthening of the collagen fibril were observed from the stress-strain plots especially at higher strain levels (B). Failure of the fibril occurred at 11% strain with a stress of 0.06 GPa (C). The tested fibril is $50 \pm 2 \mu\text{m}$ in length and $305 \pm 10 \text{ nm}$ in diameter.

Stress-strain curves of 11 separate collagen fibrils were determined and the average modulus determined from the maximum slopes of the stress-strain curves is given in Table 6.1. With macro-tensile testing, the data presented in the literature on the Young's modulus of dry collagen fibers range from 1 to 8 GPa and is 0.15 to 1 GPa for tendons and collagen fibers in the hydrated state [7,29,30]. These results show that the value of Young's moduli of single collagen fibrils at ambient conditions or in PBS buffer are in the

same range of the Young's moduli of tendon tissue and collagen fibers measured at these conditions.

Sasaki *et al.* [12] reported a Young's modulus of 430 MPa for collagen fibrils immersed in a saline solution by performing X-ray diffraction measurements on a loaded tendon sample. In their measurements a linear stress-strain relationship of collagen fibrils in a saline solution up to 4% strain was found. The fact that they applied a force on the whole tendon instead of on an individual fibril could be the reason for the difference in the shape of the stress-strain curve measured compared with our measurements. By testing hydrated single collagen fibrils isolated from sea cucumber using a micro-electromechanical device Eppell *et al.* [17] found a stress-strain relationship with an initial toe region followed by a heel and linear region, similar to our results. The Young's modulus of the fibrils was determined to be 0.3 - 0.4 GPa at the toe region and 6 GPa at the linear region. The difference in the Young's modulus from their measurements and ours still can be explained in two ways. Firstly, they used a diameter of fibril at ambient conditions for calculating the cross-sectional area of the hydrated sample, which may lead to overestimation of the Young's modulus. Secondly, it has been shown from our results obtained for fibrils at ambient conditions and in PBS buffer that the hydration state has a significant influence on the stress-strain behavior. The collagen fibril used by Eppell *et al.* was not fully immersed in water, which may lead to a difference in the degree of hydration as compared to fibrils immersed in PBS which results in a different value for the Young's modulus. Our methodology allowed for the first time to determine the failure stress and the strain at break of single collagen fibrils. The strain at break (11-15%) is comparable to fibers isolated from tendon [31] and tendon tissue [7].

6.3.3 Influence of cross-linking

For biomedical applications of collagen-based materials chemical cross-linking of collagen is important. Cross-linking is an efficient method to retard the degradation by collagenase and also to inhibit immunological reactions. Cross-linking by glutaraldehyde and activation methods in polypeptide chemistry like EDC/NHS are nowadays commonly used procedures to stabilize collagen-based materials and both methods were applied to study the influence of cross-linking on the mechanical properties of individual collagen fibrils.

The tensile tests were performed on collagen fibrils at ambient conditions and fibrils fully immersed in PBS buffer. The stress-strain behavior of individual collagen fibrils cross-

linked with EDC/NHS is depicted in Fig. 6.6 and those cross-linked with glutaraldehyde in Fig. 6.7. A similar shape of the stress-strain curves was found for the cross-linked fibrils compared to the native collagen fibrils. At ambient conditions a linear stress-strain curve was found at lower strain ($\leq \sim 4\%$) irrespective of the cross-linking method used. At higher strain hysteresis and irreversible lengthening was observed. The slope of the stress-strain curves for collagen fibrils placed in PBS buffer increased up to 5-6% strain. Above $\sim 10\%$ strain hysteresis with irreversible lengthening of the fibril was found irrespective of the cross-linking method used. Differences in Young's moduli of fibrils were found for the differently cross-linked fibrils. For EDC/NHS cross-linked fibrils, the average Young's modulus of the tested fibrils was 2.5 ± 0.2 GPa at ambient conditions and 700 ± 100 MPa for fibrils in PBS buffer, which was comparable to native fibrils (Table 6.1). A ~ 2.5 times increase in the Young's modulus was found for fibrils cross-linked with glutaraldehyde both at ambient conditions and in PBS buffer (Table 6.1) compared to the value for native fibrils. Failure of the cross-linked fibrils was only determined for fibrils immersed in buffer. After cross-linking the fibrils either with EDC/NHS or glutaraldehyde, the strain at break increased. The EDC/NHS cross-linked fibrils ($N = 3$) broke at $30 \pm 3\%$ strain with a maximum stress of 170 ± 20 MPa. For glutaraldehyde cross-linked fibrils ($N = 3$), the fibrils broke at $22 \pm 3\%$ strain with a maximum stress of 290 ± 40 MPa.

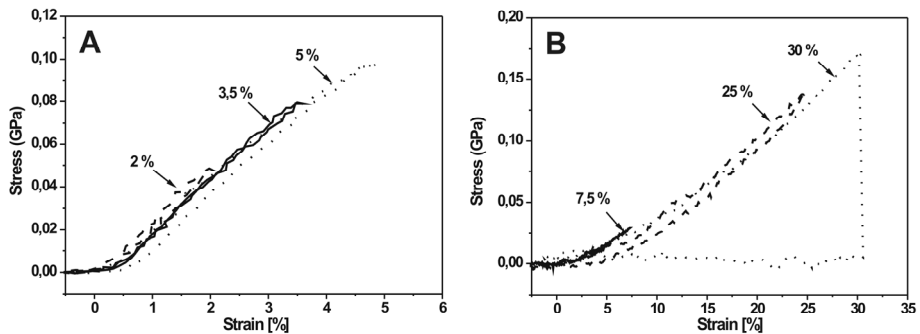


Figure 6.6 Representative stress-strain curves of an individual collagen type I fibril cross-linked by EDC/NHS, at ambient conditions (A) and in PBS buffer (B). Stretching and relaxation cycles of the fibril up to different percentages of strain are indicated. Failure of the fibril occurred at 30% strain with a stress of 0.17 GPa (dotted line) in PBS buffer. The strain rate for all stretching and relaxation cycles is $4 \mu\text{m/s}$. The fibril tested at ambient conditions is $45 \pm 2 \mu\text{m}$ in length and $205 \pm 10 \text{ nm}$ in diameter. The fibril immersed in PBS buffer is $53 \pm 2 \mu\text{m}$ in length and $300 \pm 10 \text{ nm}$ in diameter.

The results presented here clearly show that the two cross-linking agents affect the mechanical properties of collagen fibrils differently. The failure stress, strain at break and Young's modulus increased after cross-linking with glutaraldehyde. The EDC/NHS

cross-linking, which is widely used to overcome the toxicity problem of glutaraldehyde, also increased the failure stress and strain at break of the collagen fibrils, but the stiffness of the fibril remained unchanged.

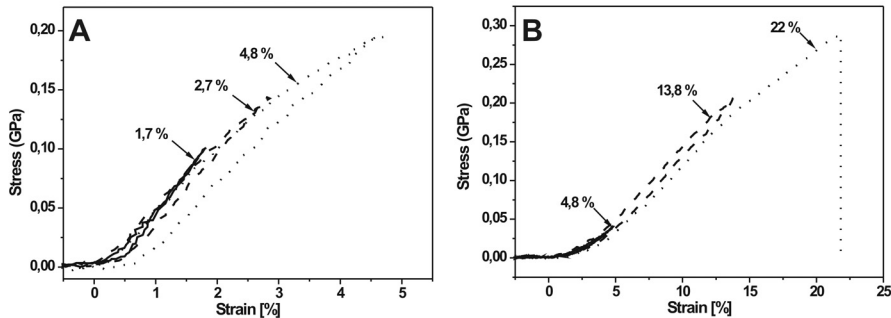


Figure 6.7 Representative stress-strain curves of an individual collagen type I fibril cross-linked with glutaraldehyde, at ambient conditions (A) and in PBS buffer (B). Stretching-relaxation cycles of the fibril up to different percentages of strain are indicated. Failure of the fibril occurred at 22% strain with a stress of 0.29 GPa (dotted line) in PBS buffer. The strain rate for all stretching-relaxation cycles is 4 $\mu\text{m/s}$. The fibril tested at ambient conditions is $69 \pm 2 \mu\text{m}$ in length and $210 \pm 10 \text{ nm}$ in diameter. The fibril immersed in PBS buffer is $90 \pm 2 \mu\text{m}$ in length and $295 \pm 14 \text{ nm}$ in diameter.

The changes in the mechanical properties of single collagen fibrils after cross-linking with EDC/NHS and glutaraldehyde can be explained by the type of cross-links introduced between fibrillar subunits. The carbodiimide in combination with the N-hydroxysuccinimide (EDC/NHS) activates the carboxylic acid groups of glutamic or aspartic acid residues, which subsequently react with amine groups of (hydroxy)lysine residues forming an amide bond and with hydroxyl groups of serine, hydroxyproline, and hydroxylysine residues forming an ester bond [23,32]. This cross-linking reaction forms intra- and inter-molecular covalent bonds between collagen molecules and leads to an increase in the failure stress and strain at break, and consequently an increase of toughness of the fibril with respect to native fibrils. However, sliding between micro-fibrils is not hampered by this cross-linking because inter-microfibrillar cross-linking is unlikely [26]. Glutaraldehyde cross-linking however enables covalent binding of two amine groups of (hydroxy)-lysine residues over distances of at least 1.3 nm due to condensation reactions. This leads to the formation of oligomeric cross-links. Glutaraldehyde thus may generate intra- and inter-molecular cross-links as well as inter-microfibrillar cross-links. We hypothesize that the inter-microfibrillar cross-links, hamper the sliding between micro-fibrils causing the observed increase in Young's modulus.

Table 6.1 Mechanical properties of individual collagen fibrils at ambient conditions and in PBS buffer (from tensile tests at strain rate 4 $\mu\text{m/s}$). Values are means \pm SD.

Sample	<i>At ambient conditions</i>		<i>In PBS buffer</i>			
	E (GPa)^d	σ_c (GPa)^e	E (GPa)^d	σ_c (GPa)^e	σ_{max} (GPa)	ϵ_{max} (%)
Native ^a	2.5 \pm 0.9	0.08 \pm 0.02	0.6 \pm 0.2	0.02 \pm 0.01	0.06 \pm 0.01	13 \pm 2
EDC/NHS ^b	2.5 \pm 0.2	0.09 \pm 0.02	0.7 \pm 0.1	0.06 \pm 0.01	0.17 \pm 0.01	30 \pm 3
Glu ^c	5.9 \pm 0.5	0.18 \pm 0.02	1.8 \pm 0.3	0.15 \pm 0.02	0.29 \pm 0.01	22 \pm 3

a. Native collagen fibrils

b. Collagen fibrils cross-linked by EDC/NHS

c. Collagen fibrils cross-linked by glutaraldehyde

d. Moduli were determined from the maximum slope of the stress-strain curve of single collagen fibrils.

e. The stress for the transition from reversible to irreversible lengthening of the fibril.

6.4 Conclusions

In the present study, tensile properties of individual collagen fibrils isolated from bovine Achilles tendon were determined using a slightly adapted home-built AFM system. A piezo tube was added to the AFM system in order to allow stretching of individual collagen fibril to large strains. The stress-strain behavior, Young's modulus and the failure stress and strain of individual collagen fibrils were for the first time determined both for fibrils at ambient conditions and in PBS buffer. For native collagen fibrils, the Young's modulus was 2.5 ± 0.9 GPa at ambient conditions and decreased to 0.6 ± 0.2 GPa when the fibrils were immersed in PBS buffer. Failure of the native collagen fibrils was observed only in PBS at 11-15% strain with a stress of 0.06 ± 0.01 GPa.

The strain at break of individual collagen fibrils increased to 30% and 22% after cross-linking with EDC/NHS and glutaraldehyde, respectively. Fibrils cross-linked with EDC/NHS have Young's moduli comparable to those of native collagen fibrils. However, the Young's modulus of collagen fibrils cross-linked with glutaraldehyde increased to 5.9 ± 0.5 GPa for fibrils at ambient conditions and to 1.8 ± 0.3 GPa for fibrils in PBS buffer. These results are best explained by the inter-microfibrillar cross-links formed by glutaraldehyde which are not possible upon cross-linking by an activation method such as EDC/NHS cross-linking.

Acknowledgement

This research was financially supported by the Softlink program of ZonMw. Project number: 01SL056.

References

1. Prockop DJ, Kivirikko KI. Collagens-molecular-biology, diseases, and potentials for therapy. *Annu. Rev. Biochem.* **1995**; 64: 403-434.
2. Silver FH, Freeman JW, Seehra GP. Collagen self-assembly and the development of tendon mechanical properties. *J. Biomech.* **2003**; 36: 1529-1553.
3. Puxkandl R, Zizak I, Paris O, Keckes J, Tesch W, Bernstorff S, Purslow P, Fratzl P. Viscoelastic properties of collagen: synchrotron radiation investigations and structural model. *Phil. Trans. R. Soc. Lond. B* **2002**; 357: 191-197.
4. Wang JHC. Mechanobiology of tendon. *J. Biomech.* **2006**; 39: 1563-1582.
5. Dowling BA, Dart AJ. Mechanical and functional properties of the equine superficial digital flexor tendon. *Vet. J.* **2005**; 170: 184-192.
6. Magnusson SP, Hansen P, Kjaer M. Tendon properties in relation to muscular activity and physical training. *Scand. J. Med. Sci. Sports* **2003**; 13: 211-223.
7. Butler DL, Kay MD, Stouffer DC. Comparison of material properties in fascicle-bone units from human patellar tendon and knee ligaments. *J. Biomech.* **1986**; 19: 425-432.
8. Yamamoto E, Hayashi K, Yamamoto N. Mechanical properties of collagen fascicles from stress-shielded patellar tendons in the rabbit. *Clin. Biomech.* **1999**; 14: 418-425.
9. Silver FH, Christiansen D, Snowhill PB, Chen Y, Landis WJ. The Role of mineral in the storage of elastic energy in turkey tendons. *Biomacromolecules* **2000**; 1: 180-185.
10. Cribb AM, Scott JE. Tendon response to tensile stress: an ultrastructural investigation of collagen: proteoglycan interactions in stressed tendons. *J. Anat.* **1995**; 187: 423-428.
11. Mosler E, Folkhard W, Knörzer E, Nemetschek-Gansler H, Nemetschek T, Koch MHJ. Stress-induced molecular rearrangement in tendon collagen. *J. Mol. Biol.* **1985**; 182: 589-596.
12. Sasaki N, Odajima S. Elongation mechanism of collagen fibrils and force-strain relations of tendon at each level of structural hierarchy. *J. Biomech.* **1996**; 29: 1131-1136.
13. Thompson JB, Kindt JH, Drake B, Hansma HG, Morse DE, Hansma PK. Bone indentation recovery time correlates with bond reforming time. *Nature* **2001**; 414: 773-776.
14. Gutsman T, Fantner GE, Kindt JH, Venturoni M, Danielsen S, Hansma PK. Force spectroscopy of collagen fibers to investigate their mechanical properties and

- structural organization. *Biophys. J.* **2004**; 86: 3186-3193.
15. Bozec L, Horton M. Topography and mechanical properties of single molecules of type I collagen using atomic force microscopy. *Biophys. J.* **2005**; 88: 4223-4231.
 16. Graham JS, Vomund AN, Phillips CL, Grandbois M. Structural changes in human type I collagen fibrils investigated by force spectroscopy. *Exp. Cell Res.* **2004**; 299: 335-342.
 17. Eppell SJ, Smith BN, Kahn H, Ballarini R. Nano measurements with micro-devices: mechanical properties of hydrated collagen fibrils. *J. R. Soc. Interface* **2006**; 3: 117-121.
 18. van der Rijt JAJ, van der Werf KO, Bennink ML, Dijkstra PJ, Feijen J. Micromechanical testing of individual collagen fibrils. *Macromol. Biosci.* **2006**; 6: 697-702.
 19. Wang PC, Takezawa T. Reconstruction of renal glomerular tissue using collagen vitrigel scaffold. *J. Biosci. Bioeng.* **2005**; 99: 529-540.
 20. Buma P, van Tienen T, Veth RP. The collagen meniscus implant. *Expert Rev. Med. Devic.* **2007**; 4: 507-516.
 21. Caruso AB, Dunn MG. Functional evaluation of collagen fiber scaffolds for ACL reconstruction: Cyclic loading in proteolytic enzyme solutions. *J. Biomed. Mater. Res. Part A* **2004**; 69: 164-171.
 22. Kato YP, Silver FH. Formation of continuous collagen fibres: evaluation of biocompatibility and mechanical properties. *Biomaterials* 1990; 11: 169-175.
 23. Olde Damink LHH, Dijkstra PJ, van Luyn MJA, van Wachem PB, Nieuwenhuis P, Feijen J. Cross-linking of dermal sheep collagen using a water-soluble carbodiimide. *Biomaterials* **1996**; 17: 765-773.
 24. van der Rijt JAJ. Micromechanical testing of single collagen type I fibrils. *Ph. D thesis*, University of Twente, Enschede, The Netherlands, **2004**. ISBN 90-365-2082-7.
 25. Yang L, van der Werf KO, Koopman BFJM, Subramaniam V, Bennink ML, Dijkstra PJ, Feijen J. Micromechanical bending of single collagen fibrils using atomic force microscopy. *J. Biomed. Mater. Res. A* **2007**; 82: 160-168. (Chapter 3 of this thesis)
 26. Yang L, van der Werf KO, Fitié CFC, Bennink ML, Dijkstra PJ, Feijen J. Mechanical properties of native and cross-linked type I collagen fibrils. *Biophys. J.* **2007**; Online. (Chapter 4 of this thesis)
 27. van der Werf KO, Putman CAJ, de Grooth BG, Segerink FB, Schipper EH, van Hulst NF, Greve, J. Compact stand-alone atomic force microscope. *Rev. Sci. Instrum.* **1993**; 64: 2892-2897.
 28. Misof K, Rapp G, Fratzl P. A new molecular model for collagen elasticity based on synchrotron x-ray scattering evidence. *Biophys. J.* **1997**; 72: 1376-1381.
 29. An KN, Sun YL, Luo ZP. Flexibility of type I collagen and mechanical property of connective tissue. *Biorheology* **2004**; 41: 239-246.
 30. Pins GD, Silver FH. A self-assembled collagen scaffold suitable for use in soft and

- hard tissue replacement. *Mat. Sci. Eng. C* **1995**; 3: 101-107.
31. Miyazaki H, Hayashi K. Tensile tests of collagen fibers obtained from the rabbit patellar tendon. *Biomed. Microdevices* **1999**; 2: 151-157.
 32. Everaerts F, Torrianni M, Hendriks M, and Feijen J. Quantification of carboxyl groups in carbodiimide cross-linked collagen sponges. *J. Biomed. Mater. Res. A* **2007**; 83: 1176-1183.

Viscoelastic Behavior of Collagen Type I Fibrils: Evidence for the Existence of Microfibrils?*

Lanti Yang¹, Kees O. van der Werf², Martin L. Bennink², Pieter J. Dijkstra¹, Jan Feijen¹

¹ *Polymer Chemistry and Biomaterials, Faculty of Science & Technology and Institute for Biomedical Technology (BMTI), University of Twente, P.O. Box 217, 7500 AE, Enschede, The Netherlands*

² *Biophysical Engineering, Faculty of Science & Technology and MESA+ Institute for Nanotechnology, University of Twente, P.O. Box 217, 7500 AE, Enschede, The Netherlands*

Abstract

The mechanical behavior of single collagen fibrils was studied using a slightly adapted AFM system. Single collagen fibrils were attached between an AFM cantilever and a glass surface to perform tensile tests at different strain rates and stress relaxation measurements. The Young's modulus of collagen fibrils immersed in PBS buffer increased with 30% by increasing the strain rate from 0.1 to 10 $\mu\text{m/s}$, indicating that the stress-strain behavior of individual collagen fibrils is rate-dependent. Stress relaxation of the fibrils subjected to 5-7% strain for 5 - 10 min was also measured. The stress relaxation process of individual collagen fibrils could be described by a two-term Prony series. For native individual collagen fibrils in PBS buffer, a fast ($\tau_1 = 1.8 \pm 0.4$ s) and a slow ($\tau_2 = 60 \pm 10$ s) relaxation process was found. After cross-linking the fibrils with EDC/NHS, τ_2 increased to 225 ± 10 s while τ_1 remained unchanged. After cross-linking of fibrils with glutaraldehyde, τ_1 and τ_2 increased to 3.7 ± 1.0 and 250 ± 80 s, respectively. Based on these results, we propose that sliding of microfibrils with respect to each other correlates with the fast relaxation process whereas sliding of collagen molecules with respect to each other is related to the slower part of the stress relaxation.

* This chapter is to be submitted for publication.

7.1 Introduction

Collagen, the most abundant protein in the human body, is crucial for the strength and stability of a wide range of human tissues. Collagen based tissues usually exhibit viscoelastic properties, i.e. their stress-strain behavior is time dependent. Viscoelastic properties of tissues are considered to be important for their function [1].

Tensile tests at different strain rates, stress relaxation and creep experiments have been performed on collagen fibers and tissues to explore the relationship between their viscoelastic properties and the hierarchical structure of collagen based tissues [2-8]. Using X-ray diffraction measurements during stress relaxation and creep tests of rat skin and bovine intramuscular connective tissue, Purslow and co-workers suggested that relaxation processes within the collagen fibers or at the fiber-matrix interface rather than alignment of collagen fibers are responsible for the viscoelastic properties of these tissues [1]. Puxkandl *et al.* [9] determined the elongation of tendon and the collagen fibrils inside the tendon simultaneously using X-ray diffraction. Based on their results, it was suggested that the fibrils and interfibrillar matrix arranged in series act as a viscoelastic system.

These studies suggest that there is a contribution of collagen fibers and fibrils to the viscoelastic behavior of collagen-based tissues. However, due to the limitation of techniques available to perform tensile and stress relaxation tests on the micro- and nano-scale level, little information is available on the possible mechanism of the mechanical behavior of collagen fibrils which will provide insight in understanding the viscoelastic behavior of collagen-based tissues. Using tensile testing combined with synchrotron radiation diffraction on tissue samples, Mosler and co-workers [10-12] suggested that stretching of the collagen molecules and their sliding with respect to each other are the two major mechanisms for the elongation of collagen fibrils. On the other hand, Sasaki and co-workers [13] hypothesized from the simultaneous X-ray diffraction and tensile testing on tendon samples that molecular elongation is the main mechanism for the elongation of collagen fibrils.

The existence of sub-structures in collagen fibrils has been a debate for years. Recent studies suggest the presence of microfibrils in fibrils. A longitudinal microfibrillar structure with a width of 4 - 8 nm was visualized in both hydrated [14,15] and dehydrated [16] collagen type I fibrils using tapping mode AFM imaging. Three-dimensional image reconstructions of 36 nm-diameter corneal collagen fibrils also showed a 4 nm repeat in a transverse section, which was related to the microfibrillar structure [17]. Using X-ray

diffraction culminating in an electron density map, Orgel *et al.* [18] suggested the presence of right-handed supertwisted microfibrillar structures in collagen fibrils. The question arises as to whether the microfibrillar structures play a role in the mechanical properties of single collagen fibrils.

In Chapter 6, we have presented the results of micro-tensile tests of individual insoluble collagen type I fibrils (diameter ~ 200 nm) using a home-built AFM system [19]. The stress-strain behavior of single collagen fibrils was determined both for fibrils at ambient conditions and in PBS buffer. When fibrils were loaded up to relatively high stresses, hysteresis was observed in the stress-strain behavior, indicative of irreversible lengthening, which can only be explained with the fibrils displaying viscoelastic properties.

Here we further investigate the time dependent mechanical properties of single collagen fibrils to get more information on the viscoelastic behavior of the fibrils. In this respect, we carried out tensile tests at different strain rates and stress relaxation measurements of individual collagen fibrils using a home-built AFM system. In order to get additional information on the presence of microfibrils in fibrils, we performed micro-tensile tests and stress relaxation measurements of collagen fibrils either cross-linked with 1-ethyl-3-(3-dimethyl aminopropyl)carbodiimide hydrochloride (EDC) or with glutaraldehyde. It has to be noted that cross-linking with EDC leads to “zero-length” cross-links, which affords additional inter- and intra-molecular cross-links in the collagen fibrils [20,21]. Cross-linking with glutaraldehyde introduces cross-links which can be at least 1.3 nm in length, leading to not only intra- and inter-molecular cross-links but also cross-links between microfibrils [22]. The results of this study may give additional clues for the existence of microfibrils and to explain the possible contribution of microfibrillar structures to the viscoelastic behavior of collagen fibrils.

7.2 Materials and Methods

7.2.1 Sample preparation for micro-tensile tests

The general procedure for the isolation of (non)cross-linked collagen fibrils was described previously [23]. In brief, a suspension of collagen fibrils was prepared from bovine Achilles tendon collagen type I (Sigma-Aldrich, Steinheim, Germany) by homogenization and filtration. This suspension was further diluted to obtain a suitable suspension (~ 1 mg/ml) for depositing single fibrils on a substrate.

Next to this preparation, suspensions containing chemically cross-linked fibrils were also

prepared. Cross-linking of the fibrils was performed in the diluted suspensions (to avoid cross-linking between the fibrils) using either the water-soluble carbodiimide 1-ethyl-3-(3-dimethyl-aminopropyl)carbodiimide hydrochloride (EDC) in the presence of N-hydroxysuccinimide (NHS) or glutaraldehyde as previously described [23,24]. The degree of cross-linking of the collagen fibrils is related to the increase of the denaturation (shrinkage) temperature (T_d) and decrease of free amino group content after cross-linking. T_d values were determined by DSC (DSC 7, Perkin Elmer, Norwalk, CT, USA). Free amino group contents of native and cross-linked samples was determined using the 2,4,6-trinitrobenzenesulfonic acid (TNBS) assay [23]. According to our previous finding, both cross-linking methods introduce a high degree of cross-linking. The T_d of the native fibrils was 55.0 °C and increased to 75.0 °C after cross-linking with EDC and NHS. The free amino group content decreased from 28 per 1000 amino acids to a value of 9 [19]. After cross-linking with glutaraldehyde, the denaturation temperature increased to 76.0 °C and the primary amino group content decreased to a value of 8/1000 amino acids [19].

Deposition of single collagen fibrils on partly Teflon (Teflon AF, 1601S Dupont, Wilmington, DE, USA) coated glass substrates (Microscope cover glasses, $\varnothing=15$ mm, Marlenfeld GmbH, Germany) has been described in detail in our previous work [19,25].

7.2.2 Micro-tensile tests of individual collagen fibrils

A schematic representation of the instrument used for the micro-tensile tests of single collagen fibrils is given in Fig. 7.1. A collagen fibril was fixed between the AFM cantilever (Multi 130A, $k = 35$ N/m Veeco, Dourdan, France) and the glass surface by small glue droplets [19]. The AFM cantilever was then moved above the glue droplet on the glass surface. After this, the sample plate was moved downward by the piezo tube (Micros, Piezosystem Jena, Jena, Germany) until a ~ 4 nN deflection signal of the AFM cantilever was reached. The distance between the AFM cantilever and the glass surface at this point was defined as the initial length of the fibril.

A saw-tooth loading pattern was provided using a calibrated 400 μm piezo tube controlled by LabView (Version 6.1, National Instruments, Austin, Texas, USA). Individual collagen fibrils were extended at different strain rates ranging from 0.1 to 10 $\mu\text{m/s}$. For tensile tests of fibrils in PBS buffer, the collagen fibrils fixed between the AFM cantilever and the glass surface were first immersed in ~ 1 ml PBS buffer and equilibrated for 15 min before carrying out the tensile tests. The Young's moduli of the collagen fibrils were derived from the maximum slope of the stress-strain curve as described previously [19].

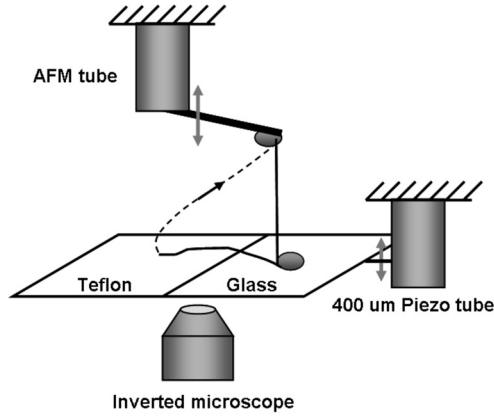


Figure 7.1 Schematic representation of the set-up for mechanical measurements (not to scale). An AFM is placed on top of an inverted microscope. A collagen fibril was fixed between the glass surface and the AFM cantilever using small glue droplets. A calibrated piezo tube with an extension range of 400 μm was attached to the sample holder, and was used to stretch and relax the collagen fibril.

Using the AFM in force distance mode gives force-extension data. In order to obtain the correct force, the spring constant of each tip-less cantilever was calibrated by pushing against a pre-calibrated cantilever as described elsewhere [26]. The cross-sectional area of the fibril was determined from tapping mode AFM images made along different positions of the fibril. Knowing the force applied on the cantilever, the length and the cross-sectional area of the fibril, the force-extension data were converted into stress-strain data [19].

7.2.3 Stress relaxation measurements

Individual collagen fibrils were loaded to approximately 5-7% strain at a loading rate of 4 $\mu\text{m/s}$. Then, the strain was maintained constant and the stress was recorded during a 5-10 min period. The time was measured from the moment the strain was kept constant. The normalized stress $\sigma(t) / \sigma(0)$ as a function of time was fitted to a two-term Prony series model (Fig. 7.2) [27] and is expressed by:

$$g(t) = \sigma(t)/\sigma(0) = [1 - A_1 \left(1 - e^{-\frac{t}{\tau_1}}\right) - A_2 \left(1 - e^{-\frac{t}{\tau_2}}\right)] \quad (7.1)$$

Where $g(t)$ is the normalized stress at time t , A_i and τ_i ($i = 1,2$) are the factors and relaxation times (s).

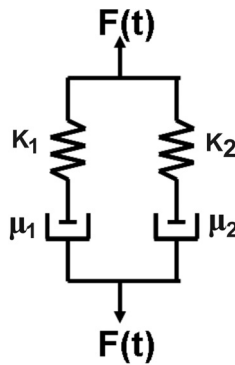


Figure 7.2 Model of two-term Prony series [27]. In this model, two Maxwell elements (a spring (K_i) and a viscous damper (μ_i) connected in series) are assembled in parallel ($i = 1,2$).

7.3 Results and Discussion

7.3.1 Strain rate dependency

It is well known that the mechanical behavior of tendons and ligaments is nonlinear and that it is dependent on the rate of the applied strain [2-8]. This viscoelastic behavior may result both from the interaction between proteoglycans and collagen in tissue and from the collagen itself [28]. In the following the dependence of the stress-strain behavior of single collagen fibrils on the strain rate will be discussed. Incubating a diluted suspension of collagen fibrils (~ 1 mg/ml) on a glass surface partly coated with Teflon afforded a sufficient amount of adsorbed isolated collagen fibrils and that were crossing the Teflon-glass boundary. Using an optical microscope, fibrils with at least $40 \mu\text{m}$ in length crossing the Teflon-glass boundary were selected for the microtensile tests. Before gluing, the diameter and the uniformity of the selected fibril were determined using atomic force microscopy imaging in tapping mode. Diameters of all tested fibrils were in the range of $150 - 250$ nm. A selected collagen fibril was fixed between an AFM cantilever and a glass surface and stretched with different rates ranging from 0.1 to $10 \mu\text{m/s}$. The typical stress-strain behavior of the fibrils at ambient conditions and in PBS buffer at strain rates of $0.1 \mu\text{m/s}$, $1 \mu\text{m/s}$ and $10 \mu\text{m/s}$ is shown in Fig. 7.3 A-F.

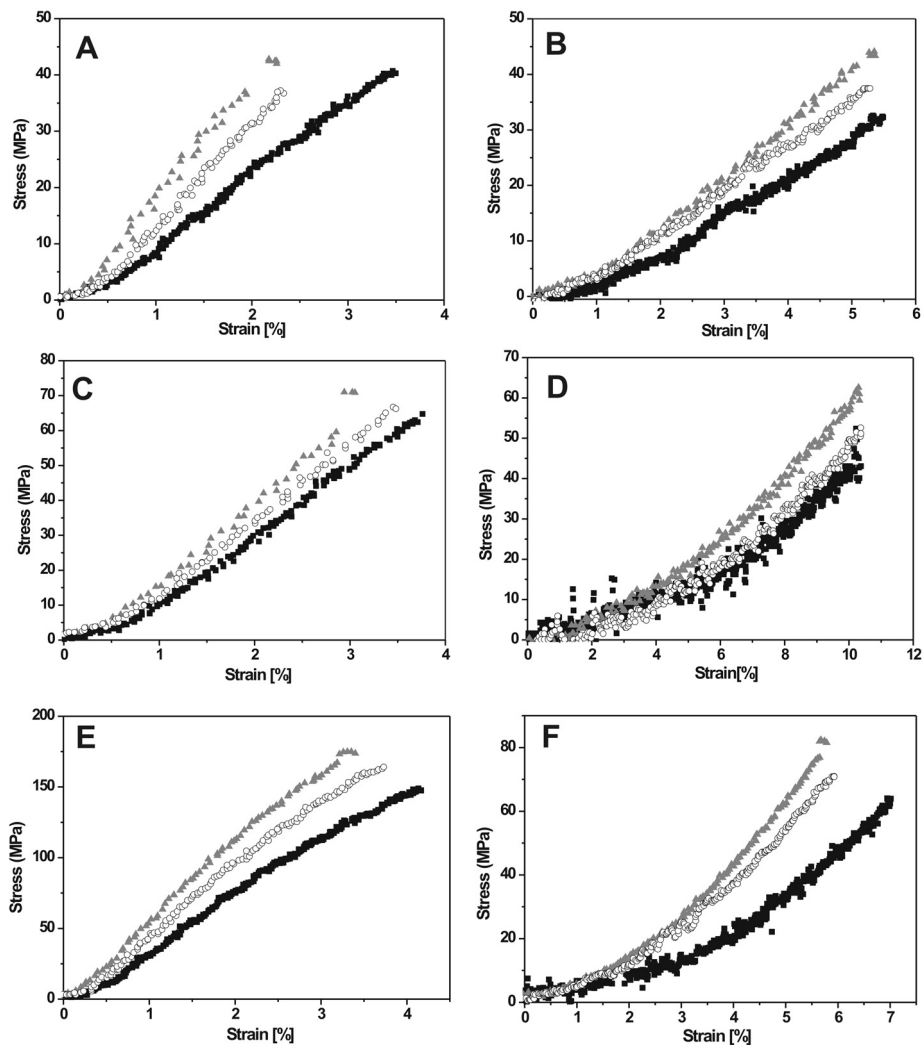


Figure 7.3 Examples of stress-strain responses of individual collagen fibrils at strain rates of 0.1 $\mu\text{m/s}$ (filled squares), 1.0 $\mu\text{m/s}$ (open circles) and 10 $\mu\text{m/s}$ (triangles). Native collagen fibrils at ambient conditions (A) and in PBS buffer (B), EDC/NHS cross-linked fibrils at ambient conditions (C) and in PBS buffer (D), and glutaraldehyde cross-linked fibrils at ambient conditions (E) and in PBS buffer (F).

The Young's modulus of 11 collagen fibrils in total at ambient conditions was determined from tensile tests at each strain rate and the results are presented in Table 7.1. The Young's modulus of native collagen fibrils at ambient conditions increased with $\sim 60\%$ when increasing the strain rate from 0.1 to 10 $\mu\text{m/s}$. With the same strain rate increase, collagen fibrils cross-linked with either EDC/NHS or glutaraldehyde showed a $\sim 30\%$ increase in

the Young's modulus for fibrils at ambient conditions. Similar experiments on (non)cross-linked collagen fibrils but now immersed in PBS buffer showed a $\sim 30\%$ increase in the Young's modulus by increasing the strain rate a 100 times. It has to be noted that when a fibril was stretched multiple times at one of the selected strain rates, no significant differences were observed in the stress-strain behavior of the fibril tested (difference in the Young's modulus determined $< 5\%$). This clearly shows that earlier performed tensile tests have no significant influence on the mechanical properties of the fibril in the range of strain applied. Yamamoto *et al.* reported that the elastic modulus of collagen fascicles obtained from the rabbit patellar tendon immersed in PBS buffer was 183 ± 26 and 248 ± 13 MPa for strain rates of 0.01 and 1 percent /s, respectively, and the latter value was 36 percent larger than the former one [29]. It is noteworthy that the approximately 30% increase in the modulus for fibrils in buffer by increasing the strain rate 100 times is similar to the increase of the Young's modulus observed from the tensile tests of collagen fascicles also increasing the strain rate 100 times.

Table 7.1 Young's modulus of collagen fibrils either at ambient conditions or in PBS buffer determined by tensile testing at different strain rates.

Strain rate	Young's modulus (GPa) ^a (at ambient conditions)			Young's modulus (GPa) ^a (in PBS buffer)		
	Native	EDC/NHS ^b	Glu ^c	Native	EDC/NHS ^b	Glu ^c
0.1 $\mu\text{m/s}$	1.6 ± 0.1	2.0 ± 0.1	4.4 ± 0.2	0.70 ± 0.04	0.65 ± 0.03	1.4 ± 0.07
1.0 $\mu\text{m/s}$	2.0 ± 0.1	2.2 ± 0.1	5.7 ± 0.3	0.82 ± 0.04	0.78 ± 0.04	1.6 ± 0.08
10 $\mu\text{m/s}$	2.6 ± 0.1	2.5 ± 0.1	5.9 ± 0.3	0.94 ± 0.05	0.83 ± 0.04	1.9 ± 0.1

Values are mean \pm SD.

- The Young's modulus is determined from the maximum slope of the stress-strain curve [19].
- Collagen type I fibrils cross-linked with EDC/NHS.
- Collagen type I fibrils cross-linked with glutaraldehyde.

7.3.2 Stress relaxation behavior

The stress relaxation behavior of collagen fibrils was studied by extending the collagen fibrils to 5-7% strain and measuring the force at constant strain for a 5 - 10 min period. The normalized stress $\sigma(t) / \sigma(0)$ against time gave stress relaxation curves for (non)cross-linked collagen fibrils at ambient conditions and in PBS buffer as depicted in Fig. 7.4 A-F. All samples relaxed rapidly at first and then progressively slower thereafter.

The bi-exponential Maxwell model (Eq. 7.1), namely the two-term Prony series [27], used for rubber modified polymers has been used to describe the stress relaxation of collagen

fibers of tendon [3] and soft tissues such as skin [7]. In our experiments, one, two and three term Maxwell models were used to fit the stress relaxation data. The curve fitting of the relaxation data revealed that the two-term Maxwell model gave the best fits of the stress relaxation process of individual collagen fibrils. As shown in Fig. 7.4 A-F, the curves for native collagen fibrils and collagen fibrils cross-linked with EDC/NHS or glutaraldehyde could all be fitted by the two-term Prony series. Fitting the data to this model afforded the relaxation times τ_1 and τ_2 which ranged from 1.5 to 4.5 s and 60 to 250 s, respectively depending on the conditions and type of cross-linker used. The almost two orders of magnitude difference in τ_1 and τ_2 indicates that there are two distinct processes involved in the relaxation of individual collagen fibrils, a fast τ_1 and slow τ_2 relaxation.

The water content of viscoelastic materials has been reported to affect the stress relaxation behavior of the materials [3]. At ambient conditions, the humidity of the environment was not controlled, which may lead to differences in the water content of the collagen fibrils. When immersing the collagen fibrils in PBS buffer, the individual collagen fibrils were fully hydrated after equilibration. Therefore, it is more appropriate to compare the influence of cross-linking on the stress relaxation behavior of collagen fibrils for fibrils immersed in buffer. As shown in Fig. 7.5, different cross-linking agents affect the relaxation times of the collagen fibrils differently. For collagen fibrils cross-linked with glutaraldehyde, the relaxation times τ_1 and τ_2 were determined to be 3.7 ± 1.0 and 250 ± 80 s, respectively, which were both higher than those of native fibrils. However for EDC/NHS cross-linked collagen fibrils only τ_2 (225 ± 10 s) higher than that of the native fibrils. The differences in the stress relaxation behavior are most likely related to the differences in the type of cross-links formed by glutaraldehyde and EDC/NHS. Glutaraldehyde cross-linking enables covalent binding of two amine groups of (hydroxy)-lysine residues at a distance of 1.3 nm [22]. Therefore, it is expected that glutaraldehyde cross-links generate intra- and inter-molecular cross-links as well as inter-microfibrillar cross-links. However, “zero-length” amide and ester cross-links are formed using EDC/NHS [20,21]. In the latter case only intra- and inter-molecular cross-links can be formed.

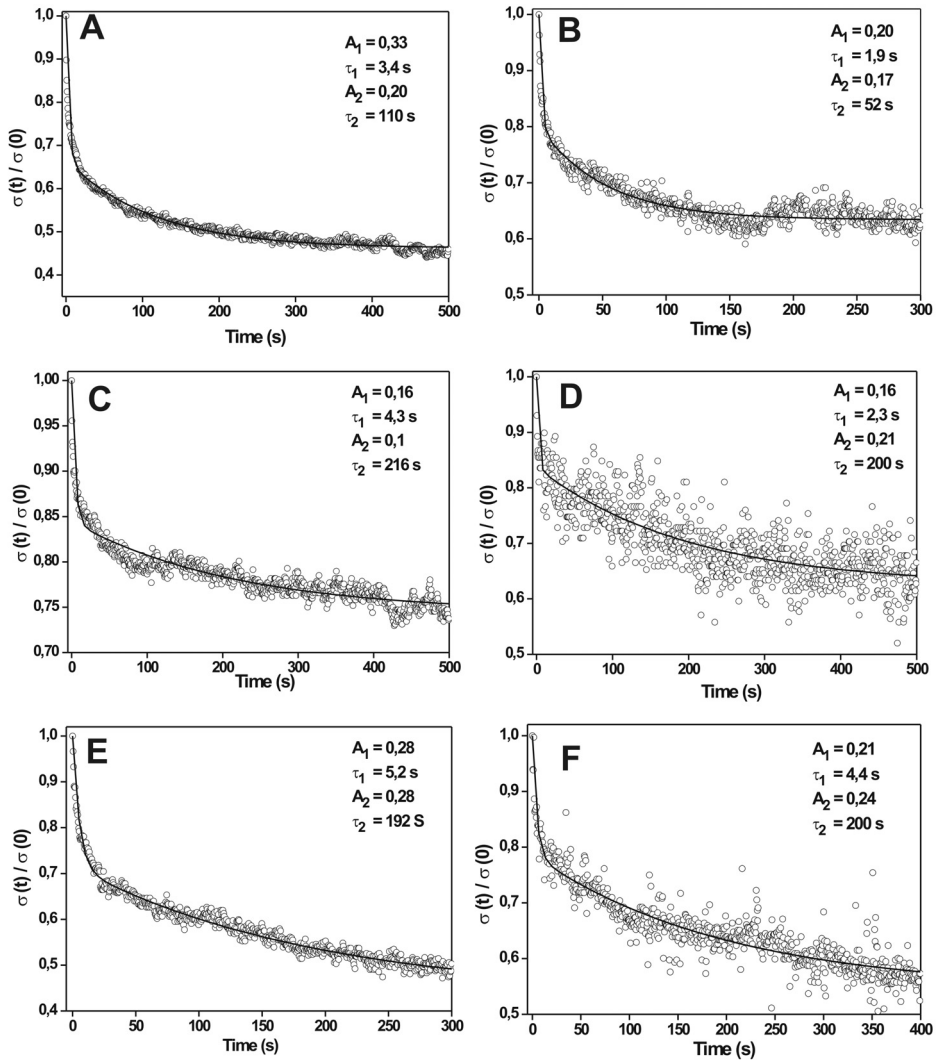


Figure 7.4 Normalized stress relaxation curves of individual collagen fibrils at ambient conditions (A) and in PBS buffer (B); EDC/NHS cross-linked collagen fibrils tested at ambient conditions (C) and in PBS buffer (D); Glutaraldehyde cross-linked collagen fibrils tested at ambient conditions (E) and in PBS buffer (F). The data (open circles) were curve fitted to Eq. 7.1 (fitting: solid lines).

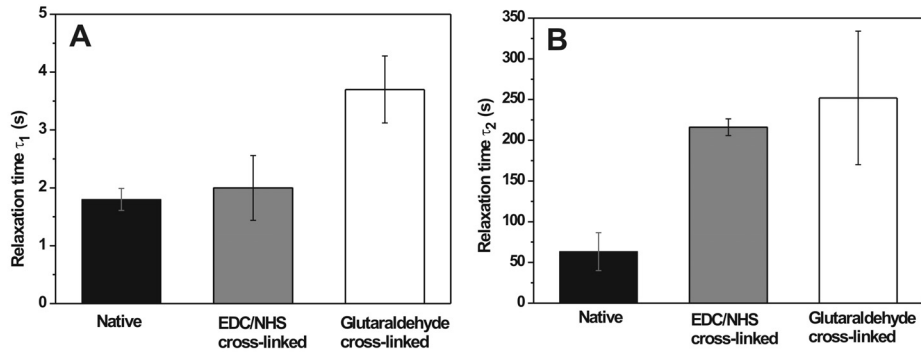


Figure 7.5 Relaxation times τ_1 (A) and τ_2 (B) of native, EDC/NHS and glutaraldehyde cross-linked collagen fibrils (PBS, 20°C). Each column (mean \pm S.D.) results from measurements of 3 individual fibrils.

7.3.3 Proposed model for the stress relaxation of individual collagen fibrils

From the results of tensile testing at different strain rates and the stress relaxation behavior of individual collagen fibrils, it is evident that collagen fibrils show viscoelastic properties. On a higher hierarchical structure level, sliding between collagen fibers has proven to be the major mechanism for the mechanical behavior of tendon [28]. Within the collagen fibrillar structure, the collagen molecule is regarded as an elastic rod [30]. The viscoelastic behavior of a collagen fibril in principle can be caused by the sliding of collagen molecules with respect to each other and the sliding of collagen microfibrils with respect to each other.

Using tensile testing combined with synchrotron radiation diffraction for tissue samples, Mosler and co-workers reported that there are two mechanisms that contribute to the elongation of collagen fibrils, namely the stretching of the collagen molecules and their sliding with respect to each other [10]. By applying a constant load, the continuous change in the intensity of the diffraction spectra up to 200 s indicates that sliding of the molecules takes place, which can be attributed to the viscous behavior of the collagen fibril [10]. From the stress relaxation measurements on rat tail tendon, Usha *et al.* [3] suggested that the relaxation time in the order of 200 s was related to the sliding between collagen molecules which was hindered by hydrogen bonding. In our research, by applying a constant strain, a continuous decay in stress with a fast and slow relaxation process (τ_1 and τ_2) was observed. The slow relaxation process with a characteristic time τ_2 of 60 s for native collagen fibrils can be related to the sliding between the molecules. Upon cross-linking either by EDC/NHS or glutaraldehyde additional intra- and inter-molecular

cross-links are introduced. The sliding process between molecules will be hindered, which can explain the increase of τ_2 to ~ 250 s for cross-linked collagen fibrils.

Our results indicate that there is a second viscous element with a short characteristic time τ_1 contributing to the viscoelastic behavior of collagen fibrils. This sliding behavior will occur at all hierarchical levels within the collagen fibril but predominantly between units exhibiting the weakest interaction [28]. In insoluble collagen type I fibrils, molecules are cross-linked at the telopeptide region [11]. However, there are only a few cross-links present between microfibrils (an assembly of five collagen molecules) [18]. Based on our results, it is hypothesized that sliding between microfibrils is the viscous element responsible for the fast relaxation component during the stress relaxation process. This hypothesis is further supported by the data of the stress relaxation experiments. Collagen fibrils cross-linked by glutaraldehyde with additional cross-links between microfibrils show a clear increase in the value of τ_1 . EDC/NHS cross-linking, however, which is a “zero-length” cross-linker able to form cross-links between collagen molecules but not between microfibrils, did not affect the value of τ_1 . Based on the results, we propose that the sliding between collagen microfibrils is most likely the other viscous element in the viscoelastic behavior of an individual collagen fibril. A model of the sliding mechanism responsible for the viscoelastic behavior of collagen fibrils is presented in Fig. 7.6. The sliding between collagen microfibrils is one of the mechanisms which introduces a rapid and significant decay of stress in the stress relaxation process. The sliding between collagen molecules, limited by the natural cross-linking at the telopeptide region, proceeds more slowly with relaxation times in the range of hundreds of seconds.

In our previous work (chapter 4) [24], we found that the shear modulus of single collagen fibrils is two orders of magnitude lower than the Young’s modulus, which confirms the mechanical anisotropy of single collagen fibrils. The similar value for the shear moduli for native and EDC/NHS cross-linked collagen fibrils placed in buffer indicates that the sliding of microfibrils with respect to each other is probably the main factor influencing the shear modulus of single collagen fibrils. In this study, the results of stress relaxation behavior of (non)cross-linked collagen fibrils further supported the existence of a microfibrillar structure and the role of microfibrils in the mechanical behaviour of single collagen fibrils.

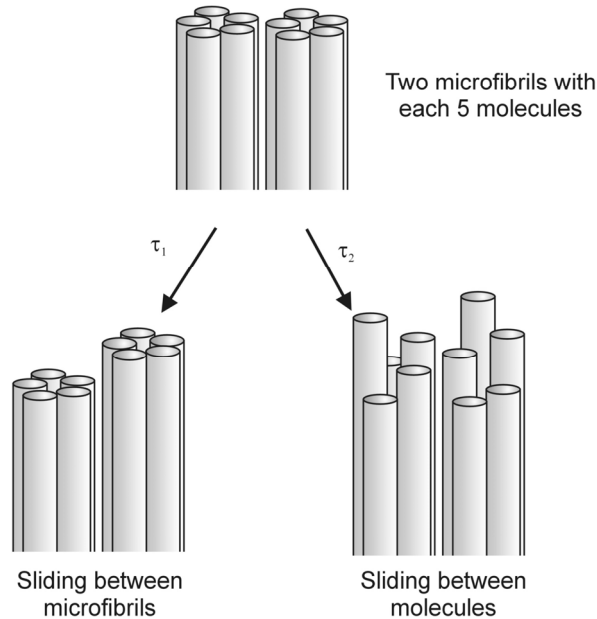


Figure 7.6 Schematic drawing of the sliding mechanism of collagen molecules and microfibrils in individual collagen fibrils. The fast relaxation ($\tau_1 = 1.5 - 5$ s) results from the sliding between microfibrils. The slow relaxation ($\tau_2 = 50 - 250$ s) results from the sliding between collagen molecules.

7.4 Conclusions

Using an atomic force microscope we have performed tensile test at various strain rates and stress relaxation experiments on native collagen fibrils isolated from bovine Achilles tendon and collagen fibrils cross-linked with different cross-linking agents to study the relationship between fibril structure and mechanical behavior. EDC/NHS was used to increase the number of cross-links between individual collagen molecules. Glutaraldehyde was used for its ability to increase the number of cross-links between collagen molecules as well as microfibrils. A 60% and 30% increase in the Young's modulus were measured for native collagen fibrils and cross-linked collagen fibrils at ambient conditions, respectively, when increasing the strain rate from 0.1 to 10 $\mu\text{m/s}$. For (non)cross-linked collagen fibrils immersed in PBS buffer, the Young's modulus increased 30% with the same range of strain rate increase.

In a second set of experiments the stress relaxation behavior of native and cross-linked collagen fibrils were measured and the data were fitted with a two-term Prony series. The results indicate that there are two distinct processes contributing to the stress relaxation

behavior of collagen fibrils: a fast relaxation process with a characteristic time τ_1 of 1.8 ± 0.4 s and a slow relaxation process with τ_2 of 60 ± 10 s for native fibrils immersed in PBS buffer. The relaxation times were influenced differently by the two different cross-linking agents. EDC/NHS cross-linked collagen fibrils only showed a longer relaxation time τ_2 with respect to the native fibrils. For collagen fibrils cross-linked with glutaraldehyde, the relaxation times τ_1 and τ_2 are both longer than those of native fibrils. It is proposed that τ_1 is related to the sliding of collagen microfibrils with respect to each other, and τ_2 is related to the sliding of molecules with respect to each other. The sliding of microfibrils is faster than the sliding of molecules because there are fewer cross-links between microfibrils. The existence of microfibrils has been a debate for years. This study together with our previous work supports the existence of microfibrils and the role of such structures in the mechanical behavior of single collagen fibrils.

Acknowledgement

This research was financially supported by the Softlink program of ZonMw. Project number: 01SL056.

References

1. Purslow PP, Wess TJ, Hukins DWL. Collagen orientation and molecular spacing during creep and stress-relaxation in soft connective tissues. *J. Exp. Biol.* **1998**; 201: 135-142.
2. Haut TL, Haut RC. The state of tissue hydration determines the strain-rate-sensitive stiffness of human patellar tendon. *J. Biomech.* **1997**; 30: 79-81.
3. Usha R, Subramaniam V, Ramasami T. Role of secondary structure on the stress relaxation processes in rat tail tendon (RTT) collagen fibre. *Macromol. Biosci.* **2001**; 1: 100-107.
4. Lynch HA, Johannessen W, Wu JP, Jawa A, Elliott DM. Effect of fiber orientation and strain rate on the nonlinear uniaxial tensile material properties of tendon. *J. Biomech. Eng.-T ASME* **2003**; 125: 726-731.
5. Robinson PS, Lin TW, Reynolds PR, Derwin KA, Iozzo RV, Soslowsky LJ. Strain-rate sensitive Mechanical properties of tendon fascicles from mice with genetically engineered alterations in collagen and decorin. *J. Biomech. Eng.-T ASME* **2004**; 126: 252-257.
6. Komatsu K, Kanazashi M, Shimada A, Shibata T, Viidik A, Chiba M. Effects of age on the stress-strain and stress-relaxation properties of the rat molar periodontal ligament. *Arch. Oral Biol.* **2004**; 49: 817-824.
7. Wu JZ, Cutlip RG, Welcome D, Dong RG. Estimation of the viscous properties of

- skin and cutaneous tissue in uniaxial stress relaxation tests. *Biomed. Mater. Eng.* **2006**; 16: 53-66.
8. Wu JJ. Quantitative constitutive behaviour and viscoelastic properties of fresh flexor tendons. *Int. J. Artif. Organs* **2006**; 29: 852-857.
 9. Puxkandl R, Zizak I, Paris O, Keckes J, Tesch W, Bernstorff S, Purslow P, Fratzl P. Viscoelastic properties of collagen:synchrotron radiation investigations and structural model. *Phil. Trans. R. Soc. Lond. B* **2002**; 357: 191-197.
 10. Mosler E, Folkhard W, Knorz E, Nemetschek-Gansler H, Nemetschek T, Koch MHJ. Stress-induced molecular rearrangement in tendon collagen. *J. Mol. Biol.* **1985**; 182: 589-596.
 11. Folkhard W, Mosler E, Geercken W, Knorz E, Nemetschek-Gansler H, Nemetschek T, Koch MHJ. Quantitative analysis of the molecular sliding mechanism in native tendon collagen - time-resolved dynamic studies using synchrotron radiation. *Int. J. Biol. Macromol.* **1987**; 9: 169-175.
 12. Folkhard W, Geercken W, Knorz E, Mosler E, Nemetschek-Gansler H, Nemetschek T. Structural Dynamic of native tendon collagen. *J. Mol. Biol.* **1987**; 193: 405-407.
 13. Sasaki N, Odajima S. Elongation mechanism of collagen fibrils and force-strain relations of tendon at each level of structural hierarchy. *J. Biomech.* **1996**; 29: 1131-1136.
 14. Raspanti M, Congiu T, Guizzardi S. Tapping-mode atomic force microscopy in fluid of hydrated extracellular matrix. *Matrix Biol.* **2001**; 20: 601-604.
 15. Habelitz S, Balooch M, Marshall SJ, Balooch G, Marshall GW. In situ force microscopy of partially demineralized human dentin collagen fibrils. *J. Struct. Biol.* **2002**; 138: 227-236.
 16. Baselt DR, Revel JP, Baldschwieler JD. Subfibrillar structure of type I collagen observed by atomic force microscopy. *Biophys. J.* **1993**; 65: 2644-2655.
 17. Holmes DF, Gilpin CJ, Baldock C, Ziese U, Koster AJ, Kadler KE. Corneal collagen fibril structure in three dimensions: structural insights into fibril assembly, mechanical properties, and tissue organization. *Proc. Natl. Acad. Sci. USA* **2001**; 98: 7307-7312.
 18. Orgel JPRO, Irving TC, Miller A, Wess TJ. Microfibrillar structure of type I collagen in situ. *Proc. Natl. Acad. Sci. USA* **2006**; 103: 9001-9005.
 19. Yang L, van der Werf KO, Bennink ML, Dijkstra PJ, Feijen J. Microtensile testing of individual native and cross-linked collagen type I fibrils. (Chapter 6 of thesis)
 20. Olde Damink, LHH, Dijkstra PJ, van Luyn MJA, van Wachem PB, Nieuwenhuis P, Feijen J. Cross-linking of dermal sheep collagen using a water-soluble carbodiimide. *Biomaterials* **1996**; 17: 765-773.
 21. Everaerts, F., Torrianni M, Hendriks M, Feijen J. Quantification of carboxyl groups in carbodiimide cross-linked collagen sponges. *J. Biomed. Mater. Res. A* **2007**; 83: 1176-1183.

22. Olde Damink LHH, Dijkstra PJ, van Luyn MJA, van Wachem PB, Nieuwenhuis P, Feijen J. Glutaraldehyde as a crosslinking agent for collagen-based biomaterials. *J. Mater. Sci.- Mater. M* **1995**; 6: 460-472.
23. Yang L, van der Werf KO, Koopman BFJM, Subramaniam V, Bennink ML, Dijkstra PJ, Feijen J. Micromechanical bending of single collagen fibrils using atomic force microscopy. *J. Biomed. Mater. Res. A* **2007**; 82: 160-168. (Chapter 3 of this thesis)
24. Yang L, van der Werf KO, Fitié CFC, Bennink ML, Dijkstra PJ, Feijen J. Mechanical Properties of Native and Cross-linked Type I Collagen Fibrils. *Biophys. J.* **2007**; Online. (Chapter 4 of this thesis)
25. van der Rijt JAJ, van der Werf KO, Bennink ML, Dijkstra PJ, Feijen J. Micromechanical testing of individual collagen fibrils. *Macromol. Biosci.* **2006**; 6: 697-702.
26. Torii, A., Sasaki M, Hane K, Okuma S. A method for determining the spring constant of cantilevers for atomic force microscopy. *Meas. Sci. Technol.* **1997**; 7: 179-184.
27. Wineman AS, Rajagopal KR. *In Mechanical response of polymers: an introduction. Cambridge University Press. New York, 2000.*
28. Screen HR, Lee DA, Bader DL, Shelton JC. An investigation into the effects of the hierarchical structure of tendon fascicles on micromechanical properties. *Proc. Instn. Mech. Engrs.* **2004**; 218: 109-119.
29. Yamamoto E, Hayashi K, Yamamoto N. Mechanical properties of collagen fascicles from the rabbit patellar tendons. *J. Biomech. Eng.-T. ASME* **1999**; 121: 124-131.
30. Engel J. Versatile collagens in invertebrates. *Science* **1997**; 277: 1785-1786.

Microscale Mechanical Properties of Single Elastic Fibers; the Role of Fibrillin-microfibrils*

Lanti Yang^{1†}, Kees O. van der Werf², Martin L. Bennink², Pieter J. Dijkstra¹, Jan Feijen¹

¹ *Polymer Chemistry and Biomaterials, Faculty of Science & Technology and Institute for Biomedical Technology (BMTI), University of Twente, P.O. Box 217, 7500 AE, Enschede, The Netherlands*

² *Biophysical Engineering, Faculty of Science & Technology and MESA+ Institute for Nanotechnology, University of Twente, P.O. Box 217, 7500 AE, Enschede, The Netherlands*

Mieke M.J.F. Koenders^{1†}, Ronnie G. Wismans¹, Dieter P. Reinhardt², Toin H. van Kuppevelt¹

¹ *Department of Biochemistry, Nijmegen Center for Molecular Life Sciences, University Nijmegen Medical Center, Nijmegen, the Netherlands*

² *Department of Anatomy and Cell Biology, McGill University, Montreal, Canada*

Abstract

Micromechanical properties of single elastic fibers and fibrillin-microfibrils, isolated from equine *ligamentum nuchae* using chemical and enzymatic methods were determined with atomic force microscopy (AFM). Young's moduli of single elastic fibers immersed in water, devoid of or containing fibrillin-microfibrils, were determined using bending tests. Bending freely suspended elastic fibers on a micro-channeled substrate by a tip-less AFM cantilever generated a force versus displacement curve from which the Young's modulus was calculated. For single elastic fibers, Young's moduli in the range of 0.3 - 1.5 MPa were determined, values not significantly affected by the absence or presence of fibrillin-microfibrils. To further understand the role of fibrillin-microfibrils in vertebrate elastic fibers, layers of fibrillin-microfibrils were subjected to nano-indentation tests. From the

* This chapter is to be submitted for publication. † Authors contribute equally to this work.

slope of the force versus indentation curves, Young's moduli ranging between 0.56 and 0.74 MPa were calculated. The results suggest that fibrillin-microfibrils are not essential for the mechanical properties of single vertebrate elastic fibers.

8.1 Introduction

Elastic fibers are essential structures which endow resilience to the extracellular matrix (ECM) by a passive, entropy-driven mechanism allowing stretching and recoil [1]. In vertebrates, the elasticity of several tissues and organs such as skin, lung, muscle, ligaments and cartilage [2-4] is provided by elastic fibers. Using macro-mechanical testing, the elasticity of elastic fiber-rich tissues has been a subject of study for years. The Young's modulus of elastic fiber-rich tissue samples of purified dog or sheep aorta was determined to be in the range of 0.13 - 0.65 MPa [5]. Young's moduli between 0.1 - 0.8 MPa were calculated for tissue samples of purified pig aorta enriched with elastic fibers [6]. The Young's modulus of single elastic fibers isolated from bovine *ligamentum nuchae* was, for the first time, determined by Aaron *et al.* [7] using a microtest apparatus attached to a polarizing microscope and was in the range of 0.4 - 1.2 MPa. The vertebrate elastic fibers contain at least two morphological components: amorphous elastin, which accounts for 90% of the elastic fibers, and microfibrils which are 10 - 12 nm in diameter [1,8]. Fibrillin-1 is the major component of the microfibrils [3], although other, less abundant, molecules like microfibril-associated glycoproteins [9-11], emilins [12-14], and latent transforming growth factor- β binding protein [15-17] have been identified.

Fibrillin-microfibrils are considered necessary for the assembly of a functional elastic fiber. During elastic fiber formation, fibrillin-microfibrils appear first and serve as a scaffold for the deposition of tropo-elastin [8]. Invertebrates lack elastin, and the essential elastic recoil of their tissue can only be provided by fibrillin-microfibrils, suggesting that fibrillin-microfibrils are elastic [18-20]. The Young's modulus of the invertebrate microfibrillar network is in the range of 0.2 - 1.1 MPa [19-21]. The question arises as to whether vertebrate fibrillin-microfibrils also have similar mechanical properties and play a role in the mechanical properties of vertebrate organs and elastic fibers. Work on mammalian ciliary zonular filaments, a structure solely composed of fibrillin-microfibrils, gave insight into the mechanical properties of vertebrate fibrillin-microfibrils. X-ray diffraction and biomechanical testing of zonular filaments indicated that fibrillin-microfibrils have a Young's modulus in the range of 0.19 - 1.88 MPa, similar in magnitude to invertebrates fibrillin-microfibrils and elastic fibers [22-24]. However, using molecular combing, the Young's modulus of single fibrillin-microfibrils from zonular

filaments was estimated to be 78 - 96 MPa, which is two orders of magnitude higher than the modulus determined from tissue samples [25]. From these data, the authors suggested that fibrillin-microfibrils play a role in reinforcing the vertebrate elastic fibers. Recent work by Lillie *et al.* also indicated that removal of fibrillin-microfibrils from the elastic fibers of porcine aorta results in a slightly decreased Young's modulus at low strain and a slightly increase of modulus at high strain for the tissue sample [6]. To date, there is still debate about the value of the Young's modulus of fibrillin-microfibrils and how these microfibrils contribute to the mechanical properties of vertebrate elastic fibers.

Since elastin is one of the most abundant proteins in human tissues, elastic fibers are regarded as highly suitable scaffolding material for tissue engineering applications. For the use of elastic fibers as a biomaterial, purity of the material is an important issue. Contamination with proteins may lead to unwanted immunological reactions. Efforts have been made to use purified intact elastic fibers as scaffolds in tissue engineering [26-29]. From the work of Daamen *et al.*, it is suggested that purified intact elastic fibers devoid of fibrillin-microfibrils are preferred for scaffold purposes [29]. The mechanical properties of the purified elastic fibers devoid of or containing fibrillin-microfibrils should also be determined for an adequate use of these fibers in tissue engineering.

This study reports on the biomechanical properties of single purified elastic fibers. Highly purified elastic fibers, devoid of or containing fibrillin-microfibrils, were successfully extracted from equine *ligamentum nuchae* and subjected to an atomic force microscope (AFM). Micromechanical bending tests, similarly as previously described (chapter 3) [30], were for the first time performed on single elastic fibers to determine the Young's modulus of the fibers. The Young's modulus of fibrillin-microfibrils was determined using AFM-based nano-indentation. The contribution of fibrillin-microfibrils to the mechanical properties of the vertebrate single elastic fibers was evaluated using the combined results from bending and nano-indentation experiments.

8.2 Materials and Methods

All experimental procedures were performed at room temperature, unless stated otherwise.

8.2.1 Isolation of elastic fibers

Elastic fibers, devoid of or containing fibrillin-microfibrils, were isolated from equine *ligamentum nuchae* using a modification of previously published work of Daamen *et al.*

[31,32]. *Ligamentum nuchae* was pulverized under liquid nitrogen conditions using a pulverisette with a 1 mm sieve (Fritsch pulverisette 19, Idar-Oberstein, Germany). The pulverized tissue was subjected three times to an overnight extraction with 10 vol. (10 ml/g) of 1 M NaCl containing 0.02% (w/v) NaN_3 at 4°C. After each extraction step, insoluble material was recovered by centrifugation at 5000 x g at 4°C for 20 min. After the last extraction step, the pellet was washed with demineralised water and resuspended in 10 vol. of ethanol. After 90 min, the suspension was filtered through a paper funnel. This procedure was repeated with 10 vol. of chloroform/methanol (2:1) for 90 min, 10 vol. of acetone for 30 min, and 10 vol. of ether for 30 min. The resulting residue was dried in a desiccator. The dried material was extracted with 15 vol. of 97% formic acid with 1% (w/v) cyanogen bromide for 24 h under non-oxidizing conditions. After extraction, the suspension was diluted with 45 vol. of demineralised water and centrifuged at 5000 x g at 4°C for 15 min. The pellet was washed with demineralised water until a pH of 6-7 was reached. After washing, the pellet was resuspended in 10 vol. of demineralised water and this suspension was divided in two parts. One half of the suspension was used to isolate elastic fibers devoid of fibrillin-microfibrils (method I) and the other half was used to isolate elastic fibers containing fibrillin-microfibrils (method II).

Method I: After centrifugation, the pellet was resuspended in 5 vol. of 0.5 M Tris HCl pH 6.8 containing 4 M ureum, 1 M β -mercaptoethanol, and 0.02% (w/v) NaN_3 and incubated overnight. This extraction step was repeated three times and after each step insoluble material was recovered by centrifugation at 5000 x g at 4°C for 20 min. The resulting pellet was washed for 6 times with 5 vol. of demineralised water. After centrifugation, the pellet was resuspended in 5 vol. 0.1 M NH_4HCO_3 , pH 8.2 containing 0.02% (w/v) NaN_3 and 10,000 U trypsin (T-4665, Sigma, St. Louis, USA) and incubated for 4h at 37°C. The suspension was centrifuged and the pellet was washed with demineralised water, followed by three overnight extractions with 5 vol. 1 M NaCl containing 0.02% (w/v) NaN_3 . The resulting pellet was washed with demineralised water and the end product was stored at -80°C.

Method II: After centrifugation, the pellet was resuspended in 5 vol. 0.2 M Tris HCl pH 7.4 containing 0.05 M CaCl_2 , 0.02% (w/v) NaN_3 , and 500 U collagenase type VII (Sigma, St. Louis, MO, USA) and incubated for 4 h at 37 °C. The suspension was centrifuged and the pellet was washed with demineralised water, followed by three overnight extractions with 5 vol. 1 M NaCl containing 0.02% (w/v) NaN_3 . The resulting pellet was washed with demineralised water and the end product was stored at -80 °C.

8.2.2 Purity assessment

Gel electrophoresis: Elastic fiber preparations were analyzed under reducing conditions (5% β -mercaptoethanol) on a 10% (w/v) polyacrylamide gel. Proteins were visualized by silver staining using a 0.1% (w/v) AgNO_3 solution.

Transmission Electron Microscopy (TEM): Elastic fiber preparations were embedded in 1.5% (w/v) agarose, fixed in 2% (v/v) glutaraldehyde in 0.1 M phosphate buffer (pH = 7.4), post fixed with 1% (w/v) osmium tetroxide, dehydrated in ascending series of ethanol, and embedded in epon 812. Ultrathin sections (60 nm) were picked up on formvar-coated grids, post stained with lead citrate and uranyl acetate, and subsequently imaged using electron microscope (JEOL 1010, Tokyo, Japan).

Scanning Electron Microscopy (SEM): Lyophilized elastic fiber preparations were mounted on stubs and sputtered with an ultrathin layer of gold in a polaron E5100 SEM coating system. Specimens were studied with a SEM apparatus (JEOL JSM-6310, Tokyo, Japan) operating at 15 kV.

Immune Fluorescence Assay (IFA): Elastic fiber preparations were suspended in demineralised water and frozen in liquid nitrogen. 4 μm cryosections were cut and incubated in 1% (w/v) bovine serum albumin (BSA, fraction V, Sigma, St. Louis, MO, USA) in PBS to block aspecific binding sites. Sections were incubated overnight at 4°C with rabbit anti-bovine type I collagen (1:50, Chemicon, Temecula, USA), rabbit anti-fibrillin-1 (1:500, clone rF6H, kind gift of Dr. Dieter Reinhardt), and mouse anti-bovine elastin (1:500, clone BA-4, Sigma, St. Louis, MO, USA) diluted in PBS containing 1% (w/v) BSA. After washing with PBS, bound antibody was detected with 1:100 diluted goat anti-mouse IgG Alexa 488 or goat anti-rabbit IgG Alexa 488 (Molecular Probes, Eugene, OR, USA) in PBS containing 1% (w/v) BSA for 90 min. Sections were washed in PBS and mounted in mowiol (4-88, Calbiochem, La Jolla, CA, USA).

8.2.3 Micromechanical bending tests of elastic fibers using AFM

Quartz glass substrates with parallel micro-channels were prepared by reactive ion etching using a RIE Elektrotech system (Elektrotech Twin PF 340, UK). The width and depth of the channels were determined by AFM (home-built instrument) and SEM (LEO Gemini 1550 FEG-SEM, Oberkochen, Germany) measurements.

Diluted suspensions of elastic fiber preparations, devoid of or containing fibrillin-

microfibrils, were prepared by adding 15 mg of preparation I or II to 20 ml demineralised water. Glass substrates were incubated in the diluted suspension for 10 min, and dried overnight.

A home-built AFM combined with an optical microscope was used for micromechanical bending tests. Bending experiments were performed using modified triangular silicon nitride cantilevers (coated sharp microlevers MSCT-AUHW, type F, spring constant $k = 0.5$ N/m, Veeco, Cambridge, UK). The tip of the AFM cantilever was removed using a focused ion beam (FIB) (FEI, Nova Nanolab 600 dual beam machine, Eindhoven, the Netherlands), which facilitated the positioning of the cantilever above the fiber because the width of the cantilever is slightly wider than the fiber diameter. The spring constant of each tipless cantilever was calibrated by pushing on a pre-calibrated cantilever as described elsewhere [33]. Before starting the measurement, the glass substrate containing the elastic fibers was immersed in 1 ml demineralised water and left to equilibrate for 15 min. Micromechanical bending tests were performed by bending the elastic fiber at the middle point of the channel using an AFM cantilever. Deflection versus piezo displacement curves were directly obtained from the micromechanical bending tests. From the results, forces versus displacement curves were derived to estimate the Young's modulus of single elastic fibers. Local indentation of elastic fibers during bending was estimated by indenting the same fiber located on the glass surface.

8.2.4 Diameter of the elastic fibers in water

The diameter of the elastic fibers used in the micromechanical bending tests was determined by Scanning Electron Microscopy (SEM) (LEO Gemini 1550 FEG-SEM, Oberkochen, Germany). The diameter of an elastic fiber in water was estimated from SEM images made with an environmental SEM system (Philips XL 30 ESEM-FEG, Eindhoven, the Netherlands) at water pressure of 5.4 Torr and temperature of 5°C.

8.2.5 Isolation of fibrillin-microfibrils

Fibrillin-microfibrils were isolated from equine *ligamentum nuchae* as described [34]. Briefly, tissue was dissected into small pieces and incubated in 50 mM Tris HCl pH 7.4 containing 0.4 M NaCl, 10 mM CaCl₂, type Ia collagenase (Sigma, St. Louis, MO, USA), 2 mM phenylmethylsulphony fluoride (PMSF), and 5 mM N-ethylmaleimide (NEM) for 18 h. Samples were centrifuged at 5000 x g at 4°C for 5 min and the supernatant was size fractionated on a sepharose CL-4B column (Amersham, Piscataway, NJ, USA) in 20 mM Tris HCl (pH = 7.4) containing 0.4 M NaCl and 2 mM CaCl₂ using a flow rate of 0.2

ml/min. The excluded volume contained fibrillin-microfibrils, as detected by dot-blot immunohistochemistry with rabbit anti-fibrillin-1 (1:500, clone rF6H).

8.2.6 Imaging of fibrillin-microfibrils using AFM

The excluded volume containing fibrillin-microfibrils was diluted 10 times in water. The diluted suspension of fibrillin-microfibrils was brought onto a cleaned glass substrate. After drying, the glass substrate was washed with demineralised water in order to remove any unattached material. The fibrillin-microfibrils were imaged by tapping mode in air using a home-built AFM system with V-shaped Si₃N₄ cantilevers (coated sharp microlevers MSCT-AUHW, type F, spring constant $k = 0.5$ N/m, Veeco, Cambridge, UK). A tapping frequency of ~ 120 kHz and a tapping amplitude of $\sim 400 - 600$ nm were used.

8.2.7 Nano-indentation of fibrillin-microfibrils using AFM

A suspension of fibrillin-microfibrils from the non-diluted excluded volume was brought onto a cleaned glass substrate to obtain multi-layers of fibrillin-microfibrils. After drying and washing with demineralised water, the fibrillin-microfibrils layers were imaged using AFM, as described above to obtain information of the morphology about the microfibrils. Using an initial large scale image, the desired area for indentation was selected. Before starting the measurements, the glass substrate containing the fibrillin-microfibrils was immersed in 1 ml demineralised water and left to equilibrate for 15 min. Nano-indentation was performed at different locations on the surface using the V-shaped Si₃N₄ cantilevers (coated sharp microlevers MSCT-AUHW, type C, spring constant $k = 0.01$ N/m, Veeco, Cambridge, UK) applying an AFM piezo displacement of 500 nm and a frequency of 10 Hz. The spring constant of each cantilever was calibrated by pushing on a pre-calibrated cantilever as described elsewhere [33]. To obtain a force versus indentation curve, the sensitivity (S) of the applied method, i.e. the ratio between the bending of the cantilever and the deflection as measured by the quadrant detector, was derived from the force versus displacement curve using a glass surface. The Young's modulus of fibrillin-microfibrils was calculated from the force versus indentation curve.

8.3 Results and Discussion

8.3.1 Elastic fiber preparations

To visualize major contaminations (e.g. globular proteins), purified elastic fiber preparations, devoid of or containing fibrillin-microfibrils, were subjected to gel electrophoresis. Contaminants and elastin degradation products are soluble and will

penetrate the gel, whereas the insoluble elastic fiber preparations will not. The consecutive extraction steps and the specific enzyme digestion used in method I and II successfully removed contaminants from the starting material, as indicated by the clear absence of protein bands (Fig. 8.1A). Moreover, no signs of degradation products of elastin were present. Similarly, scanning electron microscopy (SEM) revealed intact elastic fibers with a smooth surface (Fig. 8.1B and C).

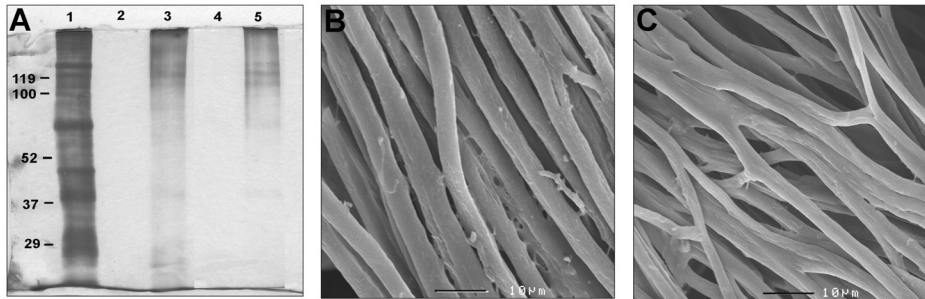


Figure 8.1 (A) Gel electrophoresis of purified elastic fiber preparations. Note that, compared to crude *Ligamentum nuchae* (lane 1), purified elastic fibers devoid of (method I, lane 2) or containing (method II, lane 4) fibrillin-microfibrils did not contain any visible protein bands that indicate contamination or elastin breakdown. Elastic fiber preparations before purification with method I (lane 3) or method II (lane 5) still contained some protein bands, indicating that method I and II successfully removed the contaminations from these preparations. (B) SEM images of purified elastic fiber preparations after purification with method I (B) and method II (C) (Bar = 10 μm). Note the smooth and intact surface of the elastic fibers.

Transmission electron microscopy (TEM) and immune fluorescence assay (IFA) were applied to detect collagen, fibrillin-1 containing microfibrils, and elastin in the elastic fiber preparations. Staining for elastin in elastic fiber preparations devoid of fibrillin-microfibrils (method I) was abundant, whereas staining for type I collagen and fibrillin-1 was absent (Fig. 8.2A and B for elastin and fibrillin-1). Elastic fiber preparations containing fibrillin-microfibrils (method II) displayed abundant elastin and fibrillin-1 staining (Fig. 8.2D and E). On the other hand, type I collagen was absent (data not displayed). Abundant black dots, as an indication of fibrillin-microfibrils were only found in the TEM images of elastic fibers containing fibrillin-microfibrils, which was in line with the results of IFA (Fig. 8.2C and F). In conclusion, two elastic fiber preparations were prepared, one preparation contained pure, intact elastic fiber devoid of fibrillin-microfibrils (method I) and the other preparation contained pure, intact elastic fibers containing fibrillin-microfibrils (method II).

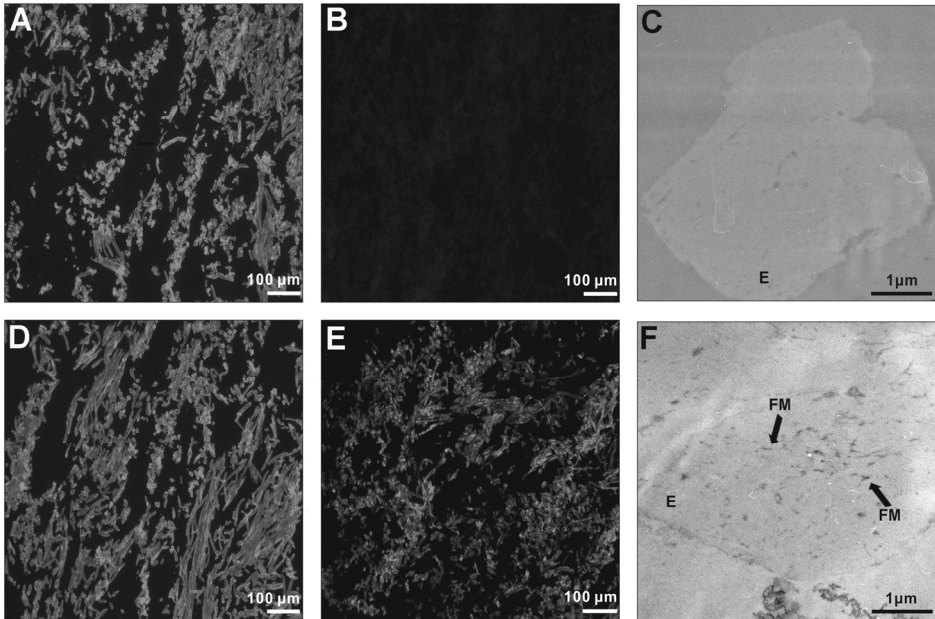


Figure 8.2 (A-B, D-E) Fluorescence microscope images of immunostaining of elastic fiber preparations. Elastic fibers devoid of fibrillin-microfibrils (method I) were immunostained for elastin (A) and fibrillin-1 (B). Likewise, elastin (D) and fibrillin-1 (E) were detected in elastic fibers containing fibrillin-microfibrils (method II). Note that in both preparations elastin was abundantly present, whereas fibrillin-1 was only present in elastic fibers purified by method II. (C, F) TEM images of the sectional area of the elastic fiber preparations. Note that fibrillin-microfibrils were only detected in elastic fibers purified by method II (F). *E* = elastin, *FM* = fibrillin-microfibrils.

8.3.2 Mechanical properties of single elastic fibers

Reactive ion etching was used to prepare the glass substrates with well defined micro-channels with a width of 5 μm – 10 μm and a depth of 600 nm. After incubating the glass substrates with the diluted elastic fiber preparations, single elastic fibers spanning the micro-channels were selected for micro-mechanical AFM bending tests using an inverted optical microscope. SEM images clearly showed that the single elastic fibers were spanning the micro-channels of the glass substrate (Fig. 8.3A). These fibers were bent with a tip-less cantilever along the fiber axis. With the piezo movement versus deflection curves obtained directly from the AFM bending data, the force (*F*) and the displacement (*z*) in the *z*-direction were calculated using the following equations:

$$z = A - D \times S \quad (8.1)$$

$$F = D \times S \times k \quad (8.2)$$

in which A is the piezo movement in the z -direction, D is the deflection measured (in Volts), S is the sensitivity of the cantilever, and k is the calibrated spring constant of the cantilever. A force versus displacement curve was obtained by plotting displacement (z) on the x -axis and force (F) on the y -axis.

By exerting a force on the elastic fibers at the middle point of the channel, a displacement from bending was induced as well as a local indentation of the fiber. In order to determine the modulus of an elastic fiber by bending tests, the displacement has to be corrected for this indentation. Local indentation can be estimated from the force versus displacement curve of indenting an elastic fiber on the glass surface (indentation curve in Fig. 8.3B). By subtracting for each force the displacement resulting from only indentation from the total displacement as obtained by measuring at the middle point (bending curve in Fig. 8.3B), the displacement resulting from only the bending can be obtained (Fig. 8.3C). In the remainder of this paper, the mentioned displacement is only displacement due to bending.

A linear force versus displacement curve was found for bending elastic fibers devoid of or containing fibrillin-microfibrils (Fig. 8.3C). In the experiments, no difference was found in the force versus displacement curve after bending the fiber at the same position multiple times, which ensured the reproducibility of the measurements and indicated that no permanent deformation of the elastic fiber had occurred. The slope (dF/dz) of the curve in Fig. 8.3C was used to calculate the Young's modulus. During the AFM manipulation, it became clear that the AFM cantilever was able to laterally move elastic fibers on the glass substrate. Therefore, elastic fibers were assumed to be supported, instead of being fixed at the two ends of the channel. The Young's modulus of the elastic fibers can then be described by the model of bending isotropic materials, using the expression [35]:

$$E = \frac{l^3}{48l} \times \frac{dF}{dz} \quad (8.3)$$

In which I is the moment of inertia, equal to $\frac{1}{4}\pi R^4$ (elastic fibers were considered a rod with a circular cross-section with radius R), l is the length of the elastic fiber spanning the channel, and dF/dz is the slope of the force versus displacement curve obtained from bending experiments of the two elastic fiber preparations.

The diameter of all the tested elastic fiber preparations was determined using SEM imaging of dry fibers. However, during the micromechanical bending test, the glass

substrate containing the elastic fibers was immersed in water. This may lead to swelling of the elastic fibers, thereby affecting the diameter. Therefore, the diameters of an elastic fiber in the dry and in the hydrated state were estimated by environmental SEM imaging under high (5.4 Torr) and very low water pressure (0.6 Torr) (Fig. 8.4). SEM images made at the high water pressure can be used to determine the dimensions of fully hydrated elastic fibers. By measuring the diameters of a large number of elastic fibers, the diameters of hydrated elastic fibers turned out to be 1.1 times larger than the diameters of dry fibers.

As shown in Fig. 8.5, for elastic fibers devoid of fibrillin-microfibrils an average Young's modulus of 0.79 ± 0.17 MPa (mean diameter 3.9 ± 0.5 μm (\pm S.D.)) was found and elastic fibers containing fibrillin-microfibrils had an average Young's modulus of 0.90 ± 0.23 MPa (mean diameter 4.3 ± 1.1 μm (\pm S.D.)). Statistically this difference is not significant.

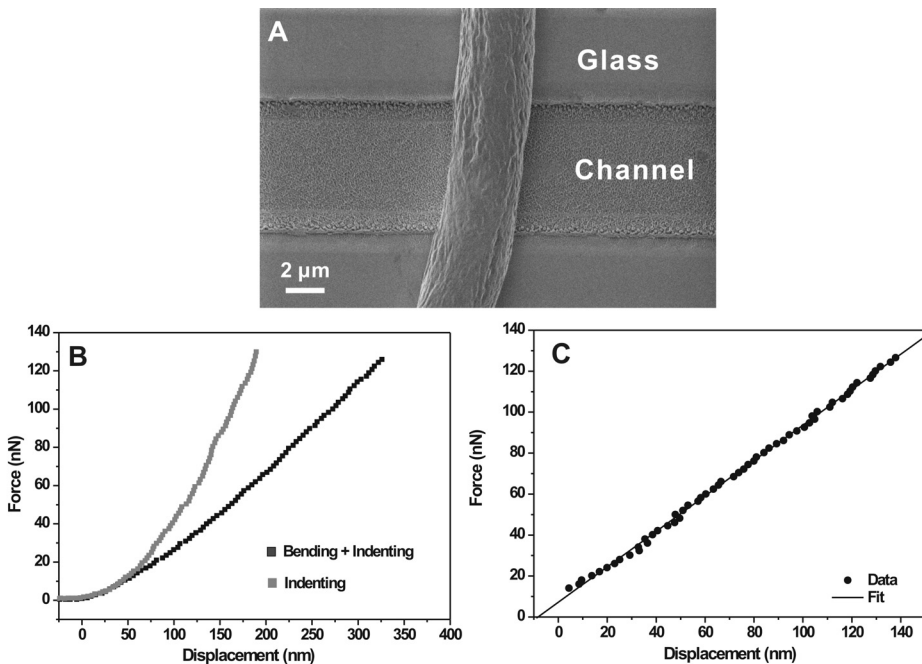


Figure 8.3 (A) SEM image of an elastic fiber spanning a micro-channel in the glass substrate. (B) Force versus displacement curves obtained from bending an elastic fiber immersed in water at the middle point of the channel (black cube) and indenting the same elastic fiber on the glass substrate (gray cube). (C) Force versus displacement only representing the bending of the fiber obtained after subtracting for each force the displacement from local indentation.

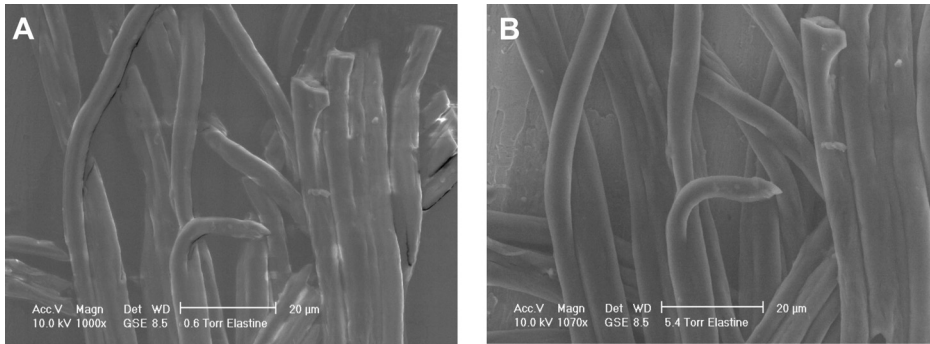


Figure 8.4 SEM images of elastic fibers devoid of fibrillin-microfibrils in dry state (0.6 Torr water pressure) (A) and in hydrated state (5.4 Torr water pressure) (B). Note the small increase in the diameter of hydrated elastic fibers as compared to dry fibers.

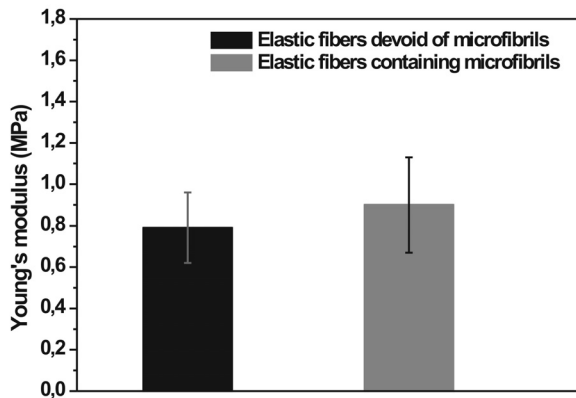


Figure 8.5 Young's moduli of elastic fibers devoid of (black bars, $N = 8$, $D = 3.9 \pm 0.5 \mu\text{m}$) and containing fibrillin-microfibrils (gray bars, $N = 9$, $D = 4.3 \pm 1.1 \mu\text{m}$). The error in the Young's modulus is presented as S. E. M.

The Young's moduli of single elastic fibers ranged between 0.3 and 1.5 MPa, which is comparable to the range stated in literature for single elastic fibers and tissues [18]. The mechanical properties of single elastic fibers from bovine *ligamentum nuchae* were studied, for the first time, by Aaron *et al.* [7]. Using a microtest apparatus it was shown that the Young's modulus of a single elastic fiber is in the range of 0.4 - 1.2 MPa. From macro-mechanical tests on elastin-rich tissue strips, elastic fibers of purified dog or sheep aorta, Young's moduli in the range of 0.13 - 0.65 MPa were determined [5]. Young's moduli between 0.1 - 0.8 MPa were obtained for elastic fibers in strips of purified pig aorta [6]. The comparable Young's moduli derived from our micromechanical AFM bending test and from macrotests/microtests of elastin rich tissue strips/single elastic

fibers indicate that the purification procedure did not affect the mechanical properties of the elastic fibers. Although the value is well within stated ranges, it has to be noted that the full range for the value of Young's modulus, as determined from our measurements, was considerable (0.3 - 1.5 MPa). This range probably resulted from the assumption that elastic fibers are circular in cross-section, as seen in Eq. 8.3. As reported previously [32], SEM imaging indicates that some elastic fibers have an irregular cross-sectional area. Interestingly, no significant differences in the values of the Young's modulus for the purified elastic fibers devoid of or containing fibrillin-microfibrils were found from our measurements. This result suggests that fibrillin-microfibrils do not influence the modulus of elastic fibers.

8.3.3 Fibrillin-microfibril preparations

In order to better explain the obtained results on the Young's modulus for elastic fibers and to provide more insight in the mechanical properties of fibrillin-microfibrils, isolated fibrillin-microfibrils were prepared for micro-mechanical tests.

Isolated fibrillin-microfibrils deposited on a glass substrate were imaged by AFM (Fig. 8.6). As reported previously [36], AFM images displayed the typical "beads-on-a-string" structure for fibrillin-microfibrils. A distance between two beads of 65 ± 7 nm was determined from the images (Fig. 8.6C).

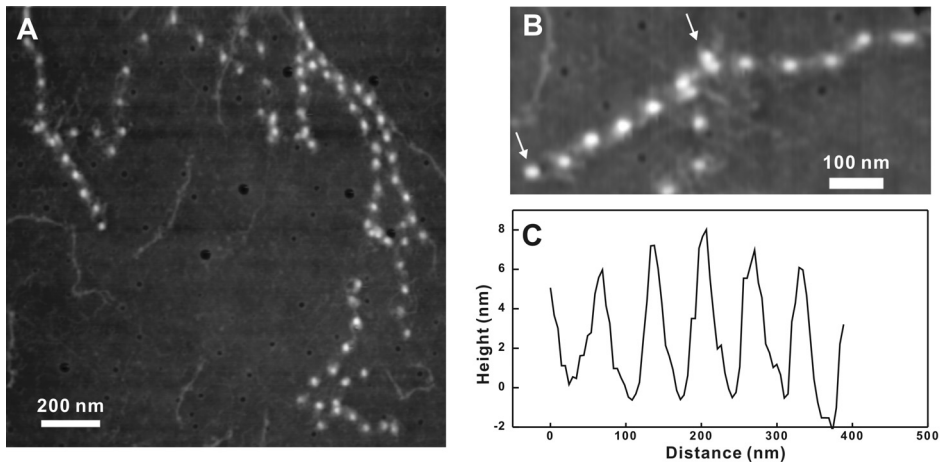


Figure 8.6 (A) Tapping mode atomic force microscopy (AFM) height image of fibrillin-microfibrils deposited on a glass surface. (B) Zoom in of tapping mode AFM height image of fibrillin-microfibrils. Note the typical fibrillin-microfibrils beads-on-a-string appearance. (C) Line scan along a fibrillin-microfibril. 6 repeats are shown as indicated by the arrows in image B. The mean distance between the beads was calculated to be 65 ± 7 nm.

8.3.4 Mechanical properties of fibrillin-microfibrils

Because fibrillin-microfibrils are three orders of magnitude smaller than elastic fibers, poly(methyl methacrylate) (PMMA) coated glass substrates with nano-channels in PMMA of 100 - 200 nm in width, instead of 5 - 10 μm , were at first prepared. A suspension of fibrillin-microfibrils was contacted with the PMMA substrate containing nano-channels. After drying, the substrate was washed with demineralised water and subsequently dried at ambient conditions. The PMMA substrate containing the micro-channels was then subjected to tapping mode AFM imaging. However, AFM images at different positions of the substrates containing channels showed that the fibrillin-microfibrils adhered to the bottom of the channel instead of spanning the nano-channels and therefore micromechanical AFM bending tests could not be performed (data not shown). Efforts were made to make the surface either hydrophilic by oxygen plasma treatment or positively charged by coating a layer of positively charged protein. Changing the surface properties of PMMA did not promote the spanning of the fibrillin-microfibrils over the channels.

Using high concentrations of fibrillin-microfibrils in the suspension to deposit the microfibrils onto the glass substrate enabled the formation of microfibril layers (Fig. 8.7A) with thicknesses of $\sim 60 - 100$ nm. AFM nano-indentation tests of fibrillin-microfibrils were performed at several locations by approaching the AFM tip to the layered surface until a cantilever deflection was observed. A plot of the cantilever deflection versus the piezo movement in the z-direction was recorded for each indentation, and converted to a force versus indentation curve using Eq. 8.1 and 8.2. A typical force versus indentation curve from nano-indentation of fibrillin-microfibrils is depicted in Fig. 8.7B. No difference was found in the force versus displacement curve after indenting multiple times at the same position, which ensured the reproducibility of the measurements and indicated that no permanent deformation of the fibrillin-microfibrils had occurred.

AFM nano-indentation tests have been used to determine the Young's modulus of different biological samples [37,38] using the theory of Hertz [39] and the mechanics of Sneddon [40]. The relationship between force and indentation is influenced by the geometry of the AFM tip. In this study, the radius of the tip was ~ 20 nm, which was in the same order as the indentation depth. Therefore, the tip can be assumed to be parabolic with a radius of curvature R at the apex. The force applied on the cantilever (F) as a function of the indentation (x) can then be described using the following expression:

$$F = \frac{4\sqrt{R}}{3} E^* \chi^{1.5} \quad (8.4)$$

Where E^* is the relative Young's modulus, defined as:

$$\frac{1}{E^*} = \frac{1 - \nu_{tip}^2}{E_{tip}} + \frac{1 - \nu_{sample}^2}{E_{sample}} \quad (8.5)$$

In which ν_{sample} is the Poisson ratio of the sample and ν_{tip} the Poisson ratio of the tip. The experimental data of the force versus indentation curve could be fitted with Eq. 8.4 (Fig. 8.7B). An average E^* of 0.74 ± 0.17 MPa (\pm S. E. M.) was calculated from several force versus indentation curves obtained from nano-indentation at different locations of the sample. The Young's modulus of the AFM tip (~ 200 GPa) is much higher than the Young's modulus of the fibrillin-microfibrils in the hydrated state, therefore the $1/E^*$ is further simplified to:

$$\frac{1}{E^*} \approx \frac{1 - \nu_{sample}^2}{E_{sample}} \quad (8.6)$$

Using a typical Poisson ratio of 0 - 0.5 for elastic materials, the Young's modulus (E_{sample}) of fibrillin-microfibrils was estimated to be in the range of 0.56 ± 0.12 to 0.74 ± 0.17 MPa (\pm S. E. M.).

It has to be considered that there are still some limitations in the method, influencing the accuracy of the determined Young's modulus. For example, in the model the sample and the tip surface are assumed to be smooth, however, in practice they are usually rough. This uncertainty of the contact area will influence the measurements and can lead to deviations in the order of a few percent [41]. The obtained value was still comparable to Young's moduli estimated for vertebrate or invertebrate fibrillin-microfibrillar networks. The invertebrate microfibrillar network in abdominal lobster oarta has a modulus of ~ 1.06 MPa [19]. The Young's modulus of fibrillin-microfibrils isolated from sea cucumber dermis is approximately 0.2 MPa [20], whereas, the microfibrillar network in jellyfish has an estimated Young's modulus of 0.9 MPa [21]. In vertebrates, the Young's modulus of bovine zonular filaments, a structure solely composed of fibrillin-microfibrils, is in the range of 0.19 - 1.88 MPa [22-24,42].

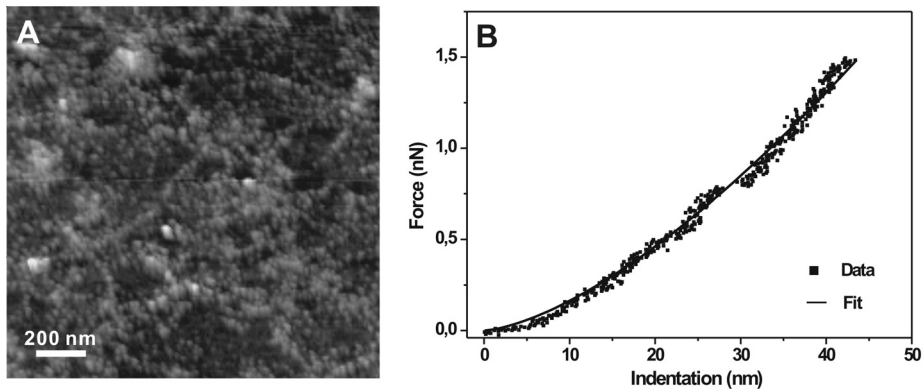


Figure 8.7 (A) Contact mode AFM height image of fibrillin-microfibrils layers deposited on a glass surface (Bar = 200 nm). (B) Typical force versus indentation curves obtained from nano-indentation of fibrillin-microfibrils layers. A relative Young's modulus (E^*) of 0.86 MPa was calculated from fitting the experimental data to Eq. 8.4.

The current study was designed to determine the role of fibrillin-microfibrils in the mechanical properties of a single elastic fiber. Highly purified elastic fibers, devoid of or containing fibrillin-microfibrils, were extracted from equine *ligamentum nuchae* and subjected to micromechanical AFM bending tests in order to determine the Young's modulus. It has to be highlighted that, compared to macromechanical tests, AFM is a very accurate method for determining the mechanical properties of micro- and nano-sized materials [43,44]. The determined Young's moduli for single elastic fibers devoid of or containing fibrillin-microfibrils were not significantly different, indicating that fibrillin-microfibrils do not influence the mechanical properties of a single elastic fiber from equine *ligamentum nuchae*. As presented in our results, fibrillin-microfibrils have a Young's modulus similar as that of elastic fibers, which can be the reason for the above finding.

Recently, Sherrat *et al.* used a molecular combing technique to determine the Young's modulus of fibrillin-microfibrils isolated from bovine zonular filaments [25]. A Young's modulus of 78 - 96 MPa was determined, a value nearly two orders of magnitude higher than the Young's moduli reported in literature for microfibrillar networks as well as the values determined by us for isolated fibrillin-microfibrils. The authors imply that individual fibrillin-microfibrils act as relatively stiff elastic polymers, reinforcing the elastic fibers. However, our direct measurements on the mechanical properties of single elastic fibers devoid of or containing fibrillin-microfibrils did not show a reinforcing effect of these microfibrils. Recent published work by Megill *et al.* gives an explanation

for this paradox [21]. The authors suggest that the mechanical behavior of fibrillin-microfibrils must be fitted by a J-shaped model, instead of the linear model that is derived from the molecular combing experiments by Sherrat *et al.* Based on reinterpretation of the molecular combing experiments, Megill *et al.* suggest a Young's modulus of 1 MPa for fibrillin-microfibrils, a value that is in the range with our data. Taken all three comments into account, we suggest that fibrillin-microfibrils have Young's moduli in the range of 0.56 - 0.74 MPa.

8.4 Conclusions

An AFM-based mechanical technique was applied to study the micro-scale mechanical behavior of single elastic fibers and fibrillin-microfibrils. Highly purified and intact elastic fibers devoid of or containing fibrillin-microfibrils were successfully isolated using chemical and enzymatic methods. As determined from micro-mechanical bending tests, the Young's moduli of single elastic fibers was in the range of 0.3 - 1.5 MPa. The Young's moduli for purified elastic fibers were in the same range as those for elastic fiber-rich tissues. The Young's modulus of single elastic fibers was not significantly affected by the absence or presence of fibrillin-microfibrils. Fibrillin-microfibrils have a Young's modulus in the range of 0.56 - 0.74 MPa as determined with nano-indentation tests, which is comparable with the Young's modulus of elastic fibers. It is concluded that fibrillin-microfibrils do not significantly influence the mechanical properties of single vertebrate elastic fibers.

Acknowledgements

The authors wish to thank the Department of Pathology, Faculty of Veterinary Medicine, Utrecht University, the Netherlands for providing equine *ligamentum nuchae*.

This research is financially supported by the Softlink program of ZonMw. Project number: 01SL056.

References

1. Rosenbloom J, Abrams WR, Mecham R. Extracellular matrix 4: the elastic fiber. *FASEB J.* **1993**; 7: 1208-1218.
2. Kielty CM, Shuttleworth CA. Fibrillin-containing microfibrils: structure and function in health and disease. *Int. J. Biochem. Cell Biol.* **1995**; 27: 747-760.

3. Sakai LY, Keene DR, Engvall E. Fibrillin, a new 350-kD glycoprotein, is a component of extracellular microfibrils. *J. Cell Biol.* **1986**; 103: 2499-2509.
4. Sherratt MJ, Wess TJ, Baldock C, Ashworth JL, Purslow PP, Shuttleworth CA, Kielty CM. Fibrillin-rich microfibrils of the extracellular matrix: ultrastructure and assembly. *Micron* **2001**; 32: 185-200.
5. Sherebrin MH. Mechanical anisotropy of purified elastin from the thoracic aorta of dog and sheep. *Can. J. Physiol. Pharmacol.* **1983**; 61: 539-545.
6. Lillie MA, David GJ, Gosline JM. Mechanical role of elastin-associated microfibrils in pig aortic elastic tissue. *Connect. Tissue Res.* **1998**; 37: 121-141.
7. Aaron BB, Gosline JM. Elastin as a random-network elastomer - a mechanical and optical analysis of single elastin fibers. *Biopolymers* **1981**; 20: 1247-1260.
8. Kielty CM, Sherratt MJ, Shuttleworth CA. Elastic fibres. *J. Cell Sci.* **2002**; 115: 2817-2828.
9. Gibson MA, Hughes JL, Fanning JC, Cleary EG. The major antigen of elastin-associated microfibrils is a 31-kDa glycoprotein. *J. Biol. Chem.* **1986**; 261: 1429-1436.
10. Gibson MA, Kumaratilake JS, Cleary EG. The protein-components of the 12-nanometer microfibrils of elastic and nonelastic tissues. *J. Biol. Chem.* **1989**; 264: 4590-4598.
11. Gibson MA, Hatzinikolas G, Kumaratilake JS, Sandberg LB, Nicholl JK, Sutherland GR. Further characterization of proteins associated with elastic fiber microfibrils including the molecular cloning of MAGP-2 (MP25). *J. Biol. Chem.* **1996**; 271: 1096-1103.
12. Bressan GM, Dagagordini D, Colombatti A, Castellani I, Marigo V, Volpin D. Emilin, a component of elastic fibers preferentially located at the elastin-microfibrils interface. *J. Cell. Biol.* **1993**; 121: 201-212.
13. Colombatti A, Doliana R, Bot S, Canton A, Mongiat M, Mungiguerra, Paron-Cilli S, Spessotto P, The EMILIN protein family. *Matrix Biol.* **2000**; 19: 289-301.
14. Doliana R, Mongiat M, Bucciotti F, Giacomello E, Deutzmann R, Volpin D, Bressan GM, Colombatti A. EMILIN, a component of the elastic fiber and a new member of the C1q/tumor necrosis factor superfamily of proteins. *J. Biol. Chem.* **1999**; 74: 16773-16781.
15. Isogai Z, Ono RN, Ushiro S, Keene DR, Chen Y, Mazzieri R, Charbonneau NL, Reinhardt DP, Rifkin DB, Sakai LY. Latent transforming growth factor beta-binding protein 1 interacts with fibrillin and is a microfibril-associated protein. *J. Biol. Chem.* **2003**; 278: 2750-2757.
16. Oklu R, Hesketh R. The latent transforming growth factor beta binding protein (LTBP) family. *Biochem. J.* **2000**; 352: 601-610.
17. Sinha S, Nevett C, Shuttleworth CA, Kielty CM. Cellular and extracellular biology of the latent transforming growth factor-beta binding proteins. *Matrix Biol.* **1998**; 17: 529-545.

18. Faury G. Function-structure relationship of elastic arteries in evolution: from microfibrils to elastin and elastic fibres. *Pathol. Biol.* **2001**; 49: 310-325.
19. McConnell CJ, Wright GM, DeMont ME. The modulus of elasticity of lobster aorta microfibrils. *Experientia* **1996**; 52: 918-921.
20. Thurmond FA, Trotter JA. Morphology and biomechanics of the microfibrillar network of sea cucumber dermis. *J. Exp. Biol.* **1996**; 199: 1817-1828.
21. Megill WM, Gosline JM, Blake RW. The modulus of elasticity of fibrillin-containing elastic fibres in the mesoglea of the hydromedusa *Pollyorchis penicillatus*. *J. Exp. Biol.* **2005**; 208: 3819-3834.
22. Wright DW, McDaniels CN, Swasdison S, Accavitti MA, Mayne PM, Mayne R. Immunization with undenatured bovine zonular fibrils results in monoclonal antibodies to fibrillin. *Matrix Biol.* **1994**; 14: 41-49.
23. Wess TJ, Purslow PP, Sherratt MJ, Ashworth J, Shuttleworth CA, Kielty CM. Calcium determines the supramolecular organization of fibrillin-rich microfibrils. *J. Cell Biol.* **1998**; 141: 829-837.
24. Ziebarth NM, Wojcikiewicz EP, Manns F, Moy VT, Parel JM. Atomic force microscopy measurements of lens elasticity in monkey eyes. *Mol. Vis.* **2007**; 13: 504-510.
25. Sherratt MJ, Baldock C, Haston JL, Holmes DF, Jones CJP, Shuttleworth CA, Wess TJ, Kielty CM. Fibrillin microfibrils are stiff reinforcing fibres in compliant tissues. *J. Mol. Biol.* **2003**; 332: 183-193.
26. Buttafoco L, Engbers-Buijtenhuijs P, Poot AA, Dijkstra PJ, Daamen WF, van Kuppevelt TH, Vermes I, Feijen J. First steps towards tissue engineering of small-diameter blood vessels: Preparation of flat scaffolds of collagen and elastin by means of freeze drying. *J. Biomed. Mater. Res. B* **2006**; 77: 357-368.
27. Buttafoco L, Kolkman NG, Engbers-Buijtenhuijs P, Poot AA, Dijkstra PJ, Vermes I, Feijen J. Electrospinning of collagen and elastin for tissue engineering applications. *Biomaterials* **2006**; 27: 724-734.
28. Daamen WF, van Morerkerk HTB, Hafmans T, Buttafoco L, Poot AA, Veerkamp JH, van Kuppevelt TH. Preparation and evaluation of molecularly-defined collagen-elastin-glycosaminoglycan scaffolds for tissue engineering. *Biomaterials* **2003**; 24: 4001-4009.
29. Daamen WF, Nillesen STM, Hafmans T, Veerkamp JH, van Luyn MJA, van Kuppevelt TH. Tissue response of defined collagen-elastin scaffolds in young and adult rats with special attention to calcification. *Biomaterials* **2005**; 26: 81-92.
30. Yang L, van der Werf KO, Koopman BFJM, Subramaniam V, Bennink ML, Dijkstra PJ, Feijen J. Micromechanical bending of single collagen fibrils using atomic force microscopy. *J. Biomed. Mater. Res. A* **2007**; 82: 160-168. (chapter 3 of this thesis)
31. Daamen WF, Hafmans T, Veerkamp JH, van Kuppevelt TH. Comparison of five procedures for the purification of insoluble elastin. *Biomaterials* **2001**; 22: 1997-2005.

32. Daamen WF, Hafmans T, Veerkamp JH, van Kuppevelt TH. Isolation of intact elastin fibers devoid of microfibrils. *Tissue Eng.* **2005**; 11: 1168-1176.
33. Torii A, Sasaki M, Hane K, Okuma S. A method for determining the spring constant of cantilevers for atomic force microscopy. *Meas. Sci. Technol.* **1996**; 7: 179-184.
34. Kielty CM, Shuttleworth CA. Abnormal fibrillin assembly by dermal fibroblasts from two patients with Marfan syndrome. *J. Cell. Biol.* **1994**; 124: 997-1004.
35. Gere JM, Timoshenko SP. *In* Mechanics of materials. *Stanley Thornes Ltd., Cheltenham, 1999.*
36. Kielty CM, Cummings C, Whittaker SP, Shuttleworth CA, Grant ME. Isolation and ultrastructural analysis of microfibrillar structures from foetal bovine elastic tissues. Relative abundance and supramolecular architecture of type VI collagen assemblies and fibrillin. *J. Cell Sci.* **1991**; 99: 797-807.
37. Vinckier A, Semenza G. Measuring elasticity of biological materials by atomic force microscopy. *FEBS Lett.* **1998**; 430: 12-16.
38. Radmacher M, Fritz M, Cleveland JP, Walters DA, Hansma PK. Imaging adhesion forces and elasticity of lysozyme adsorbed on mica with the atomic force microscope. *Langmuir* **1994**; 10: 3809-3814.
39. Timoshenko S, Goodier J. *In* Theory of elasticity. 3rd edition. *McGraw-Hill, New York, 1987.*
40. Sneddon IN. The relation between load and penetration in the axisymmetric boussinesq problem for a punch of arbitrary profile. *Int. J. Engng. Sci.* **1965**; 3: 47-57.
41. Bouzakis KD, Michailidis N, Hadjiyiannis S, Skordaris G, Erkens G. The effect of specimen roughness and indenter tip geometry on the determination accuracy of thin hard coatings stress-strain laws by nanoindentation. *Mater. Charact.* **2002**; 49: 149-156.
42. Wright DM, Duance VC, Wess TJ, Kielty CM, Purslow PP. The supramolecular organisation of fibrillin-rich microfibrils determines the mechanical properties of bovine zonular filaments. *J. Exp. Biol.* **1999**; 202: 3011-3020.
43. Jacot JG, Dianis S, Schnall J, Wong JY. A simple microindentation technique for mapping the microscale compliance of soft hydrated materials and tissues. *J. Biomed. Mater. Res. A* **2006**; 79: 485-494.
44. Matsumoto T, Abe H, Ohashi T, Kato Y, Sato M. Local elastic modulus of atherosclerotic lesions of rabbit thoracic aortas measured by pipette aspiration method. *Physiol. Meas.* **2002**; 23: 635-648.

Summary

Collagen is the principal, tensile stress-bearing component of connective tissue. Several research groups have studied the hierarchical structure of collagen and have attempted to relate the structure to its function and mechanical properties. At this moment, the role of microfibrils in fibrils and the contribution of each level of the collagen hierarchical structure to the overall mechanical properties of collagen based tissues are not fully understood. Next to collagen, many tissues for instance blood vessels, contain elastic fibers which are mainly responsible for providing elasticity to tissues and organs in vertebrates. The elastic fibers contain elastin and fibrillin-microfibrils. The role of fibrillin-microfibrils in the mechanical properties of elastic fibers has been a debate for years.

The aim of the work described in this thesis is to acquire a better insight in the relationship between the mechanical properties and structure of collagen fibrils and elastic fibers using AFM-based micromanipulation techniques. The mechanical properties of collagen fibrils and elastic fibers will also give information on the micro-mechanical behavior of tissues.

In **Chapter 2** the structure and mechanical properties of fibril-forming type I collagen are reviewed. The structure of this type of collagen is characterized by a hierarchical assembly of sub-structures. The collagen molecules, which are assemblies of three polypeptide chains, are the units for further assembly into fibrils and fibers. Further structural organization is found in tissues like tendons where the collagen fibers are organized in fascicles.

Especially the molecular organization of the collagen molecules in fibrils has been a debate for several years and different models were proposed. Based on recent experimental results, microfibrils formed by assembly of five collagen molecules are suggested as a sub-structure of the collagen fibril.

Tissues based on fiber forming collagens like tendon exhibit viscoelastic behavior. The mechanism for the viscoelastic behavior of tendon is not clear due to the limited amount of information on the contribution of the mechanical properties of the sub-structures to the

overall mechanical properties of collagen. Force spectroscopy measurements using AFM and micro-electromechanical devices have been performed to study the mechanical properties of single collagen fibrils and molecules. However, the current understanding of the mechanical properties of single collagen fibrils is still limited. The overall picture of the stress-strain behavior, the viscoelastic behavior and its relation to the (an)isotropy of the collagen fibrils, which is essential to provide insight in the function and structure relationship of collagen have not been studied yet. Atomic force microscopy (AFM) as a tool to determine the mechanical properties of materials is also briefly reviewed in this chapter. Recent studies have shown that AFM is a suitable technique to determine the mechanical properties of materials in the sub-micron range.

In **Chapter 3**, we report on a newly developed AFM-based micromechanical technique to study the mechanical properties of single collagen fibrils. Collagen fibrils isolated from bovine Achilles tendon were deposited on a poly(dimethyl siloxane) (PDMS) substrate containing micro-channels. Force-displacement relationships of collagen fibrils perpendicular and freely suspending the micro-channels were determined by loading them with a tip-less cantilever at the center of the channel. With the assumption that the mechanical behavior of collagen fibrils can be described by the model of bending a rod and that the fibrils are freely supported at the rims, a Young's modulus of 5.4 ± 1.2 GPa for fibrils at ambient conditions was determined. Also fibrils cross-linked with glutaraldehyde were mechanically tested and showed a Young's modulus of 14.7 ± 2.7 GPa. Assuming that the fibril was fixed at the ends of the channel the Young's moduli of native and glutaraldehyde cross-linked collagen fibrils were calculated to be 1.4 ± 0.3 GPa and 3.8 ± 0.8 GPa, respectively. The values deduced from the two models represent the minimum and maximum boundaries of the Young's modulus determined for native and glutaraldehyde cross-linked collagen fibrils.

Having proved the very good applicability of micromechanical bending as a tool to determine the mechanical properties of collagen fibrils prompted us to extend the measurements to the collagen fibrils in the hydrated state. Further improvements were made to allow multiple bending along the entire length of the suspended part of the fibril. This allowed a more precise determination of the bending modulus. Micromechanical bending in scanning mode using AFM was used to study the mechanical properties of native and carbodiimide cross-linked single collagen fibrils and is described in **Chapter 4**. Bending moduli ranging from 1.0 GPa to 3.9 GPa were determined for single collagen fibrils at ambient conditions. By bending fibrils with different length to diameter ratios

and using the unit-load equation, the shear modulus of the fibrils at ambient conditions was, for the first time, calculated to be 33 ± 2 MPa. The bending and shear modulus of the native fibrils in PBS buffer were 0.07 - 0.17 GPa and 2.9 ± 0.3 MPa, respectively. The two orders of magnitude lower shear modulus compared with the Young's modulus confirms the mechanical anisotropy of the collagen single fibrils. Carbodiimide cross-linked fibrils immersed in PBS buffer have similar bending and shear moduli as native fibrils. Since carbodiimides only introduce intra- and inter-molecular cross-links, the results indicate that the sliding of microfibrils with respect to each other is probably the main factor influencing the shear modulus of single collagen fibrils.

The scanning mode bending technique developed can also be used to determine the mechanical properties of single electrospun collagen fibers (**Chapter 5**). Electrospun collagen fibers with diameters ranging from 100 to 600 nm were successfully produced by electrospinning a solution of acid soluble collagen type I. The electrospun fibers were water soluble and became insoluble after cross-linking with glutaraldehyde vapor for 24 hours and thus could also be tested in the hydrated state. The bending moduli of the non-cross-linked electrospun fibers determined from the scanning mode bending tests ranged from 1.3 to 7.8 GPa at ambient conditions, similar to those of single native collagen fibrils. The shear modulus of the non-crosslinked electrospun collagen fibers at ambient conditions was calculated to be approximately two orders of magnitude lower than the bending modulus which clearly indicated mechanical anisotropy of the fibers. Cross-linking of the electrospun fibers with glutaraldehyde vapor increased the shear modulus of the fibers at ambient conditions from ~ 30 MPa to ~ 50 MPa. The bending and shear moduli of the cross-linked fibers immersed in PBS buffer were 0.07 - 0.26 GPa, and 5.2 MPa, respectively.

Next to the bending experiments as described in Chapters 3 and 4 the tensile properties of individual collagen fibrils were studied using a slightly adapted AFM system and the results are described in **Chapter 6**. For these experiments the fibril was glued to the substrate and the AFM cantilever by droplets of epoxy glue. An additional calibrated piezo tube which can extend up to 400 μm was added to allow stretching of the collagen fibrils up to breakage. At ambient conditions a linear stress-strain behavior of the collagen fibrils with reversible elongation up to a stress of 80 ± 20 MPa and a Young's modulus of 2.5 ± 0.9 GPa were determined. When immersing the fibrils in PBS buffer, a toe region was found up to a stress of 5 MPa. At higher stresses, the stress-strain curve became linear and a Young's modulus of 0.6 GPa was calculated. For the first time the failure stress and

strain at break of individual collagen fibrils in PBS buffer could be determined. Furthermore, the influence of cross-linking on the mechanical properties was investigated. Both carbodiimide cross-linking and glutaraldehyde cross-linking resulted in an increase of the failure stress and strain at break of collagen fibrils. Compared to native collagen fibrils, an increase of the Young's modulus was only found for collagen fibrils cross-linked with glutaraldehyde.

The successful micromechanical tensile test experiments also allowed determining of the viscoelastic behavior of single collagen fibrils. In **Chapter 7**, we describe the tensile test experiments at different strain rates and stress relaxation measurements on collagen fibrils. The results indicate that the stress-strain behavior of individual collagen fibrils is rate-dependent. Stress relaxation tests revealed that there was a fast ($\tau_1 = 1.8 \pm 0.4$ s) and a slow ($\tau_2 = 60 \pm 10$ s) relaxation process present for the native individual collagen fibrils in the fully hydrated state. After cross-linking using the carbodiimide EDC in combination with NHS, τ_2 of the tested fibrils increased to 225 ± 10 s while τ_1 remained unchanged. After cross-linking with glutaraldehyde, the relaxation times of the collagen fibrils increased to 3.7 ± 1.0 s and 250 ± 80 s, respectively. Based on these results, we propose that the fast relaxation relates to the sliding of microfibrils with respect to each other whereas the slow relaxation relates to the sliding of collagen molecules with respect to each other. These results and the results described in Chapter 4 support the existence of a microfibrillar structure and suggest a possible role of microfibrils in the viscoelastic behavior of single collagen fibrils.

In joint research with Mieke Koenders and Toin van Kuppevelt of the Department of Biochemistry at the Nijmegen Center for Molecular Life Sciences of the University Nijmegen Medical Center, Nijmegen in the Netherlands, the micromechanical bending technique was applied to elastin fibers. Fibrillin-microfibrils, one of the components of elastic fibers, are considered necessary for the assembly of a functional elastic fiber. Invertebrates lack elastin, and their essential elastic recoil can only be provided by the mechanical properties of fibrillin-microfibrils. The question arises as to whether vertebrate fibrillin-microfibrils also have similar mechanical properties. **Chapter 8** deals with a study on the role of fibrillin-microfibrils in the mechanical properties of elastic fibers. Young's moduli of single elastic fibers, devoid of or containing fibrillin-microfibrils, were determined from bending tests on elastic fibers immersed in water. For single elastic fibers, Young's moduli in the range of 0.3 - 1.5 MPa were determined, which were not affected significantly by the absence or presence of fibrillin-microfibrils. Nano-indentation tests

were performed on layers of fibrillin-microfibrils to determine the Young's modulus. From the slope of the force versus indentation curves, Young's moduli ranging from 0.56 to 0.74 MPa were calculated, which was similar to that of elastic fibers. These results suggest that the fibrillin-microfibrils do not significantly influence the mechanical properties of single vertebrate elastic fibers.

To conclude, micromechanical techniques are versatile tools to analyze the mechanical properties of collagen fibrils, electrospun collagen fibers and elastic fibers. The results allow a better understanding of the relationship between the structure of collagen type I fibrils and elastin fibers and their mechanical properties.

Samenvatting

Het eiwit collageen is de belangrijkste component in weefsels als onder andere pezen, spieren, tussenwervelschijven, gewrichtsbanden en huid en speelt een zeer belangrijke rol in het overbrengen van krachten. Verschillende onderzoeksgroepen hebben geprobeerd een verband te vinden tussen enerzijds de structuur en anderzijds de biologische functie en mechanische eigenschappen van collageen. Desondanks is het tot op heden onduidelijk wat de bijdrage is van alle individuele hiërarchische structuurniveaus (triple helices, microfibrillen, fibrillen, vezels) in de vezelbundels op de mechanische eigenschappen van collageen. Veel biologische weefsels, zoals bloedvaten, bevatten naast collageen ook elastine, een eiwit verantwoordelijk voor de elasticiteit van weefsels in gewervelde dieren. Elastische vezels bevatten naast elastine ook fibrilline-microfibrillen. De exacte rol die fibrilline-microfibrillen spelen in het bepalen van de mechanische eigenschappen van de elastische vezels is al jaren onderwerp van een wetenschappelijke discussie.

Het doel van het werk dat beschreven staat in dit proefschrift is om een beter inzicht te verkrijgen in de relatie tussen de mechanische eigenschappen en de structuur van collageenfibrillen en elastische vezels door gebruik te maken van op AFM gebaseerde micromanipulatie technieken. De mechanische eigenschappen van collageenfibrillen en elastische vezels geven ook informatie over het micromechanische gedrag van weefsels.

In **hoofdstuk 2** wordt een overzicht gegeven van de structuur en mechanische eigenschappen van het vezelvormende collageen type I. De collageenmoleculen, die zelf bestaan uit drie polypeptide ketens, vormen de bouwstenen waaruit de fibrillen en vezels zijn opgebouwd. In weefsels als pezen zijn op een hiërarchische wijze de substructuren georganiseerd zodat sterke collageen vezels worden gevormd.

De exacte moleculaire organisatie van de collageenmoleculen in fibrillen is een onderwerp van discussie en er zijn verschillende modellen voorgesteld. Gebaseerd op recente experimentele resultaten is het aannemelijk dat een microfibril, bestaande uit vijf collageen moleculen, een substructuur is van de collageenfibril.

Weefsels die zijn opgebouwd uit vezelvormende collagenen, zoals pezen, vertonen viscoelastisch gedrag. Het achterliggende mechanisme voor dit viscoelastische gedrag is

tot op heden niet duidelijk, omdat er slechts beperkte informatie is over de bijdrage van de substructuren op de mechanische eigenschappen van collageen. De mechanische eigenschappen van collageenfibrillen en -moleculen zijn gemeten met krachtspectroscopische technieken waarbij gebruik is gemaakt van een AFM en micro-elektromechanische actuatoren. Desondanks zijn de mechanische eigenschappen van collageen op het fibrilniveau nog grotendeels onduidelijk. Het spanning-rek gedrag van collageenfibrillen, het viscoelelastische gedrag en de relatie tussen de (an)isotropie van de collageenfibrillen en het viscoelastische gedrag zijn nog niet tot in detail bestudeerd. Juist deze relatie is essentieel om inzicht te verkrijgen in het verband tussen de structuur en de mechanische eigenschappen van collageen. Tot slot is in dit hoofdstuk een kort overzicht gegeven van het gebruik van krachtmicroscopie (afgekort met AFM uit het Engels afkomstige Atomic Force Microscopy) als een techniek om de mechanische eigenschappen van materialen te onderzoeken. De resultaten van recent onderzoek hebben laten zien dat AFM een erg geschikte techniek is om de mechanische eigenschappen te bepalen van materialen met afmetingen kleiner dan een micrometer.

In **hoofdstuk 3** beschrijven wij een nieuwe micromechanische techniek waarbij gebruik wordt gemaakt van AFM om de mechanische eigenschappen van individuele collageenfibrillen te bestuderen. Voor deze experimenten zijn collageenfibrillen geïsoleerd uit runderachillespees en neergelegd op een poly(dimethyl siloxaan) (PDMS) substraat waarin zich microkanalen bevinden. Voor collageenfibrillen die de microkanalen loodrecht overspannen is de relatie tussen kracht en verplaatsing gemeten door met een krachtmicroscopie met een bladveer kracht uit te oefenen (buigexperiment) op het midden van de fibril. Onder de aanname dat het mechanische gedrag van de collageenfibrillen kan worden beschreven met een model voor het buigen van een macroscopische staaf en dat de fibrillen vrij worden ondersteund aan de rand van het kanaal, is een Young's modulus van 5.4 ± 1.2 GPa bepaald voor fibrillen in lucht en bij kamertemperatuur. Voor fibrillen die met het reagens glutaraaldehyde zijn gecrosslinkt (vernet), is onder dezelfde condities en aannames een modulus van 14.7 ± 2.7 GPa bepaald. Onder de aanname dat de fibrillen tijdens de experimenten gefixeerd zijn aan de randen van de microkanalen, is uit de experimenten een modulus berekend van 1.4 ± 0.3 GPa en 3.8 ± 0.8 GPa voor de ongemodificeerde en vernette fibrillen. De waardes die met deze twee modellen zijn berekend moeten gezien worden als de onder- en bovengrens van de werkelijke waarde van de Young's modulus van de fibrillen.

Met het behalen van deze eerste resultaten hebben wij ons tot doel gesteld om de

micromechanische buigmetingen uit te breiden naar collageenfibrillen in de gehydrateerde toestand, zoals in de natuurlijke situatie. Hiertoe is de meettechniek eerst verder verbeterd door het mogelijk te maken om de kracht-verplaatsings kromme van de fibrillen te bepalen op meerdere punten over de gehele lengte van de fibril door met de bladveer over de fibril heen te scannen. Deze verbetering maakt het mogelijk om de buigmodulus van de fibrillen veel preciezer te bepalen. De mechanische eigenschappen van individuele collageenfibrillen zijn met deze scannende micromechanische buigtechniek bestudeerd (**hoofdstuk 4**). De buigmodulus van de collageenfibrillen onder omgevingscondities ligt tussen de 1.0 GPa en 3.9 GPa. Door fibrillen met verschillende lengte-diameter verhoudingen te meten en gebruik te maken van de zogenaamde “unit-load” vergelijking is het mogelijk om ook de afschuifmodulus van fibrillen te berekenen. Voor fibrillen gemeten in lucht is de afschuifmodulus 33 ± 2 MPa. De buig- en afschuifmodulus van ongemodificeerde fibrillen in een PBS bufferoplossing is respectievelijk 0.07 - 0.17 GPa en 2.9 ± 0.3 MPa. Het feit dat de afschuifmodulus twee ordegrottes lager ligt dan de Young's modulus bevestigt dat individuele collageenfibrillen mechanisch anisotroop zijn. Collageenfibrillen die gecrosslinkt zijn met een carbodiimide hebben vergelijkbare buig- en afschuifmoduli in een PBS bufferoplossing als de ongemodificeerde fibrillen. Aangezien met carbodiimide crosslinking alleen inter- en intramoleculaire crosslinks in de fibrillen worden gemaakt, is het op basis van deze resultaten waarschijnlijk dat de afschuifmodulus van collageenfibrillen voornamelijk wordt bepaald door het langs elkaar schuiven van microfibrillen.

De door ons ontwikkelde scannende micromechanische buigtechniek kan ook gebruikt worden om de mechanische eigenschappen te onderzoeken van individuele collageenvezels die verkregen zijn door middel van electrospinnen (**hoofdstuk 5**). Het is mogelijk om een oplossing van oplosbaar type I collageen te electrospinnen en zo collageenvezels te verkrijgen met een diameter tussen de 100 en 600 nm. Na het electrospinnen zijn de vezels oplosbaar in water, maar door blootstelling aan glutaraaldehyde damp (24 uur) vindt crosslinking plaats en worden de vezels onoplosbaar. Voor de gecrosslinkte vezels is het ook mogelijk om de mechanische eigenschappen in gehydrateerde toestand te onderzoeken. De buigmoduli van de niet-gecrosslinkte vezels zijn bepaald met de scannende micromechanische buigtechniek en lopen uiteen van 1.3 tot 7.8 GPa in lucht. Deze waarden zijn zeer vergelijkbaar met de eerder behaalde resultaten voor ongemodificeerde natuurlijke collageenfibrillen. De berekende afschuifmodulus voor de niet gecrosslinkte vezels is ongeveer twee ordegrottes lager dan de buigmodulus. Hieruit blijkt duidelijk dat ook de door electrospinnen verkregen collageenvezels

mechanisch anisotroop zijn. Na vernetting met glutaraaldehyde stijgt de afschuifmodulus van de vezels onder omgevingscondities van ~ 30 MPa naar ~ 50 MPa. De buig- en afschuifmodulus van deze gecrosslinkte vezels in een PBS bufferoplossing is respectievelijk 0.07 - 0.26 GPa en 5.2 MPa.

Naast de buigexperimenten die staan beschreven in hoofdstukken 3 en 4 zijn de mechanische eigenschappen van collageenfibrillen ook onderzocht met micromechanische trekexperimenten. Voor deze experimenten, die beschreven staan in **hoofdstuk 6**, is gebruik gemaakt van een aangepaste krachtmicroscoop en is de fibril vastgelijmd met epoxylijm aan zowel de bladveer van de microscoop als het substraat. Een tweede, gekalibreerd piëzo-element zorgt ervoor dat de collageenfibrillen tot maximaal 400 μm kunnen worden uitgerekt. Onder omgevingscondities vertonen de collageenfibrillen lineair spanning-rek gedrag tot een spanning van 80 ± 20 MPa, waarbij de Young's modulus gelijk is aan 2.5 ± 0.9 GPa. Voor fibrillen in een PBS-oplossing is in de spanning-rek kromme een aanloopgebied te zien tot een spanning van 5 MPa. Bij hogere spanningen is er een lineair verband tussen spanning en rek en is de Young's modulus 0.6 GPa. Tijdens deze experimenten is het voor de eerste keer mogelijk gebleken om de breukspanning en rek bij breuk te bepalen van individuele collageenfibrillen in een PBS-buffer. Ook de invloed van crosslinking op de mechanische eigenschappen is onderzocht. Zowel crosslinking met carbodiimide als met glutaraaldehyde resulteert in een toename van de breukspanning en rek bij breuk van de collageenfibrillen. Alleen de Young's modulus van met glutaraaldehyde gecrosslinkte fibrillen stijgt in vergelijking met de ongemodificeerde fibrillen.

De micromechanische trekexperimenten maken het ook mogelijk om het viscoelastische gedrag van collageenfibrillen te onderzoeken. In **hoofdstuk 7** staan trek-rek experimenten met een variabele deformatiesnelheid en spanningsrelaxatiemetingen aan collageenfibrillen beschreven. De resultaten laten zien dat het spanning-rek gedrag van individuele collageenfibrillen afhankelijk is van de deformatiesnelheid. De spanningsrelaxatiemetingen laten verder zien dat er een snel ($\tau_1 = 1.8 \pm 0.4$ s) en een langzaam ($\tau_2 = 60 \pm 10$ s) relaxatieproces aanwezig is in de gehydrateerde toestand. Na crosslinking met carbodiimide EDC in combinatie met NHS, stijgt τ_2 van de fibrillen naar 225 ± 10 s, terwijl τ_1 gelijk blijft. Na vernetting met glutaraaldehyde, stijgen beide relaxatietijden van de fibrillen naar respectievelijk 3.7 ± 1.0 s en 250 ± 80 s. Op basis van deze resultaten stellen wij een deformatiemechanisme voor waarin de snelle relaxatie veroorzaakt wordt door het langs elkaar schuiven van microfibrillen, terwijl het langzame

relaxatieproces veroorzaakt wordt door het langs elkaar glijden van collageenmoleculen. Samen met de resultaten uit hoofdstuk 4 ondersteunen deze bevindingen de hypothese dat collageenfibrillen opgebouwd zijn uit microfibrillen. De resultaten wijzen ook op een mogelijke rol van de microfibrillen in het viscoelastische gedrag van individuele collageenfibrillen.

In samenwerking met Mieke Koenders en Toin van Kuppevelt van de afdeling Biochemie van het Nijmegen Centre for Molecular Life Sciences in het Universitair Medisch Centrum in Nijmegen zijn micromechanische buigexperimenten gedaan aan elastinevezels. Er wordt algemeen aangenomen dat fibrilline-microfibrillen, een van de componenten van elastische vezels, essentieel zijn voor de bouw en eigenschappen van elastische vezels. In ongewervelde dieren komt geen elastine voor en de elastische eigenschappen van weefsels in deze organismen komen voort uit de mechanische eigenschappen van fibrilline-microfibrillen. Het is daarom interessant om te onderzoeken of fibrilline-microfibrillen van gewervelde dieren dezelfde mechanische eigenschappen bezitten. **Hoofdstuk 8** beschrijft een studie naar de mechanische eigenschappen van elastische vezels en de rol die fibrilline-microfibrillen hierin spelen. De Young's modulus van elastische vezels met en zonder fibrilline-microfibrillen is bepaald door buigexperimenten in water. Voor individuele elastische vezels zijn Young's moduli gemeten uiteenlopend van 0.3 tot 1.5 MPa onafhankelijk van de aanwezigheid van fibrilline-microfibrillen. Verder is ook de Young's modulus van een film bestaande uit fibrilline-microfibrillen bepaald door middel van nano-indentatiemetingen. Uit de hellingen van de kracht-indentatie curves zijn Young's moduli tussen de 0.56 en 0.74 MPa berekend. Deze resultaten zijn vergelijkbaar met de eerder gevonden moduli voor elastische vezels en laten zien dat de fibrilline-microfibrillen de mechanische eigenschappen van elastische vezels van gewervelde dieren niet significant beïnvloeden.

Tot slot kan geconcludeerd worden dat het gebruik van micromechanische technieken een veelzijdige methode is om de mechanische eigenschappen van collageenfibrillen, collageenvezels verkregen door electrospinnen en elastische vezels te onderzoeken. De behaalde resultaten geven een beter inzicht in de relatie tussen de structuur van collageen type I fibrillen en elastinevezels en hun mechanische eigenschappen.

Acknowledgements

When I sit in front of my computer and start looking back at the last four years of my Ph. D study in the University of Twente, I realize that there are so many people who support me in this or that way. Without all these people, the last four years would not be as pleasant as it is now.

First of all, I would like to thank my promotor, Prof. dr. J. Feijen, for offering me the opportunity to pursue my Ph. D study in PBM group at University of Twente. I really appreciate for your guidance throughout the four years especially the discussions we had during this last year. I learned a lot from your inspiring ideas, broad knowledge, and attitude in scientific researches.

I am deeply grateful to my daily supervisor Dr. P. J. Dijkstra. Dear Piet, thank you very much for your constant help throughout the four years not only in scientific work. You gave me a lot of freedom to work and at the meantime help me to structure the framework of my Ph. D research. I really appreciate your continuous support for my lab work and the amount of time you spent on the discussion, papers and thesis. I also really enjoyed the time spent together with you and Janny for dinners and parties. The hospitality from both of you makes me somehow feel at home in Enschede.

I own many thanks to Dr. M. L. Bennink, the other daily supervisor of my Ph. D study. Dear Martin, we have regular work meeting almost every week but you are always available for discussion when I just call you or pop in your office. Thank you very much for the constant help in the lab work and in writing of the papers. As a physicist, you gave me a lot of active suggestions in the research.

I would like to thank all the other promotion committee members who read the thesis and provide me valuable advices.

This project would never be done without the financial support of Softlink program of ZonMw and the cooperation with Biophysical Engineering group.

Kees, you are so busy in taking care of all the AFM setups. I can not remember how many times I came to you with some questions concerning the AFM. But you are always patient

for teaching and helping me with all the problems (we even discussed on the phone during your holiday). Dear Kees, thank you so much for your help and your brilliant ideas for the AFM measurements.

Chapter 8 will not be part of the thesis without the cooperation with people in the group of Dr. T. H. van Kuppevelt at University of Nijmegen. Mieke, thank you for all the efforts you made for this chapter. I wish you all the best with your last year's Ph. D study. I would like to thank Dr. T. H. van Kuppevelt, for supporting the cooperation.

Carel, it is really a nice experience for me to have a student and friend like you. Without your excellent work, Chapter 5 will not be in the thesis. Also many thanks for translating the summary into Dutch. I really enjoyed the time spent with you and Kicki for dinners, parties and basketball games.

Many people have contributed to the thesis with different helps. I would like to thank Mark Smithers and Aart van Apeldoorn for the SEM work, Vishwas Gadgil for the FIB work, Qi Chen for making the micro-channels in glass, and Maryana Escalante Marun for the efforts in making nano-channels in PMMA surface.

I am really lucky to meet all the nice colleagues in the PBM group who make my stay in PBM group really a wonderful memory. Karin, thank you so much for all your kind help in the administrative work. Prof. Engbersen, Dirk and André, I really appreciate your suggestions for my research during the discussion of Monday morning meetings. Hetty, Zlata, Anita, and Marc you are always willing to help for the computers, equipments and chemicals, thanks to you all. I have shared so much joyful time with all my officemates: Bas and Marcel, sometimes we were quiet but not the time when we talked about collagen. Federica, you were the first female officemate I had and I really like the time shared with you. In Zuid Horst, I moved into the "chicken room" and met several great girls: Ingrid, I really cherish the encouragement we had for each other during the last year of our Ph. D study and good luck for your defense! Wei, I really enjoy the Chinese food and tea you bring to the office. Christine, although you were always so busy, we still had a lot of fun together at the dinners. Janine, I am so lucky to have you as my last roommate during my Ph. D study. Thank you for being my paranimfen! I want to express my thanks to all the former and present PBM members for the supports and accompany during coffee breaks and trips although it would be impossible to mention all the names: Zheng and Boon Hua (you both helped me a lot when I first arrived in the group, thanks for your friendship),

Priscilla (it is so nice to have a friend like you and I am grateful for all your help), Sandra (I really appreciate your presents and friendship), Laura, Henriette, Sigrid, Kicki, Yan, Rong, Chao, Jung Seok Lee, Hongzhi, Marloes, Mark B, Ferry, Grégory, Erhan, Hans, Sytze, Andries, Martin, Miguel, Sameer, Niels, Anita K.

I would like to thank all the people in the Biophysical Engineering group for their help in this or that way. Special thanks to Martin, Kees, Vinod, Yanina, Maryana, Chien-Ching, Chandrashekhar, and Bart for the discussion we had during work meetings and in the lab. I also appreciate the nice coffee breaks and helps offered by people from MTP, RBT, and STEP group.

I would like to thank all the Chinese friends I met during my stay in Enschede, who help me a lot and shared a lot of wonderful moments with me, especially to Jing (thanks for being my paranimfen), Xiao and Zheng, Xin and Tian, Xing Yi and In Yee, Shan and Yuguo, Boon Hua and Ai Lin, Rui, Hongmei, Yujie and Qi, Chunlin and Xiaoyi, Chien-Ching and Kaifan, Weiqing. We had a lot of enjoyable time together and thank you all for your friendship!

Finally and most importantly, I would like to thank all my family members. I express my deepest gratitude to my parents Yang Rongsheng and Chang Jiachun, and my beloved husband Hao for their endless love, support and encouragement.

Lanti

January, 2008

Curriculum Vitae

Lanti Yang was born on April 15, 1979 in Harbin, P. R. China. After graduating from Shanghai Nan Yang Model Middle school, she entered the Chemistry and Chemical Engineering Department, Shanghai Jiao Tong University in 1997. In 2001, she obtained her Bachelor's degree with the award of Shanghai Excellent Graduation Thesis. In the same year, she started her Master's studies in the same university. During her Master's studies, she joined in the group of Materials Science and Technology of Polymers (MTP), University of Twente, the Netherlands in 2002-2003 as an exchange student between Shanghai Jiao Tong University and University of Twente. In 2003, she obtained her MSc degree under the supervision of Prof. Julius Vancso from University of Twente. In 2004, she graduated from Shanghai Jiao Tong University with her second MSc degree in Polymer Physics and Chemistry under the supervision of Prof. Qinghua Lu. From Jan. 15 2004, she started her Ph. D studies in the group of Prof. Jan Feijen, University of Twente, the Netherlands. Her Ph. D work focused on the mechanical properties of collagen fibrils, electrospun collagen fibers and elastic fibers studied by atomic force microscopy (AFM) based techniques. The results of her research are described in this thesis.

